STUDIES ON PHOTOIONIZATION

A thesis submitted by

MOHAMED ALI HOURIEH

for the Degree of

Doctor of Philosophy of the

University of London

Chemistry Department

Imperial College of Science and Technology

London, S. W. 7

September 1965

ABSTRACT

The design, construction and operation of a one meter normal incidence vacuum ultraviolet monochromator, combined with a non-magnetic time of flight mass spectrometer, some electronic circuits associated with the instrument and chemical kinetic studies of some organic compounds have been made with this mass spectrometer are described.

The spectrometer incorporates:

a. A simple arrangement to rotate and move the grating to keep the spectrum in focus at the exit slit.

b. A microwave excited, light source for use in studies above the limit of lithium fluoride i.e. 1050 A^{o}; 11.8e.v.

c. A flash light source for use in the spectral range (1172.5 - 685A^{o}); (10.57 e.v. - 18-08 e.v.).

d. An efficient detector for extreme ultraviolet radiation and as a device for the identification of the grating spectrum order.

Monochromatic photons were used to ionize the following organic compounds: acetone; methyl-ethyl ketone; methyl n-butyl ketone; acetaldehyde; n-propane; n-butane; benzene; mono-bromo and monoiodo-benzene. The decay curves of the parent and fragment ions have been determined experimentally, then theoretically, over the

energy range (10.57 - 18.08 e.v), allowing some estimate of kinetic energies to be made. Agreement between experiment and theory was good.

ACKNOWLEDGEMENTS

The author expresses his most sincere gratitude to Dr. D. W. Turner, for his advice, generous help and constant encouragement throughout the period covered by this work and in particular for many stimulating discussions and criticisms.

He would like to express his deep gratitude to Professor D. H. R. Barton, F.R.S., who admitted him to the organic chemical laboratories.

He would like to express his deep indebtedness to his wife, Mayla, who has shared the burden of this work, and to his parents, who have sacrificed to made his university education possible.

He is indebted to Mr. R. S. Milner, for I.B.M. computer, programming of the theoretical calculation of the ions decay in the ionization chamber. He is also highly indebted to Miss P. A. Mills, for typing this thesis.

Finally he must thank the Ministry of Education (in Syria) for a scholarship during the period covered by this research.

TABLE OF CONTENTS

	Page
ABSTRACT	2
ACKNOWLEDGEMENTS	4
TABLE OF CONTENTS	5
INTRODUCTION	7
PART A. THE VACUUM ULTRA VIOLET MONOCHROMATOR - TIME-OF-FLIGHT MASS SPECTROMETER COMBINATION	20
1. OPERATING PRINCIPLE OF A TIME-OF-FLIGHT MASS-SPECTROMETER	22
2. METHODS OF ANALYSIS BY TIME-OF-FLIGHT	26
2.1. Constant Energy and Space Focusing	26
2.2. Constant Momentum	28
3. DESIGN AND CONSTRUCTION	32
3.1. Ion Source	
3.1.1. Vacuum Ultra Violet Monochromator	32
3.1.1.1. Optical Design Consideration	32
3.1.1.2. Scanning the Spectra	33
3.1.1.3 Grating, Mounting and Driving	36
3.1.1.4. Slits	41
3.1.1.5. Vacuum System	42
3.1.1.6. Light Sources	45
A. Pulsed Microwave Discharge Light Source	45

B. Capacitor Discharge Flash Light Source 49

3.1.1.7.Detector 57

3.1.1.8.Stray Light 59

3.1.2. Ionization Chamber 60

3.2. Field Free Drift Tube 62

3.3. Ion Collection and Signal Display 63

4. MASS RESOLVING POWER, LIMITATIONS IN PERFORMANCE AND ADVANTAGES 66

5. MATERIALS 73

PART B. RESULTS AND DISCUSSION 75

1. THEORETICAL CALCULATIONS 76

1.1. Excess Kinetic Energy of Fragment Ions 76

1.2. Mechanism of Formation of High Kinetic Energy Ions During Dissociation 78

1.2.1. Diatomic Molecules 79

1.2.2. Polyatomic Molecules 85

1.3. Decay of Ions in the Ionization Chamber 90

2. PRESENT RESULTS 98

2.1. Effect of Pressure 144

2.2. Effect of Delay Time 145

PART C. APPENDICES - ELECTRONIC INSTRUMENTS 157

1. Pulse Generator and Monitor Unit 158

2. Microwave Pulse Generator 158

3. 10K.V. Power Supply 158

4. Ion Repeller Voltage Generator 159

REFERENCES 164

INTRODUCTION

The ionization and dissociation phenomena of molecules can mainly be investigated using one of three methods: Electron impact, charge exchange or photo-ionization.

A photon of energy $h\nu$, where h is the Planck's constant and ν is the radiation frequency, can be absorbed by an atom or a molecule exciting it to a higher state, provided $ev^{*} = h.\nu$. This process is an absorption of photons i.e.: photo-excitation. The probability of this process depends on the rules governing the reverse process.

When $h.\nu \geq e.V_i$, or $h.\nu = e.V_i + E$ according to Einstein's relation, where V_i is the ionization potential; one of the outermost electrons may be ejected with kinetic energy E equal to the difference between the energy of incident photon and the ionization energy of the gas atom or molecules. The wavelength of radiation necessary is given by a simple relation $\lambda_i = \frac{12398}{V_i}$ where λ_i in A^{o} and V_i in electron volts.

This process is an absorption of photons as well i.e. photoionization.

The probability of this process is maximum when $(h\nu - eV_i)$ is small (0.1 - 1 e.v.), and decreases with decreasing wavelength, the cross section or absorption coefficient.

The frequency of incident photons and the structure of molecule determine the mode of ionization, such as, for example

1. $AB + h\nu \rightarrow AB^+ + e$ without kinetic energy
2. $AB + h\nu \rightarrow AB^+ + e$ with kinetic energy
3. $AB + h\nu \rightarrow AB^* \rightarrow AB^+ + e$
4. $AB + h\nu \rightarrow AB^* \rightarrow AB^+ + e \rightarrow A^+ + B^\cdot + e$
5. $AB + h\nu \rightarrow AB^* \rightarrow A^* + B^\cdot \rightarrow A^+ + B^\cdot + e$
6. etc.

For many years the possibility that photons ionize the gas molecules was largely ignored until 1925. The reason for this was that no very good or certain data could be obtained experimentally that showed photoionization to occur in gases and vapours. It was theoretically expected but there were experimental difficulties.

In 1900 Lenard (1) reported that the light from a spark in air was capable of discharging an electroscope and inferred that the ultraviolet (u.v.) light from the spark ionized air and other gases. Hughes (2), found that ultraviolet light transmitted through fluorite was capable of producing molecular ions; but light transmitted through quartz was not effective.

It seems that it was difficult to interpret the results of these early experiments since undispersed ultraviolet radiation was used and quantum yields were not measured. A book by Hughes and DuBridge (3) described these early

experiments and states, 'It must be admitted that the state of our knowledge regarding the ionization of these gases is extremely unsatisfactory'.

In 1925 Mohler and Foote (4), then later Mohler and others (5), found that there is some ionization by line absorption in cesium vapour and the efficiency of the ionization is proportional to the pressure. He explained it by the assumption that highly excited atoms or a radiation react with neutral atoms or molecules to form molecular ions and the number of ions produced (6), may be less than the number of photons absorbed and the ratio is called the efficiency of photoionization. Thus a considerable amount of quantitative data was obtained.

During the following two decades, after Mohler's work, studies on photoionization processes in gases almost ceased. Recently, since 1950, there has been a considerable interest and intensive efforts of many institutions (7 - 34); many extensive reviews (35 - 41) and data tables (42, 43) of experimental techniques, experimental results and theoretical calculation on this process have been published since then, and as far back as the turn of the century.

The photoionization process is best understood from the theoretical point of view and it has great practical importance (provided by the need for data about atoms and molecules) to several branches of applied physics such as:

a. Gaseous electronics (44).

b. Geophysics of the upper atmosphere (45 - 51).

c. Astrophysics (both in regard to the outer layers and to the interior of the stars) (52).

d. Plasma physics as it may be applied to the construction of models for planetary and stellar atmosphere.

e. Molecular physics (38 and 53).

f. Identification of molecular orbitals (54 - 57).

Most of the investigations mentioned above were carried out by using a monochromator to provide a beam of photons of known energy. These photons were then caused to interact with gas molecules between two plate electrodes placed in an ionization chamber and the resulting photoions were detected by measuring the ionization current produced. The current (I_o) from a photomultiplier facing the photon beam in the chamber was recorded when the chamber evacuated. The sample was allowed into the ionization chamber in sufficient pressure to give about 25 per cent transmission and the corresponding photomultiplier current (I) together with the ion current (i) and the pressure recorded. The quantity (I_o-I) was proportional to the number of photons absorbed and the ion current to the number of ions formed in the ionization chamber. The photoionization efficiency defined as the number of ions formed per 100 photons absorbed is given by Ai ($I-I_o$) where A is the apparatus constant and is independent of wavelength. The pressure measurement is not required for the efficiency but is used to give the

absorption coefficient and hence the absorption cross section and photoionization cross section if required. If the photoionization cross section plotted on a semi-log scale, ionization potentials can be determined. By this method (15, 16) very accurate values have been obtained for the ionization potentials of a large number of molecules.

Another accurate method reported by Vilesove et al for measuring the kinetic energy distribution of photo-electrons during the photoionization process of aromatic amines (58) and some methyl derivative of benzene (59 and 60) by the retarding potential method in the energy range (10.5 - 11.25 e.v.) only.

In 1962 Turner and Al-Jobory (61) reported another general method for the determination of all ionization potentials of a molecule below 21.2 e.v. by photoelectron energy measurement. This method is different from the other methods in its simplicity. It does not necessitate using a monochromator, but uses the helium resonance line 584.33A^{o} (21.2 e.v.) of an undispersed radiation of a low pressure discharge tube. The ionization chamber here is different. It consists of two cylindircal grids. The axis of this assembly is made co-linear with the light source photon beam through 0.5 mm glass capillary tube. The measurement of the kinetic energy of the photo-electron is made by the retarding potential field method.

The results in this method are not affected by auto-ionization. It records true ionization potentials, while the other photoionization and electronimpact techniques fail to distinguish between ionization limits and autoionization in the strong resonance transition of inner orbital electrons. It can also show whether those electrons were bonding or none. Accurate data about 150 molecules are made available by this technique (54 - 57).

The first method mentioned above, however, has some limitations, since no information was given about the species of the ions which consist the ion current. Are they ions of similar masses or different?

It requires a mass spectrometric analysis to obtain a complete interpretation of the results and evaluate the abundance of different ions. Because of the lack of mass analysis one has to be sure that the sample being studied is very free from impurities of low ionization potential. These difficulties can be overcome by combining the photoionization chamber with a mass spectrometer.

The application of mass analysis to study photoionization process is relatively new field of research, but it was described for the first time by Terenin and Popove (61) in 1932. They were able to demonstrate that thallium iodide, bromide and chloride are ionized by

radiation transmitted by a quartz monochromator. By using a simple magnetic mass spectrometer they showed that the ions are Tl^+ and I^- or Br^- for the iodide or bromide. The ion current reached a peak value near 2125 A^o for TlI and 2000 A^o for TlBr. The cross-section for photoionization was of the order of $10^{-17} cm^2$. Recently Lossing and Tanaka (62) described some preliminary work in the use of a photoionization source for mass spectrometry. They were able to show that in the case of certain hydrocarbons the mass spectra produced were much simpler than was the case of the corresponding compounds under the influence of electron impact.

They also discussed briefly the possible applications of the technique to the measurement of ionization and appearance potential. They used in their experiment the undispersed radiation from a krypton discharge light source.

Shortly after this work and nearly simultaneously a number of investigators (63 and 64) have reported on the mass spectrometric analysis of fragmentions produced by photoionization using undispersed radiation (light source). Inghram (65) and his group were able successfully to use the combination of a vacuum monochromator and a mass spectrometer to study in detail the formation of ions by photoionization. In these experiments the residual gases in the monochromator were isolated from

those to be studied by photoionization in the mass spectrometer by using a lithium fluoride window which cut off all radiation below 1050 A^{o}. Their experiments were carried out by a Seya-Namioka type monochromator and the ionization potentials of a variety of organic compounds were determined. At the same time Vilesov et al (66) reported on similar mass spectrometric investigations in general of photoionization and photodissociation of various amines such as ammonia, hydrazine, benzylamine, and aniline, and studied (74) the relation between spectra and photoionization efficiency of benzene, toluene, P-xylene, aniline, methylamine, dimethyl aniline and benzylamine. They identified metastable and other type peaks in the spectra of the compounds. These peaks were related to a secondary process. Later (75) they studied hydrazine, methyl hydrazine, 1, 1-dimethyl hydrazine, 1, 1-diethyl hydrazine, 1-methyl 1-n-butyl hydrazine and 1, 1-di-n-butyl hydrazine with the same instrument and technique. Their experiments were carried out by a Seya-Namiska type monochromator combined to a Russian commercial mass spectrometer model MI-1305, but they also were not able to use differential pumping to dispense with the lithium fluoride window which limited the energy range to 11.2 e.v. only. Weissler et al (67) reported their advanced investigations on the photoionization of Ar; Ne; He; N_2; O_2; CO; NO; CO_2; N_2O; and NO_2

with the same experimental techniques of Inghram et al (65) except the light source used had more intense emission lines in the region 400 - 1350 A°; secondly no lithium fluoride window was used between the exit slit and ionization chamber but differential pumping. They obtained a great amount of valuable experimental data on ionization potentials and ionization cross sections and on dissociation and ionization process of diatomic molecules.

Momigny (76) examined the structure occurring in photoionization efficiency curves of cis and trans-dichloro- and di-bromo-ethylenes up to 11.2 e.v. only. He interpreted regularly spaced structures in turns of vibrational progressions involving the c-c valence vibrations of the ions. Sharp peaks are correlated with strong absorption bands present above the first ionization potential and are interpreted as being due to autoionization. Very recently Diebler and Reese (77, 78) described their windowless vacuum-ultra violet monochromator which was combined to magnetic mass spectrometer, with initial observation they made on acetylene, acetylene-d_2, benzene and benzene-d_6 in the energy range (2000 - 600 A° or 6 - 21 e.v.). Then (79) with similar technique they examined H_2, HD and D_2 in the energy range (815 - 700 A or 15.2 - 17.7 e.v.).

The mass spectrometric investigations reported

before were mostly carried out to measure the photoionization efficiency, appearance and ionization potentials or to determine the ionization cross sections. But left unanswered question about the form, dissociation kinetic energy and decay of the molecular and fragmentions. The dissociation and kinetic energy of diatomic molecules is rather well understood and carefully studied (80). By contrast, the case of polyatomic molecules is not well understood. Two complications, (81) which make the polyatomic molecule more difficult are:

a. The excitation energy of molecular ions is shared among a number of different degrees of freedom. This fragmentation may not occur immediately when the dissociation threshold is reached as it does with diatomic molecules but rather may be delayed until the molecular vibrations cooperate to produce a particular dissociation.

b. The fragment ions can carry away energy in the form of vibrational oscillation, so that the excess energy need not appear as kinetic energy or as electronic excitation of the fragment.

Some detailed studies of the dissociation of organic and inorganic polyatomic ions have been made, using electron impact methods (82 - 111), charge exchange collision with slow positive ions (112 - 122); or photoionization techniques (123 - 126).

The use of photoionization has an advantage in this

type of study because the results are more precise, accurate and more easily interpreted (127) for many reasons:

a. The photoionization process is an interaction between a photon and an electron of a molecule. The products are ion and ejected electron with or without kinetic energy.

The electron impact is a process where collision is between two electrons. The products are ion, ejected electron and colliding electron. Obviously the probability for secondary processes is higher.

b. The extra thermal energy that an ion or molecule may gain in the ionization chamber is negligible if it is not zero because the process happens at room temperature. While the thermal energy of an ion in an E.I. source (which is normally 500 - 600°K) is of the order 0.05 e.v.. This energy will increase the initial energy of the ions and these will increase the error if any kinetic energy investigations are made.

c. It is very easy to obtain monoenergetic photon of bandwidth 0.001 e.v. (17), while it is very difficult to obtain electron beams which are sufficiently monoenergetic and of accurately known energy.

d. The only difficulty facing the photoionization studies lies in obtaining sufficient light intensity to produce measurable ion beams.

The earlier investigations about kinetic energy (129-138) and half-life of the transition states were also carried out by electron impact (E.I.) methods and no single case about using photoionization technique has been reported so far.

The mass spectrometers used to study photoionization processes were the conventional magnetic type mass-spectrometers. In these mass spectrometers ions having life-time of about 10^{-6} sec. are observable as metastable ions. Ions with life-time of 10^{-7} second or shorter are seen as their decomposition products and those with life-time longer than 10^{-5} second are largely collected (84, 97, 105, 106, 107).

Such a mass-spectrometer can be used to study in detail only those ions decomposing with a rate constant of the order of 10^{6} sec^{-1}. The other point needed is the experimental observation of the change in concentration of various ions present as a continuous function of time delay between ionization and acceleration. This is difficult to achieve in conventional mass spectrometers.

One would desire an instrument which could follow the ion dissociation processes as a function of time over the range of 10^{-13} seconds to about 10^{-2} seconds.

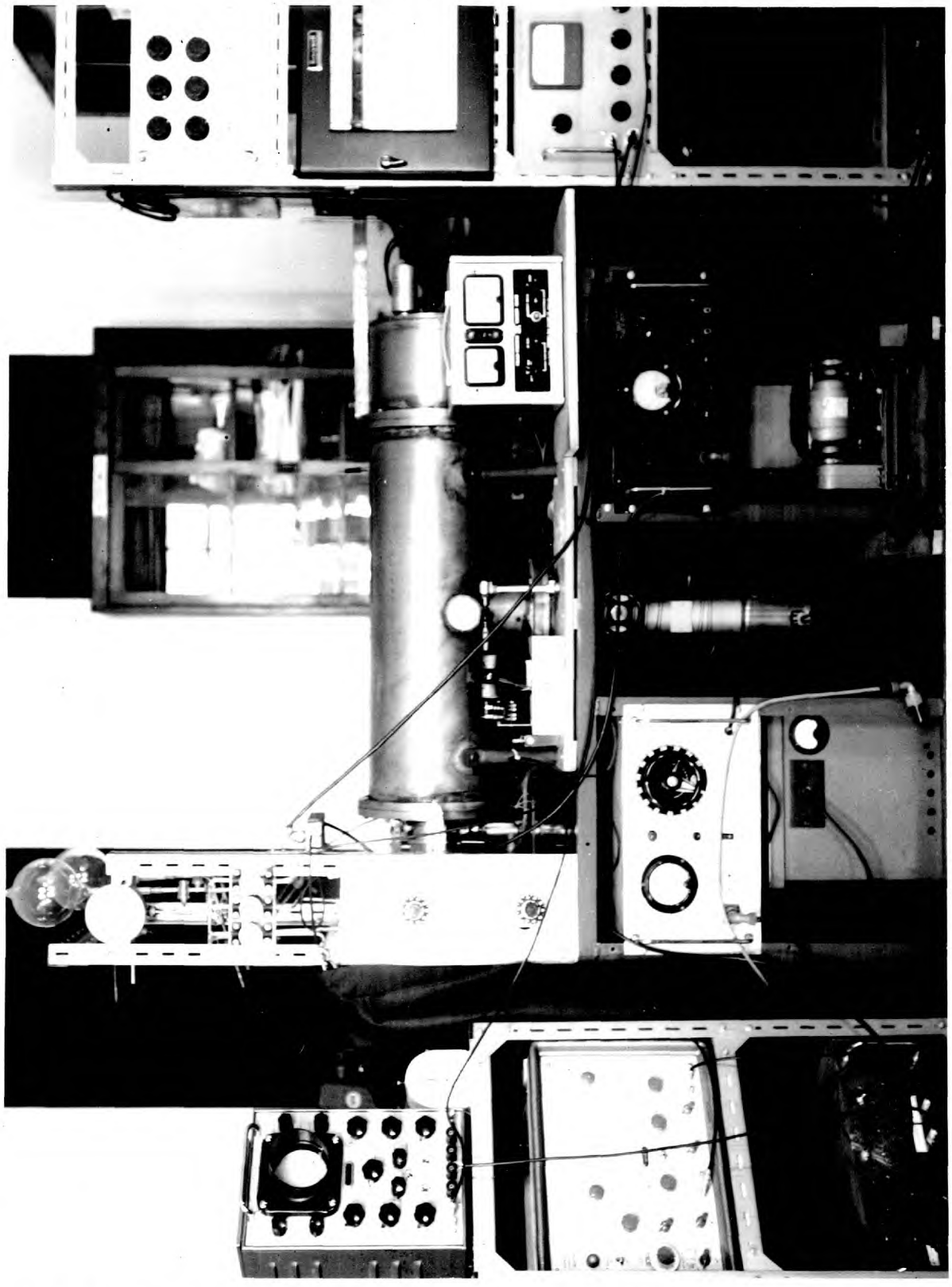
The newly developed linear pulsed time-of-flight mass spectrometers are, in theory, ideally suited to investigations over much of this range of time.

The work to be reported in this thesis is essentially based on the design and construction of a new pulsed linear time of flight mass spectrometer coupled to a normal incidence vacuum ultra-violet monochromator; to investigate the dissociation and kinetic energy of molecular and fragmentations produced in photoionization of these organic compounds: n-propane; n-butane; acetaldehyde; acetone; methyl-ethyl ketone; methyl n-butyl ketone; benzene; monobromo- and mono-iodobenzene, over the energy range of 10 - 18 e.v.

PART A

THE VACUUM ULTRAVIOLET MONOCHROMATOR

- TIME-OF-FLIGHT MASS SPECTROMETER COMBINATION



VIEW OF THE VACUUM ULTRA-VIOLET MONOCHROMATOR-TIME OF FLIGHT MASS SPECTROMETER COMBINATION

THE TIME-OF-FLIGHT MASS SPECTROMETER

Until recently, the usual method of measuring the mass-to-charge ratio (m/e) of an ion has been through observing its trajectory in an electrostatic, magnetic or a combination of the two fields.

In 1946 Stephens (139) reported the method of mass analysis by measuring the time of flight of an ion in a field free drift tube, but the first working TOF* mass spectrometer was made by Cameron and Eggers (140) in 1948. The resolution of their device (Velocitron) was very poor but their work has encouraged others (141 - 157) to investigate non magnetic TOF mass spectrometry more thoroughly.

1. Operating Principle of TOF Mass Spectrometer

A linear TOFMS is an instrument in which the mass of an ion is determined from the transit time it takes to travel a known distance through a field-free-shift-tube.

The basic elements of a TOFMS (Fig. 1) are:

---

*Hereafter the phrase 'Time-of-Flight' and 'Time-of-Flight mass spectrometer' will be abbreviated by TOF and TOFMS respectively.

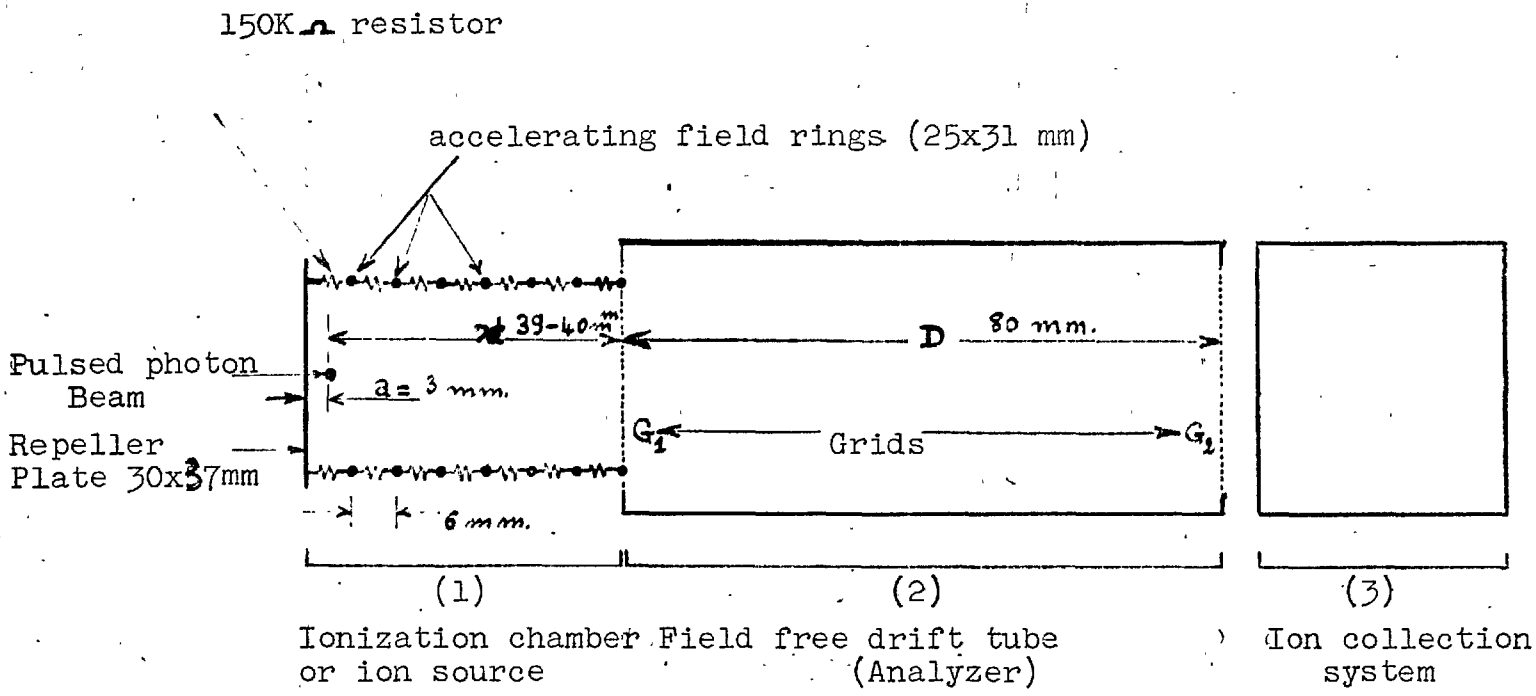


Fig. 1. Vertical cross-section of the essential parts of the linear TOF mass spectrometer

a. Ion source and accelerating region

b. Field-free drift tube

c. The detector or ion collection system.

An electron or photon beam pulse produces a number of ions of the vapor in the ion source. The ions are then accelerated through a voltage pulse of certain time-width depending on the ion source dimensions. They enter the field-free drift tube at essentially the same time with the same kinetic energy per unit charge. They then travel down the tube following a linear path with velocities inversely proportional to the square root of their mass-to-charge ratio. The pulse of ions break up into groups or bunches as soon as they enter the tube. These bunches contain ions having the same m/e and the same velocity. They arrive at the detector at different time proportional to $(m/e)^{1/2}$. The lightest bunch reaches the detector first and is followed by bunches of successively heavier mass.

As each ion bunch strikes the detector a pulse signal is produced in a pre-amplifier stage. Further electronic amplification is followed by a wide-band linear amplifier. The output signal of the amplifier is transmitted to the vertical deflection plates of an oscilloscope whose horizontal sweep is triggered by the accelerating pulse circuit. The oscilloscope display represents the mass spectrum. Each peak represents the time of arrival of each bunch

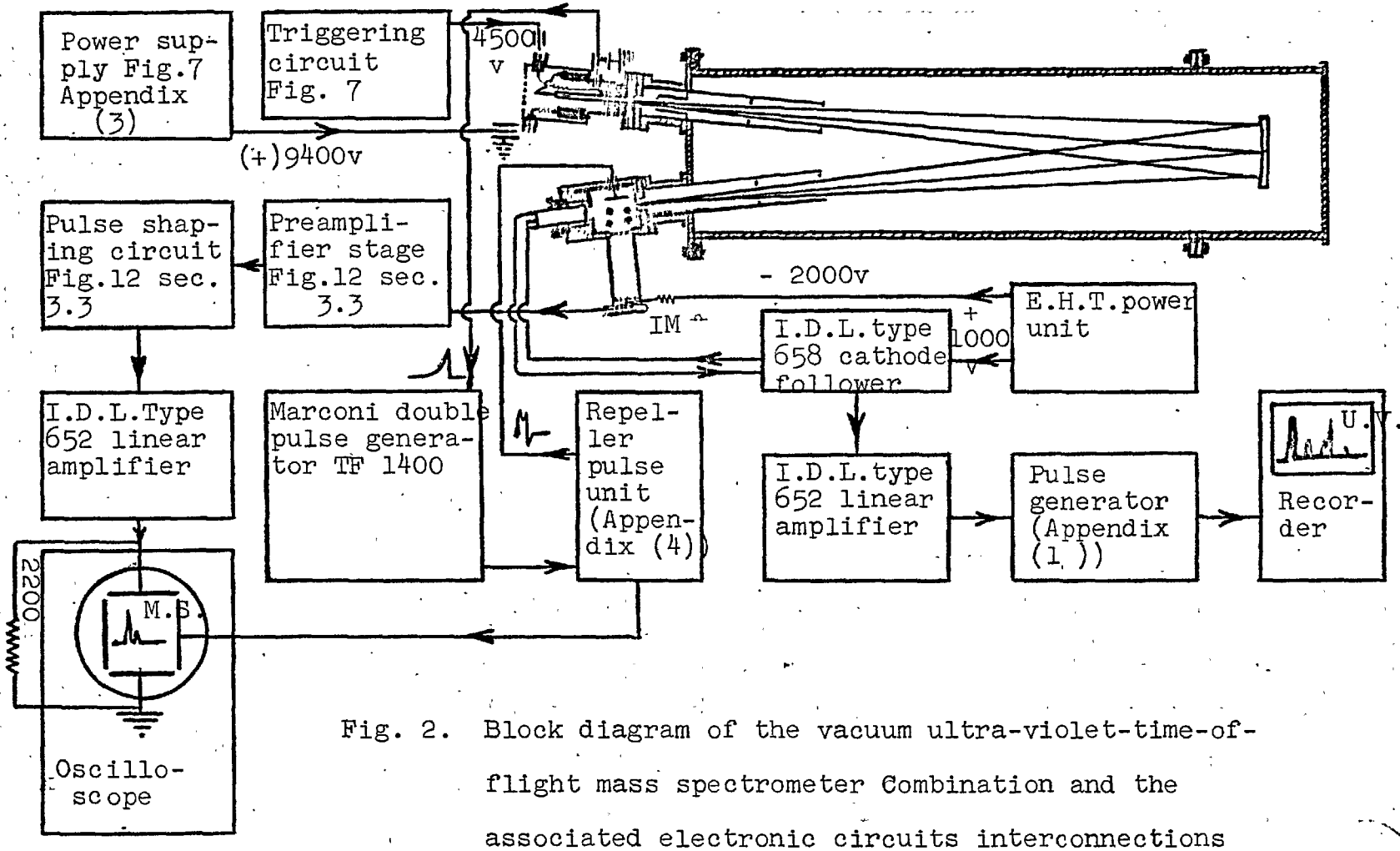


Fig. 2. Block diagram of the vacuum ultra-violet-time-of-flight mass spectrometer Combination and the associated electronic circuits interconnections

of ion. This time can be measured along the time axis. The abundance of ions is proportional to the area under the corresponding peak or approximately to the peak height.

2. Methods of Mass Analysis by TOF

Two methods for mass analysis may be applied by the TOFMS undertaken in this project:

1. The constant energy
2. The constant momentum.

Each has advantages and limitations

2.1. Constant Energy Method and Space Focusing

An ion of mass m and charge e will experience a force

$$\vec{F} = e.\vec{E} = m.\vec{\gamma} \qquad (1)$$

If an electric field of E intensity acts and lasts on it until it arrives at the first grid of the field free drift tube (Fig. 1). The particle will then travel a distance x with velocity v during time t:

$$v = \frac{dx}{dt} = \gamma t \qquad (2)$$

the distance travelled at time t is then:

$$x = \int_0^t v.dt = \frac{1}{2}\gamma t^2 \qquad (3)$$

equation (1) and (3) gives:

$$x = \frac{1}{2}\ \frac{e.E}{m}\ .\ t^2 \qquad (4)$$

the time of flight of the ion through the acceleration

region will then be:

$$t_1 = \left[\frac{m}{e} \cdot \frac{2x}{E} \right]^{1/2} \tag{5}$$

the velocity v_G of the ion when it arrives at the first grid of the drift tube is:

$$v_G = \gamma t = \left[\frac{2eEx}{m} \right]^{1/2} \tag{6}$$

the time taken by the ion to traverse the drift tube D to the detector is:

$$t_2 = \frac{D}{v_G} = \left[\frac{mD^2}{2eEx} \right]^{1/2} \tag{7}$$

the total TOF of an ion at constant energy will then be:

$$T_{TOF} = t_1 + t_2 = k\left(\frac{m}{e}\right)^{1/2} \left[\left(\frac{2x}{E}\right)^{1/2} + \left(\frac{D^2}{2ex}\right)^{1/2} \right] \tag{8}$$

where TOF is in microseconds; $\frac{m}{e}$ is the mass-to-charge ratio of the ion in a.m.u.; x is the acceleration region in centimeter (4 cm); D is the length of the drift tube in centimeter (8 cm) and E is the acceleration field in volt/cm. For Kr. m/e = 83 the TOF was 12.8 microseconds, and the acceleration field was 32 volt/cm.

The Space Focusing Condition

For optimum mass focusing (148) the time spread for similar m/e of ions in the ion bunch should be a minimum and time separation between different m/e should be maximum. This condition may be possible in a single field

system when in eq. (8) $\frac{dT}{dx} = 0$ or D = 2x i.e. the field free drift tube must be double the acceleration region length. This condition was established in the undertaken spectrometer.

2.2. Constant Momentum:

If acceleration pulse or field is ended before any ion of the bunch has passed through the field free drift tube the ions all have received the same fixed equal momentum. Since each ion in the bunch receives the same momentum we write:

$$\vec{m_1 v_1} = \vec{m_2 v_2} = \ldots\ldots\ldots \vec{m_n v_n} = \text{constant} = \vec{F}.dt$$

or in general: $mv = F.dt$ (9)

where m is the mass of the ion; v is the velocity it acquires in a field of force F at time dt.

If the voltage pulse applied to accelerate the ions has a potential V and width τ , then the momentum of an ion after the repulsion is:

$$mv = e.E.\tau \tag{10}$$

and the energy u, acquired by an ion from the pulse in electron volts is:

$$u = \frac{1}{2}\frac{m}{e}v^2 = \frac{1}{2}\left(\frac{e}{m}\right)(E.\tau)^2 \tag{11}$$

the distance travelled by the ion at the time τ is

$$d = \int_0^{\tau} v\,dt = \frac{1}{2}\gamma.\tau^2$$

or

$$d = \frac{1}{2} \frac{e.E}{m} \cdot \tau^2 \qquad (12)$$

since each ion or bunch of ions receives one pulse only during its travel through the accelerating region we write:

$$x + D = v(T_{TOF} - \tau) + d \qquad (13)$$

equations (10), (12) and (13) give the total time of flight:

$$T_{TOF} = \frac{m}{e} \frac{x+D}{E\tau} - \frac{3}{2}\tau \qquad (14)$$

$$T_{TOF} = \frac{m}{e} \cdot \frac{x(x+D)}{v\tau} - \frac{3}{2}\tau \qquad (15)$$

where T_{TOF} is in microseconds, m/e is a.m.u, x and D are in cm (x = 4 cm, D = 8 cm) τ is the accelerating pulse width in microseconds (0.3μ sec) and v is its amplitude in volts (2500v).

Replacing the instrument constants in eq. (15) gives

$$TOF = \frac{8}{125} \cdot \frac{m}{e} - 0.45 \qquad (16)$$

or

$$\frac{m}{e} = \frac{(T + 0.45)125}{8} \qquad (17)$$

Equation (14) clearly shows that the relation between TOF and m/e is linear[*]. The mass-to-charge ratio of ions was determined from equation (14) or from the experimental

---

[*]Practically, it was found linear up to m/e = 70 a.m.u. only.

calibration line shown in Figure 3.

The present mass-spectrometer can be operated by either of the methods and it can be switched from one to the other in a few seconds when required.

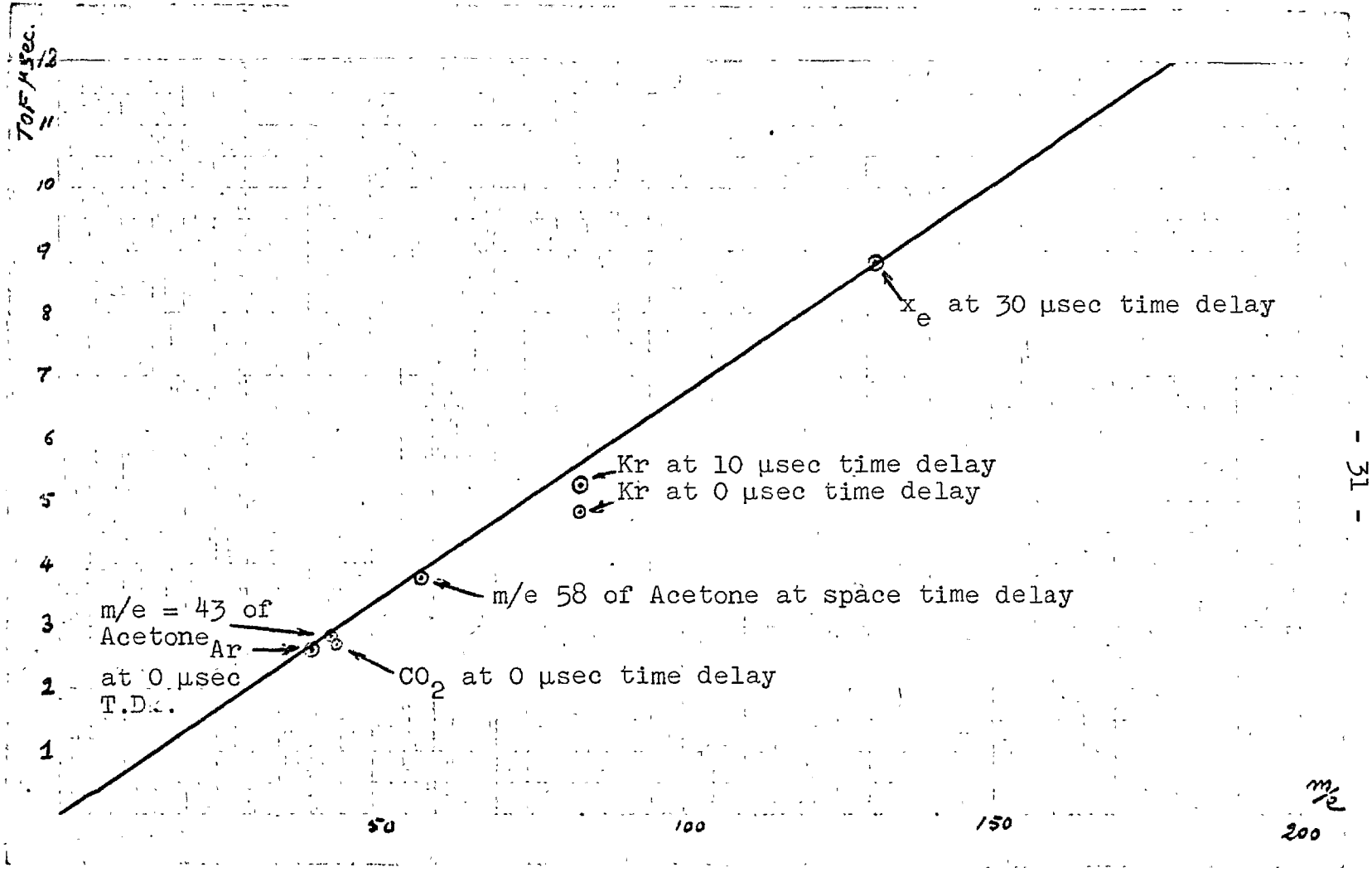


Fig. 3. m/e vs TOF calibration line

3. DESIGN AND CONSTRUCTION

3.1 Ion Source

In the present mass spectrometer a photoionization ion source was used. Ions are obtained by the interaction of photons with gas or vapour molecules. This type of source produces ions with a low kinetic energy and no multiply charged ions, and the excitation energy is uniquely determined. However, the degree of ionization is low. If high ion concentrations are desired, the energy of the light source's flashes must be increased.

The ion source here consists of two parts:

3.1.1. A photon source; a vacuum ultra-violet monochromator, capable of providing photons with energy between 4 and 18 electron volts.

3.1.2. An ionization chamber, where photons interact with vapour or gas molecules to produce ions. The ions are then accelerated into the field free drift tube.

3.1.1. Vacuum-Ultra-Violet Monochromator

3.1.1.1. Optical Design Considerations:

The important factors governing the design of vacuum spectrographs include the requirements of spectral range, dispersion and resolution, flexibility and convenience of operation.

Four types of monochromator are available*:

a) Prism spectromators - range down to 1100 A°.

b) Normal-Incidence grating monochromators - range 600 - 3000 A°.

c) Grazing incidence grating monochromators - range 30 - 600 A°.

d) Seya- Namioka grating monochromators, similar in range to (b).

In this work the normal incidence type was adopted because it has some advantages over the other types. It has nearly linear, constant dispersion down to 600 A°, more light owing to less astigmatism and is very satisfactory for the wavelength range in which molecular spectra and photoionization of all organic molecules are likely to be studied.

3.1.1.2. Scanning the Spectra:

One of the problems of the concave grating monochromator is scanning of the spectrum. Several methods have been used to solve this problem (161-173).

The most popular method was the simple rotation of the grating about its axis with no translational motion (174-177). Recently it seems fashionable to use the

---

*For a complete survey of 'Vacuum-Ultra-violet Spectroscopy' see refs 158, 159 and 160.

mounting of Seya (178); Namioka (179-180); and Greiner (181), where a similar rotation of the grating about its vertical axis through its centre occurs, but the angle between the lines connecting the grating centre to the entrance and exit slits must be 70° 30', and both slits must be placed at positions (81.8 cm from the one-meter radius grating centre), calculated from the theory. This method is very good when high focusing over a wide wavelength range is required. Obviously a certain amount of defocusing occurs, but by a proper choice of the position of the entrance and exit slits this was minimized. There are two disadvantages of this mounting: a) the astigmatism is much greater than at normal incidence, and is essentially due to the large angles of incidence and diffraction ($\alpha = \beta = 35^{\circ}$).

b) The emergent beam is likely to be partially polarized (224).

In the present monochromator to be described here, the grating has a simple rotation about its vertical axis through its centre with a fine translational motion along the axis which bisects the two slits. The grating, slits and detector (photo-multiplier) are mounted vertically on a horizontal Rowland circle, Figure 4. The two slits are fixed and the angle between them is 10° ($\alpha = \beta = 5^{\circ}$). This minimizes the astigmatism while the fine translational

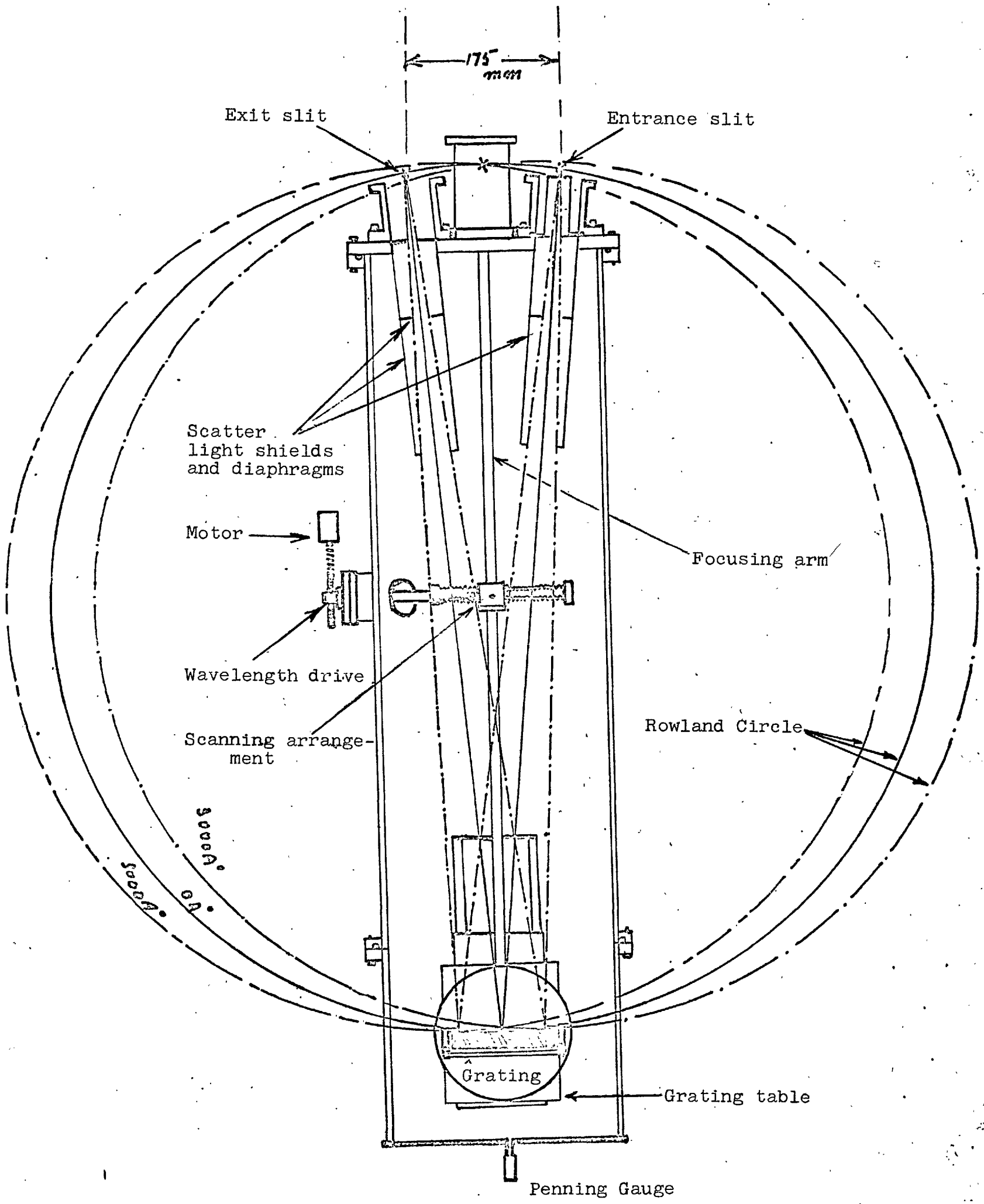


Fig. 4. Schematic diagram of the vacuum-ultra-violet monochromator and the scanning arrangement

motion keeps the image at the exit slit in good focus.

The scanning mechanism and other points of the monochromator are enclosed in a 10 mm. thick brass cylinder of 27 cm. diameter and 101 cm. long. The cylinder is mounted on a steel rack (2'6" x 4' 6" x 2'0") transportable on four rollers. It consists of two sections, the first is 80 cm. long, bolted with 8 steel bolts to an end rigid brass plate which holds the slits. This section was used for the 4-inch oil diffusion pump connection and the wavelength drive vacuum seal to the motor and gear assembly outside the cylinder. The second section of the cylinder is closed at one end which holds a Penning vacuum gauge head and is bolted also with 8 steel bolts to the main part of the cylinder. When attention to the grating or any part of the monochromator inside this cylinder is required, the second section may be slid back on three wheels along rails on the main rack.

3.1.1.3. Grating, Mount and Drive:

A. Grating: The grating is a Bausch and Lomb precision 0.99454-meter concave grating. It is a 'Tripartite', to give higher efficiency at the blazed wavelength - 1500 A^{o} in the first order - than similar concave gratings ruled with the same blaze angle ($2^{o}35'$) over the entire area but the resolving power is not as high. It has 600 lines/mm. The ruled area 56 x 96 mm. was masked with a copper disc,

having an aperture of 54 x 94 mm. The copper surface was matt blackened by a layer of copper sulphide made by immersing the disc in ammonium sulphide solution.

B. Mounting: The grating is mounted near the rear end inside the main chamber. The mount is supported about a horizontal axis upon a steel spring, kinematic mounting, so that a small rocking motion could be imparted to the grating electromagnetically at its natural resonant frequency (12 cycle per second). The electromagnet is enclosed in a little tank filled with pump oil, fitted behind the grating mount. It was powered from outside the main chamber through a metal-to-glass seal. This provision was made to allow the effect of the stray light (182) to be eliminated and to enable the monochromator to be used as a double-beams spectrometer for ultra-violet absorption studies if required.

The grating mount is placed on a brass table which is able to rotate about a vertical axis through the grating centre. The table is carried on ball bearings*. The bearings plate stands on a second plate which slides on two grooves. This arrangement allows the grating to

---

*The bearings and the internal parts of the entire monochromator were degreased thoroughly, and the moving parts were lubricated with Apiezon oil grade 'c', which has a vapour pressure of 10^{-8} mm. Hg at 20°C.

maintain the focusing condition when scanning the spectrum by the motion along the axis bisecting the slits towards or away from them.

C. Driving: The two motions of the grating (rotation and translation) are controlled simultaneously by a system of radius arms attached to the drive unit nut on the head screw, which is mounted in the middle of the main chamber. The right-hand arm is bolted to the grating table. The left-hand arm is controlled via a spring clutch by a lead screw operated from outside the vacuum. This allows for adjustment of the arms length and grating radius, hence to focus the monochromator when required. The drive nut is stopped from rotating indefinitely by two guide pins. The lead screw of the drive nut is coupled to a 3/8 inch steel shaft which passes through two rubber O-rings vacuum seal, to outside the vacuum chamber. A reversible synchro-us geared electric motor connected through a worm and wheel to the drive shaft. The motor is controlled by a reversible panel switch. It has one scanning speed only.

A revolution counter is coupled to the worm. The counter reading can be converted into Angstrom units very easily as follows:

We start from the usual grating equation:

$$n\lambda = a(\sin \alpha \pm \sin \beta) \qquad (20)$$

where α = Angle of Incidence,

β = Angle of Diffraction

a = Grating spacing = $\frac{1}{600} \times 10^{-7}$ A°

θ = Blaze angle

n = Grating order 1,2,3,....

$\gamma = \frac{\alpha+\beta}{2}$

Since the beams lie on opposite sides of the normal (Fig. 4 and 5), the smaller of the two angles is to be taken as negative:

$$n\lambda = a\ (\sin \alpha - \sin \beta) \qquad (21)$$

If the grating is rotated δ degrees then

$$\alpha = \frac{\gamma}{2} + \delta$$

$$\beta = \frac{\gamma}{2} - \delta$$

By replacing α and β in equation (21)

$$n\lambda = a[\sin(\tfrac{\gamma}{2} + \delta) - \sin(\tfrac{\gamma}{2} - \delta)]$$

or

$$n\lambda = 2a \cos \tfrac{\gamma}{2} \sin \delta$$

from Fig. 5.

$$\cos \tfrac{\gamma}{2} = 0.9962$$

or

$$n\lambda_{A^\circ} = \frac{99620}{3} \sin \delta \qquad (22)$$

The counter reading at zero order image is 7235. The number of turns of the shaft is then:

$$\frac{7235 - \text{counter reading}}{60}$$

Since 60 turns of the electric motor turns the shaft one

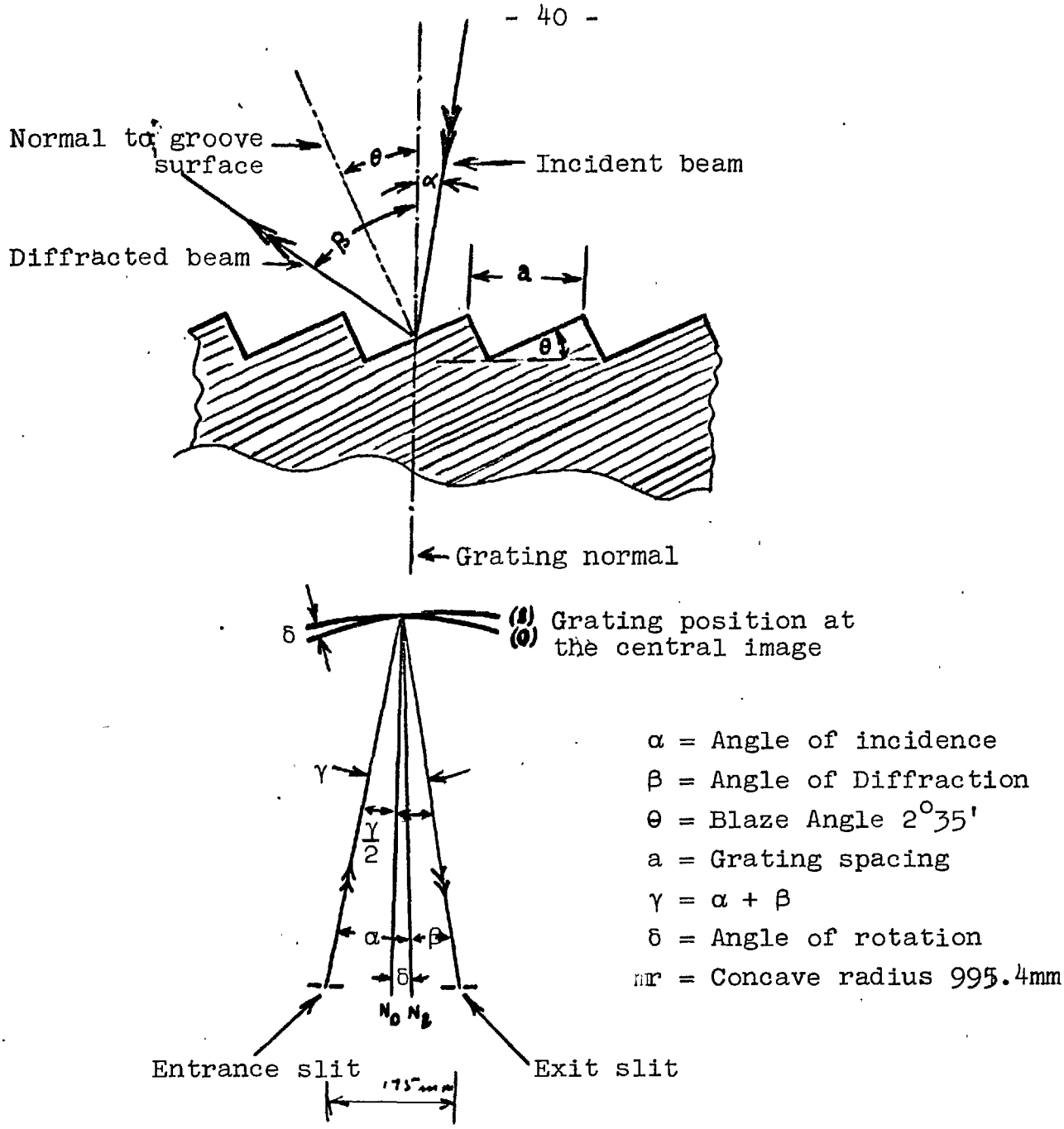


Fig. 5. Cross Sectional diagram of Diffraction Grating and angles of incidence and diffraction

turn only, i.e. move the grating arm 1 mm. For n turns of the shaft, the arm moves n millimeters and $\sin \delta \neq \tan \delta = \frac{n}{497.7}$. Replacing the value of $\sin \delta$ in equation (22) and adding 18.3 A°* equation (22) becomes

$$n\lambda^{\circ}_{A} = [\frac{99620}{3} \cdot \frac{n}{497.7}] + 18.3$$

or

$$\lambda_{A^{\circ}} = [\frac{99620}{3} \cdot \frac{n}{497.7}] + 18.3 \qquad (23)$$

for the first order.

These calculations were confirmed quite accurately by measurements on the various orders of strong lines.

Finally, it must be noted that the grating had been under use for more than three years without showing any marked falling off in intensity of the ultra-violet spectra it produced, yet the grating could not be said to possess a fresh surface, but is strong in its first and second orders.

3.1.1.4. Slits:

The slits are similarly mounted, vertically on rigid brass rings which are bolted to brass flanges placed and bolted to the rigid brass front end of the vacuum cylinder. The two slits' flanges are inclined to a point at the grating centre. The jaws are one inch long and

---

*A constant error between calculated and experimental wavelength.

made of a 1/8-inch thick stainless steel with 45° wedge towards the grating. They are of the so-called unilateral type, in which only one jaw is movable.

The two slits are controlled by one micrometer through a series of push rods and levers and can be adjusted to 0.001 mm. The jaws are sprung back against the end of the micrometer rod, when the micrometer is set back. They are adjusted and set parallel before assembling the light source and photomultiplier by focusing the central image of the grating on the entrance first, then exit slits. They are satisfactory parallel (0.01 mm.; 0.16 A° - 0.02 mm. or 3.3 A°). The slits' width or the bandwidth of the ionizing photon beam (full width at half-maximum) in the experimental work was 6.6 A°, or in the energy range covered about 0.05 electron volt.

3.1.1.5. Vacuum System:

The vacuum system consists* of:

a) Backing Pump: is a single stage gas ballast rotary pump, model 1SC 150B, capable of displacing 144 litre of air per minute at normal speed.

b) A four-inch three-stage oil vapour fractionating

---

*The vacuum products used in this project were made by Edwards High Vacuum Limited, Manor Royal, Crawley, Sussex.

diffusion pump model F403. It has a speed of 250 - 300 litre/sec. unbaffled and 150 - 170 litre/sec. at the inlet of a hand operated 4-inch isolation baffle valve type 7L4. The baffle valve mounted between the main vacuum chamber of the monochromator and the oil diffusion pump allows this to be by-passed when required.

c) Two one-inch two-stage oil vapour diffusion pumps model 102, are mounted under the slits. Each has a speed of 7 - 8 litre/sec. at the inlet of the baffle valve. These baffle valves are one-inch Speedivac Butterfly type QSB1. The oil used in these oil-diffusion pumps and for lubricating the moving parts inside the main chamber is Apiezon oil grade 'C'. It has a vapour pressure of 10^{-8}mm. at 20°C.

The vacuum connections and seals were made tight by bolts with rubber O-rings placed in polished grooves. The connections between the diffusion pumps and the baking rotary pump were made by either one or 1/2 inch copper tubing through brass union and joints and a set of 3/4 inch valve.

The grease used with the neoprene rubber O-rings was Apiezon grade 'H' (vapour pressure 10^{-9}mm. Hg at 20°C and 10^{-3}mm. Hg at 300°C) in the ionization chamber of the mass spectrometer. Apiezon grade L (vapour pressure 10^{-10}mm. Hg at 20°C) in the light source and on the O-ring

between the diffusion pump and the main chamber where a high melting grease is required. Apiezon grade 'M' (vapour pressure 10^{-7}mm. at 20°C) for those O-rings elsewhere.

The vacuum system maintained a pressure of 10^{-6} without any cold trap. When gas was flowing in the light source the vacuum in the main chamber dropped to about 5×10^{-5}mm. of Hg, in the case of a windowless light source, or to 5×10^{-6}mm. of Hg when the light source was isolated from the body of the monochromator by a one millimeter thick lithium fluoride window in front of the entrance slit.

The whole vacuum system was pumped down by the combined pumping unit, from atmospheric pressure to 1×10^{-6}mm. of Hg in 35 minutes only.

The pressure was measured by a Penning gauge type (5MF) in the main chamber above the grating, by a Piranni gauge type 6A in the ionization chamber and a similar one in the backing line and by a barometric compensated gauge type CG3 in the sampling system.

The pressure readings were displayed on a Piranni-Penning type vacuum gauge model 2A.

3.1.1.6. Light Sources:

Molecular spectroscopy in the vacuum-ultra-violet has been undertaken infrequently, partly because of the lack of satisfactory light sources. Photoelectric detection methods and high vacuum techniques have been greatly improved in recent years, good optical materials and gratings are now available commercially, but relatively few advances in light sources have been made, and a continuous search has been going on during recent years for improved light sources giving high radiation intensity needed in photo-ionization experiments. It is obviously desirable to have additional radiation sources available in order to fill the existing gaps in the spectrum.

Two new simple light sources were developed during this work:

A. Pulsed Microwave Discharge Light Source: Excitation of light sources by microwave power (183-196), has been claimed to have many advantages over other methods of excitation, notably:-

1. Absence of internal electrodes,
2. Low power consumption for a given light output,
3. High intensity,
4. Long tube life.

The discharge tube used here was a Pyrex tube of 4 cm. long and 1.4 cm. in diameter, Figure (6), inserted

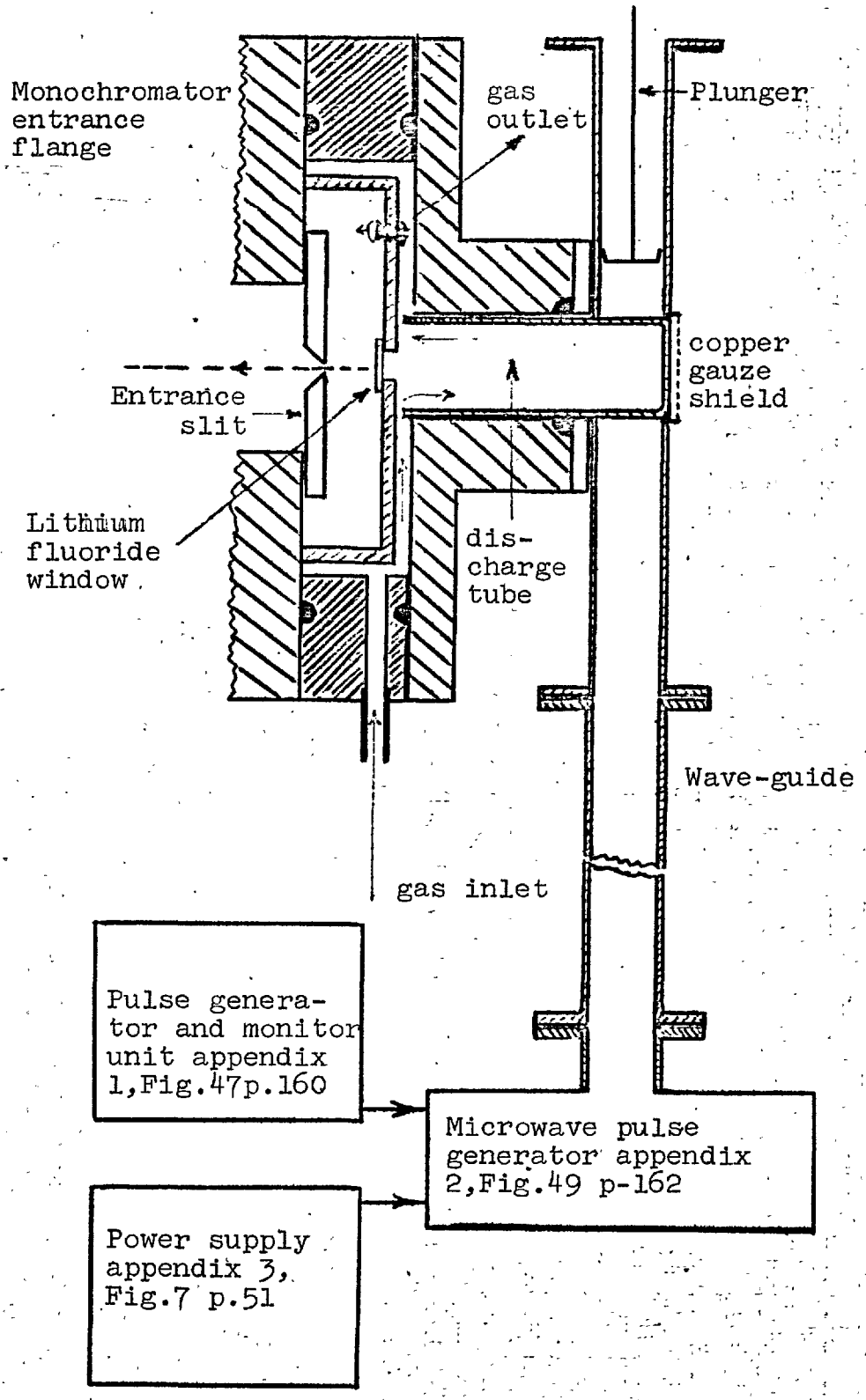


Fig. 6. Cross-sectional diagram of the microwave discharge light source.

into a 1.4 cm. in diameter hole of an x-band wave-guide (2.3 x 1 cm.), at a place of antinode of the electric field. A tuning plunger of quarter wave re-entrant edge was used to provide a very smooth adjustment by simple pushing or pulling it inside the waveguide.

The source of microwave power was a military radar transmitter using a Raytheon cavity magnetron type 725A rated 50 - 60 Kw peak at x-band frequency (9345 - 9405 m.c. or 3.21 - 3.32 cm. wavelength), with one microsecond pulse duration. Some modifications on the transmitter's circuit were made to meet our specifications. The pulser transmits about 40 K.W. peak at the same frequency and pulse duration. The transmitter was triggered by one microsecond pulses, 180 volts peak from a pulse generator and monitor unit (Appendix 1). The radiation was transmitted through one yard of flexible waveguide 2.3 x 1 cm. to the light source (Appendix 2). Between the magnetron and the light source was a Ferrite isolator, which serves to protect the magnetron from power reflected by the light source.

The carrier gas was flowing continuously through the light source. The pressure readings in the main chamber were recorded as follows:-

Ar : 2.5×10^{-5} mm. of Hg

He : 1×10^{-5} mm. of Hg

H_2 : 3×10^{-5} mm. of Hg

N_2 : 1×10^{-5} mm. of Hg

CO_2 : 1×10^{-5} mm. of Hg

As the pressure in the tube was increased, a transition from a glow filling the entire tube to a bright ring around the wall occurred. It is necessary to mention that the brightness of this light source is controlled by the position of the plunger in the waveguide and by the output of microwave radiation obtained from the power unit.

The light source when operated with the appropriate gas pressure, produces chiefly the resonance lines of the gas used. It can probably by a different mode of operation produce the molecular continuum, i.e. by increasing the gas pressure without affecting the vacuum in the main chamber, because the entrance slit was blocked by a lithium fluoride window. This window was used with this tube because the discharge needs a relatively high pressure of few mm. of Hg to strike. This window limits the useful wavelength range to longer than 1100 A° only, which is not satisfactory in the present work. The light-source, however, had several advantages over other previous microwave light sources for these reasons:

1. Simple in shape and construction,
2. No initiation by a tesla coil was required,

3. Stable over a long period of time,

4. No cooling arrangement was required, even if it was left running for a few hours continuously with full power.

B. Capacitor Discharge Flash Light Source: Many investigations of the properties of the gaseous flash discharge directed to its application as a photographic source have been reported (197 - 200). The application of the technique to atomic and molecular spectroscopy, however, was first described by Norrish and Porter in 1949 (201), when they applied it to studies in photolysis. Since that early experiment the technique of flash discharge has been used extensively in chemical and physical research to study the spectra of short-lived species (201 - 203). However, until quite recently (204 - 207) flash discharge studies have not been extended to the vacuum-ultra-violet region shorter than 1600 A^{o}.

A simple new low repetition frequency flash light source has been developed, which exhibits some of the desirable properties of a light source, such as stability and intensity in the wavelenth range* 685 - 1172 A^{o}.

*The characteristic of this light source in the wavelength range longer than 1172 A^{o} has not been studied since the grating exhibits strong lines of the second order overlapped with those of the first order. A lithium fluoride window is necessary to cut off the radiations of orders other than the first.

The light source tube was constructed, Figure (7), of a Pyrex glass tube, 15 cm. long and 1.4 cm. in diameter. The tube contains one electrode only and a capillary glass section of 10 cm. long and 2 mm. bore in which the discharge was produced.

The power dissipated was 0.18 joule per flash produced by a series of mild condensed discharge from a bank of five capacitors - of the television type rated at 20 k.v., 0.001 microfarad - connected around the discharge tube, in parallel, to have a total capacitance of 0.005 microfarad. The capacitors were charged to 8600 volts positive through eight current limiting resistors of 800 KΩ total resistance. The connection wire to the tube was made as short as possible, but no attempt was made to reduce the self-inductance of the discharge circuit to absolute minimum. To trigger the discharge, the gas in the capillary tube was ionized slightly by a 5000 volts provided by a simple circuit shown in Figure (7), through a 10 KΩ, 3 watts ballast resistor to a secondary ring electrode placed around the end of the capillary tube section, against the outer tube. The tube was about 8 mm. distant from the entrance slit and separated by two diaphragms which protect the slit from sputtering or clogging by solid materials torn from the electrode or glass wall by the discharge, which was a problem with some light source

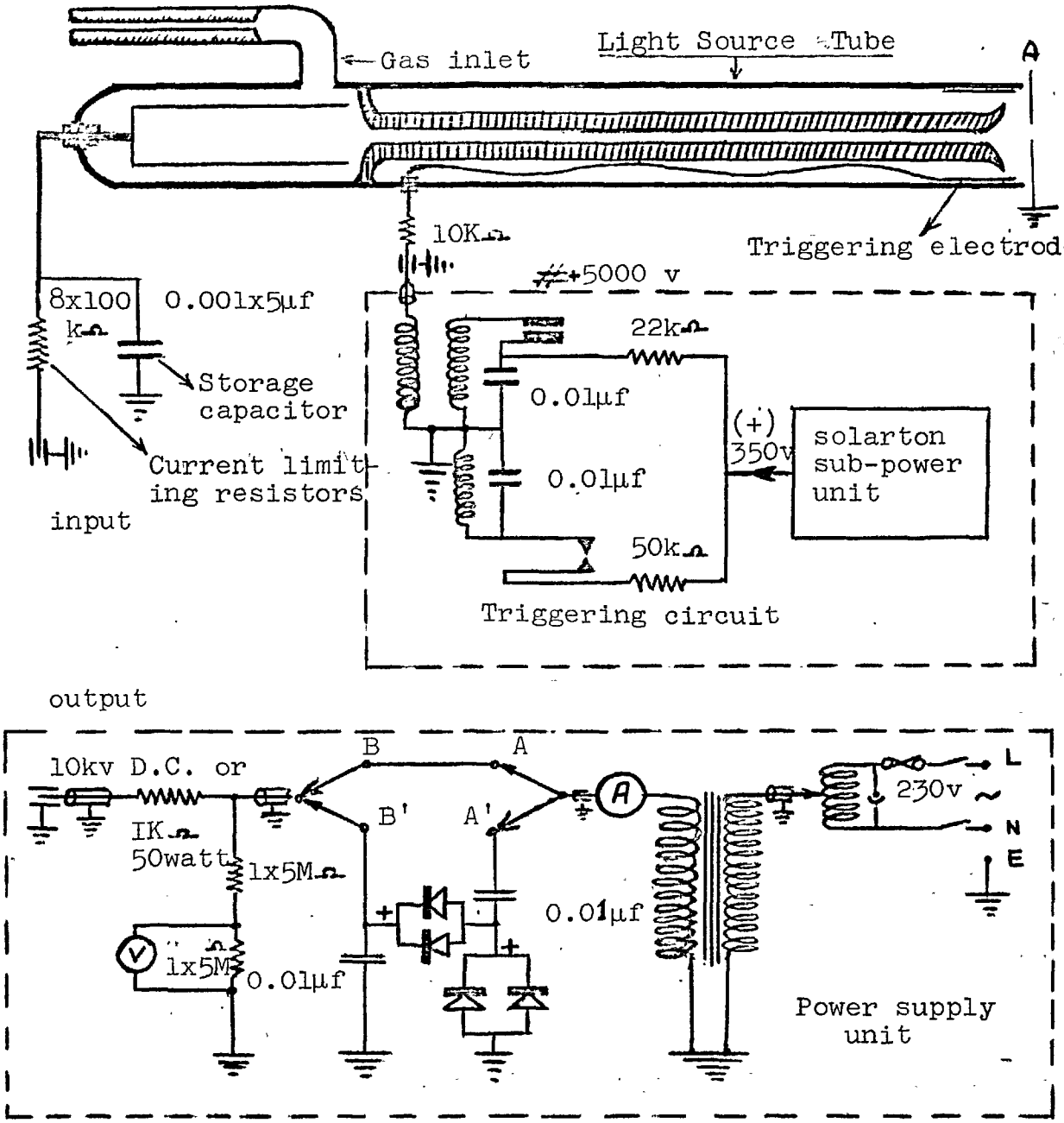


Fig. 7. Cross section diagram of the capacitor flash light source showing associated power supply and triggering units

used by other investigators (208).

The repetition frequency of the triggering pulse was about 16 - 18 pulses per second and the half-width of the light flash was about 2 - 2.5 microseconds.

The carrier gas was introduced to the tube through 10 - 12 cm. long of 0.5 mm. bore capillary tube. Using this section of capillary tubing had two advantages:-

a) To prevent the discharge between the cathode and the metal of the gas valve on the gas line,

b) To limit the discharge electrical noise from spreading outside the shielding enclosure.

The rate of the gas flow was adjusted by a vernier control needle valve.

The differential pumping system and the slit width used permitted the discharge to be operated with the following values of residual gas pressure in the main chamber:

Ar : 7.5×10^{-5} mm. of Hg

N_2 : 6.5×10^{-5} mm. of Hg

O_2 : 5.5×10^{-5} mm. of Hg

CO_2 : 4.5×10^{-5} mm. of Hg

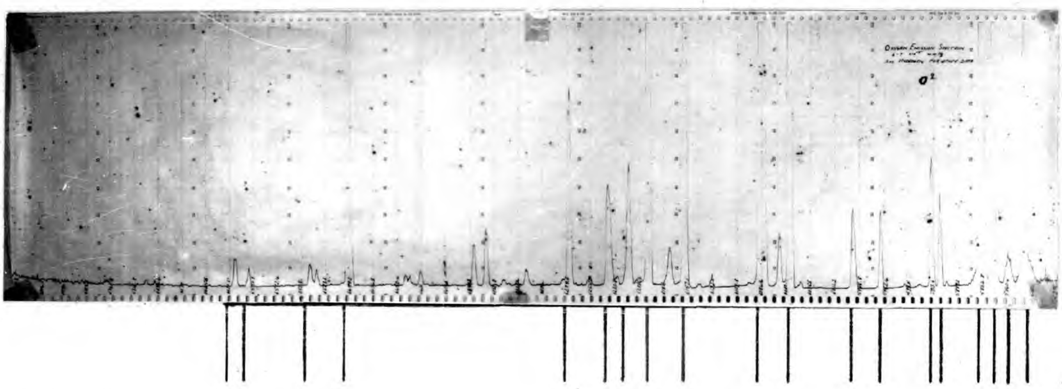
The discharge has been found highly stable at a particular pressure and voltage. It ran freely (i.e. without triggering) if the gas pressure changed above the limit mentioned earlier, and stopped completely if the pressure was lower. Within these limits it was very

steady and reproducible over a long period of time without cooling. The reproducibility might be improved by replacing the mechanical relay (spark gap) in the triggering circuit by an electronic switch or by using an ignitron (thyratron circuit) (225).

The present light-source has been operated for over 500 hours without trouble, except for occasional failure of the present type of capacitors when used for more than 25 minutes continuously.

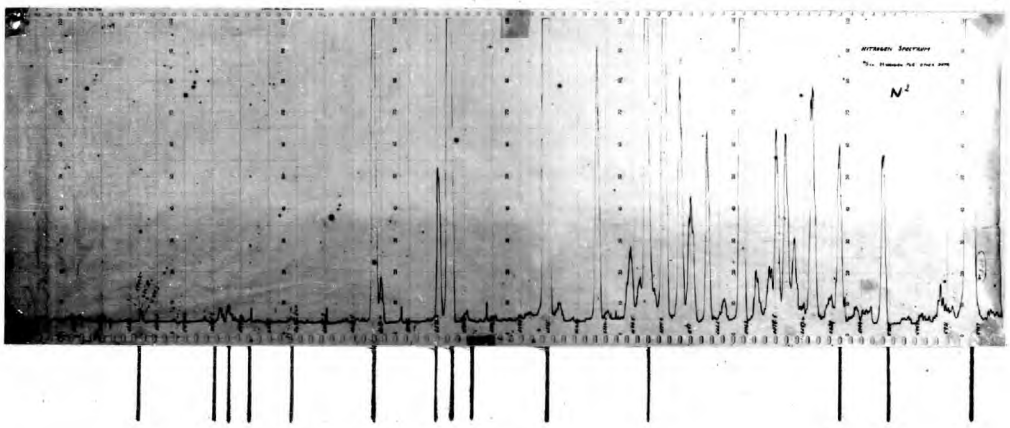
The emission spectra of six gases, Hydrogen, Helium, Argon, Oxygen, Nitrogen and Carbon Dioxide, were obtained. Oxygen and Nitrogen spectra are shown in Figures (8) and (9). It is shown that towards shorter wavelengths the resonance lines occurred further apart and were less intensive. This decrease in intensity probably caused by the discharge, by grating surface reflectance loss, or by the non-linearity of sodium salicylate in this region of wavelength. The lines towards the long wavelengths -some of them are not shown in these photographs - were very strong because the grating blaze near 1500 A^{o} in the first order and 750 A^{o} in the second order. Thus most of the spectral region from 685 A^{o}, 18 e.v. to 1172 A^{o}, 10.57 e.v., can be filled by the proper choice of gas.

These strong emission lines (Table 1) were used as a source of photons of different energies, and are the



Spectral order	1 1	1 1.	1 11 1 1	1 1	2 2	11 1122
Wavelength in A°	712.6 718.5	796.6 835.3	1217.6		707.3 718.4	796.6 802.2
Energy in Electron volts	17.39 17.25	15.56 14.84	10.18		17.52 17.25	15.57 15.45

Fig. 8. A photograph of the oxygen emission spectrum produced by the capacitor discharge flash light source. The spectrum was recorded by a photomultiplier sensitized with a layer of sodium saligylate (sec. 3.1.1.7).



Spectral order	1		III	1		1		III	1	1		2	1	2
Wavelength in A°	685.5	775.1	775.9	791	837.1	916.7	989.8	991.8	1005.1	1185.7	1177.7	685.8		765.1
Energy in Electron volts	18.07	16.2	15.97		14.84	13.53	12.52	12.50	12.39	11.42	10.52	18.07		16.2

Fig. 9. A photograph of the nitrogen emission spectrum of nitrogen recorded in the same conditions as mentioned already in Fig. 8.

TABLE 1

The Strong Emission Lines of Three Gases as a Source of Energy

Gas	First Order		Second Order	
	Wavelength A^{o}	Energy e.v.	Wavelength A^{o}	Energy e.v.
Nitrogen	685.8	18.07	685.8	18.07
	765.1	16.2	765	16.2
	775.9	15.97	771.5	16.07
	837.1	14.81		
	916.7	13.53		
	955.8	12.97		
	991.5	12.5		
	1000.5	12.39		
	1085.7	11.42		
Oxygen	712.6	17.39	707.3	17.52
	718.48	17.25	718.48	17.25
	796.6	15.56	796.66	15.56
	835.29	14.84	802.2	15.45
			835.3	14.84
			919.7	13.47
Carbon-Dioxide	1172.5	10.57		
	835.29	14.84		

only lines which can be used in photoionization and dissociation studies with the present energy of the light output - 0.18 joule per flash. The intensity of many other weak lines present may be increased if the power dissipated were increased by increasing the energy storage capacitance to an optimum value.

3.1.1.7. Detector

The ultra-violet radiation detector was a low dark current 13-stage E.M.I. photomultiplier tube type 6256B. The end window of this type is of fused quartz and possesses a one-centimeter diameter photocathode surface.

The tube was mounted end-on to the exit beam against a rubber O-ring held against the wall surrounding the tube aperture. The tube is clamped around the body vacuum tight with another rubber O-ring and threaded brass ring. It was completely shielded by a thick copper cylinder with a light tight lid. The shield contained the dynodes resistor chain and is shown in Figure (10). The output voltage pulse was taken through the cathode follower (I.D.L. type 658), to the input of a wide band linear amplifier (I.D.L. type 652), then to the reference channel of the pulse peaks height monitor (Appendix 1), the output of which was recorded.

A fluorescent layer of sodium salicylate (209), with a thickness of one milligram per cm^2 (210), deposited

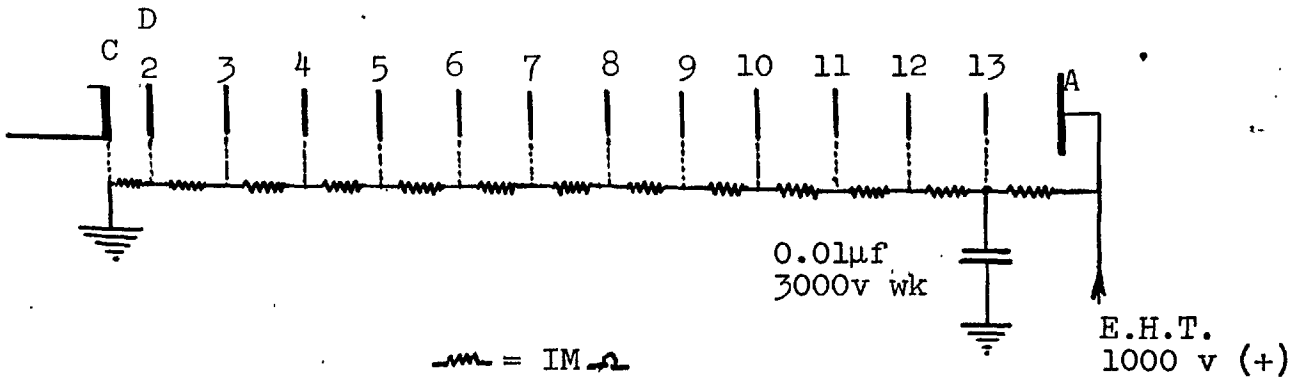


Fig. 10: The base (B 15B) connection of photomultiplier type 6256B.

on a microscope slide of 0.8 mm. thick was placed in contact with the tube window. The layer was made by dissolving the compound in methy alcohol, then dropping the solution on the glass slide surface and drying it by a gentle hot air stream from an air blower. This method was found very convenient to coat the glass surface with an even fine crystal layer. Other methods which have been used to prepare this coating are found in references 211 and 212.

The quantum efficiency of sodium salicylate has been measured by several investigators, (165 and 211-222), and was found to be linear in response and constant with wavelength in the range of excitation from 800 A^{o} to 3500 A^{o} with an indication of a 10% decrease at 800 A^{o} and about 25%/o at 584 A^{o}.

3.1.1.8. Stray Light:

Stray light is alway present in a monochromator and can lead to noticeable errors in spectrometric measurements. Care was taken to reduce as far as possible the level of the stray light reaching the exit slit. This was achieved by installing a set of copper diaphragms, to define the light beam between the slits and grating. This system of diaphragms was held in a tube placed behind each slit (Figure 4). The surfaces of these devices were

matt blackened by a layer of copper suphide to decrease surface multi-reflection.

After many experiments it was noticed that the stray light level was quite low, if not negligible, and had no serious effect on the wavelength region 600 - 1100 A^{o} but it increases below 400 A^{o}. Most of this residual stray radiation in this region undoubtedly arises from the grating surface itself and has to be tolerated, though the grating rocking arrangement (3.1.1.3. B) provides a means to discriminate against it, since only the diffracted image is focused on the exit slit.

3.1.2. Ionization Chamber

The ionization chamber was a small brass chamber, Figure (11), placed directly behind the exit slit of the u.v. monochromator. It contained:

a) The ion repeller plate, a 30 x 37 mm. nickel sheet soldered vertically to the terminal of a metal-ceramic feed-through close to the radiation beam. The other end of the feed-through was connected through a coaxial socket and plug to the output of the voltage pulse generator. This pulse generator applied pulses of 2500 volt and 0.3 microseconds duration.

b) Seven rectangular 25 x 31 mm. copper rings soldered at one end to the repeller plate and supported from the other end by the drift tube. Those rings were spaced at

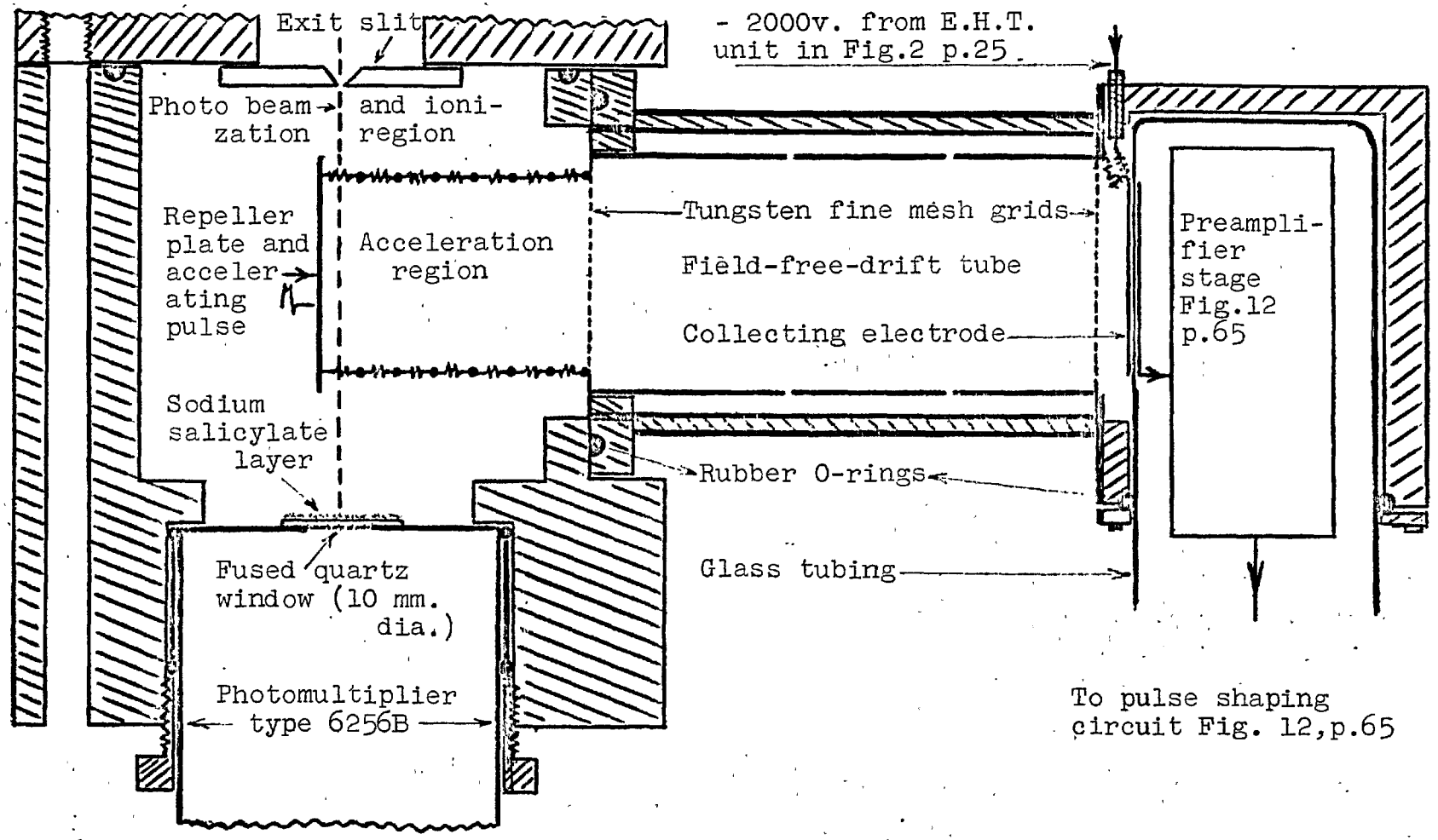


Fig. 11. Horizontal Cross-Section diagram of the ionization chamber, accelerating system, drift tube and ion collection system

6 mm. intervals. Each ring joints to the next by two resistors, 300 KΩ, and the total resistance between the plate and the ground is 500 KΩ. The paint of these resistors was completely removed by solvent to prevent contamination of the sample vapour.

The u.v. radiation beam passed 3 - 4 mm. from the repeller plate to impinge on the centre of the photomultiplier window. The interaction between the radiation and gas or vapour molecules occurred in this chamber along the radiation beam. Simultaneously, or after a time-delay, a voltage pulse repelled the ions and accelerated them towards the drift tube.

3.2. Field-Free-Drift Tube

The 'field free drift tube' was a cylindrical copper tube, 8 cm. long and 4 cm. in diameter. One tungsten fine mesh grid was soft soldered to each end of the tube to prevent any electric penetration or interference from outside, and to define a field free region.

Since the action of the drift tube depends on velocity only and not on the mass or charge of the ion after it has entered the drift tube, this tube makes the T.U.F.M.S. a uniquely suitable instrument for studying the kinetics of the processes that change the mass and charge such as charge transfer, ion dissociation and similar processes.

3.3. Ion Collection and Signal Display

Two aluminium foils 20 x 30 mm. stuck opposite one another outside and inside a 1.5 inches diameter Pyrex glass tube formed a collecting electrode and a capacitance 23.5 micromicrofarad coupling to the preamplifier grid, Figures (11) and (12). When charged (to -2k.v through an isolating resistance 1 mΩ), the positive signal created by the arrival of a group or bunch of positive ions, was further amplified by the loss of secondary electrons from the aluminium surface. A gain of about 5 fold was achieved for ions in the mass range 15 - 100 a.m.u. It is estimated that a pulse of 6×10^3 ions* could be detected by this detector.

The signal so obtained was amplified by the low noise preamplifier (valve type EC1000 Mullard) and shaped (transistor type 2G414), Figure (12). After further amplification in a wideband linear amplifier (I.D.L. type 652) set at:

Attenuation 8 db

Time constant a) Rise time 0.03 μ sec.

b) Fall time 100 μ sec.

---

*From the equation $Q = C.V. = 23.5 \times 10^{-12} \times 40 \times 10^{-6}$

$= 9.4 \times 10^{-16}$ Coulomb

and the ionic charge is 1.6×10^{-20} e.m.u.

i.e. Number of ions $= \frac{9.4 \times 10^{-17}}{1.6 \times 10^{-20}} = 6 \times 10^3$ ions per pulse

The signals displayed on an oscilloscope (Solarton type CD 513.2), whose x-sweep was triggered by the accelerating pulse generator (Appendix 4).

The traces obtained on the oscilloscope's screen were photographed and up to seven traces were superimposed on the same frame. Measurements were made directly from those photographs.

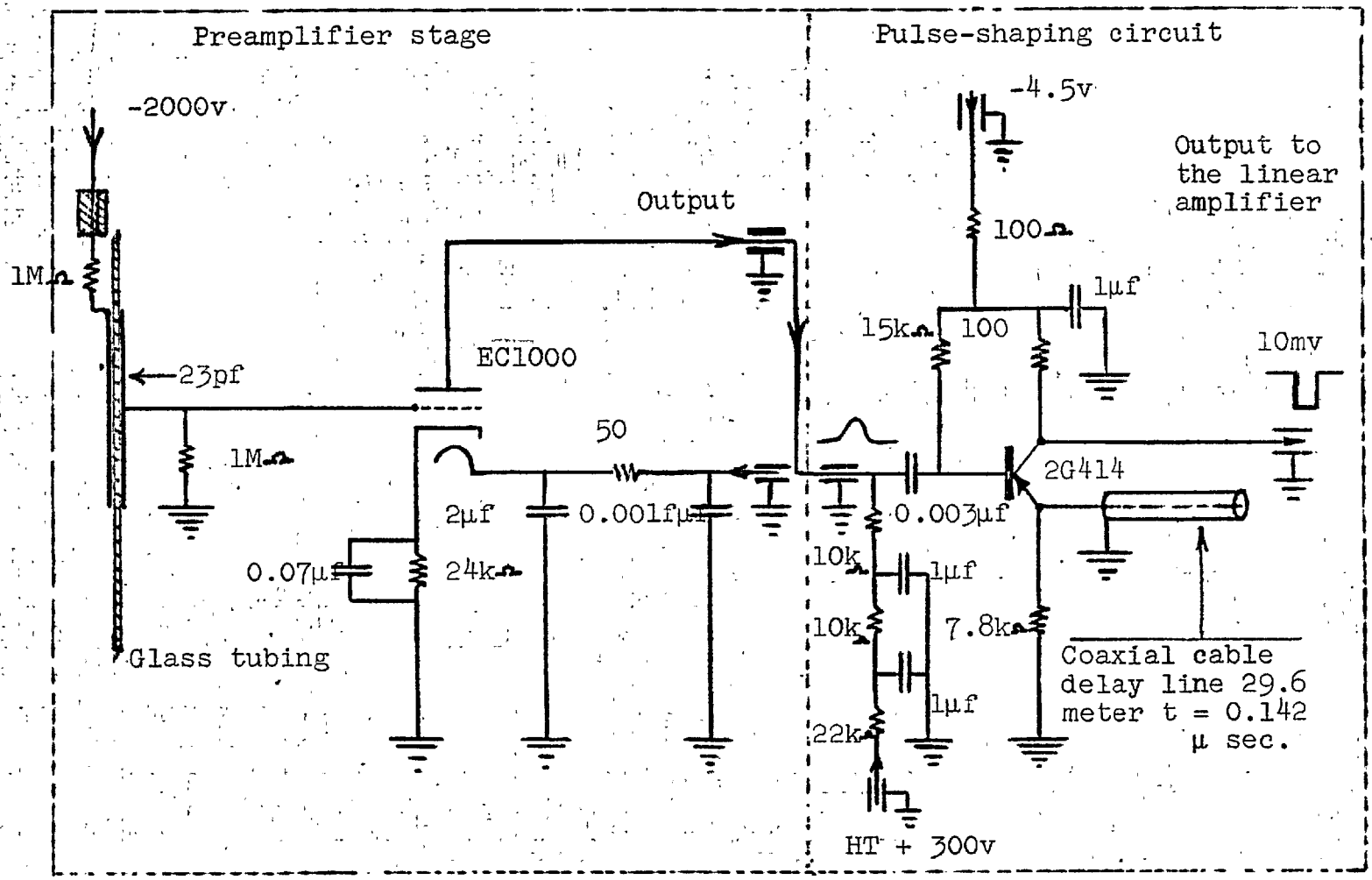


Fig. 12. Circuit diagram of the preamplifier and pulse shaping circuits

4. Mass Resolving Power, Limitations in Performance and Advantages

The present mass spectrometer can accelerate ions with constant energy or with constant momentum.

The resolution was found to be higher when the instrument operated with constant momentum. Theoretically the resolution in the case of constant momentum is double that of constant energy. That is clear from the following equations:

At constant energy, from equation (8) we have:

$$\frac{M}{\Delta M} = \frac{T}{2\Delta T} \tag{18}$$

and

at constant momentum, from equation (14) we have:

$$\frac{M}{\Delta M} = \frac{T}{\Delta T} \tag{19}$$

Practically, the resolution was not high - the instrument was unable to separate ions of masses with difference less than 3 - 4 a.m.u. This was satisfactory to identify the carbon content of any peak in the mass spectrum by measuring directly the time of flight or by comparing the peaks with standard ones of known masses. Resolution has been sacrificed by shortening the length of the drift tube (8 cm.) to shorten the time of flight, i.e. to enable the investigator to look at the fragmentation and dissociation products after very short time -

a few microseconds only - because these product may undertake further dissociation if they have to stay a longer time before detection. However, poor resolving power was one of two limitations of this spectrometer and is still the main disadvantage of T-O-F mass spectrometers, if compared with the conventional magnetic deflection mass spectrometers.

The other limitation was the mass range. The spectrometer was used with constant energy for identifying masses up to m/e = 204* a.m.u. Though no wide peaks were noticed when ions were accelerated with constant energy, peaks of masses heavier than m/e = 70 a.m.u. were unusually wide and their abundance decreased as the mass increased, until they vanished completely beyond m/e = 130 a.m.u.** A short time delay was found useful to refocus the ions slightly.

These factors were probably affected - to a limit -

---

*Iodobenzene, no higher molecular weight compounds were examined.

**When ions were accelerated with constant momentum.

the peaks' broadening - owing to time spreading of the ions bunch or pulse - and the decrease in abundance of ions, owing to scattering - towards the heavy mass side of the spectrum.

a) Thermal velocities. The most important factor of these is the thermal energy distribution as the ions leave the ionization region.

About 1°/o of the ions have energies greater than 6.5 times the most probable energy (223). At room temperature the most probable thermal energy is about 1/30 e.v. Therefore 1 per cent of the ions will have energies above

$$\frac{1}{30} \times 6.5 = 0.216 \text{ e.v.} \qquad (20)$$

Since this may be in either the positive or negative ( ) direction, the voltage spread may be considered to be

$$2 \times 0.216 = 0.432 \text{ e.v.}$$

Also since these velocities may be in any direction, a proportion of these ions will have significant components of thermal velocity perpendicular or in the axis of the ion beam (Z). The perpendicular components (x,y) will cause loss from the beam and the other (Z) will cause the time spreading, i.e. widening the individual ion peaks, and thereby losing resolution.

b) Irregularities in the accelerating field caused by irregularities in the ring shape, dimension or spacing can give the ions transverse velocity components cause

the spreading ultimate loss. This will result in general reduction in resolving power irrespective of mass.

c) Surface potential variations: This may cause scattering by unequal retardation to different ion trajectories.

d) Initial energy variations: The variations in initial energy - if any - which occur in the ionization chamber will cause the time spreading of the ion bunch.

e) Limited bandwidth: The ion signal amplifier needs a wide bandwidth and the present detector may not fulfil this condition, but because the high mass peak broadening was noticed only when the ions are accelerated with constant momentum, it follows that there is no limitation here due to insufficient amplifier bandwidth. The peak broadening was thus due to pulsed acceleration, and might be overcome if the voltage and width of the acceleration pulse were made variable, then optimum values to match the depth of the acceleration region may be selected.

The major advantages of the instrument as a TOF mass spectrometer are:

1. A unique advantage is the speed with which a spectrum can be obtained conveniently. A complete spectrum - depending on the light source frequency - can be obtained every few microseconds. Thus one can study how the relative abundance of different ions varies when the ionization

region conditions change rapidly - such as by introducing a time delay intervals between ionization and ion acceleration.

2. The entire mass spectrum can be displayed for each accelerating pulse. Thus one can measure relative intensities of the peaks more accurately.

3. The accuracy here depends on electronic circuits rather than on extremely accurate mechanical specifications.

4. As a reliable detector for the ultra-violet radiation: when the ionization chamber, drift tube, and ion detector are combined with any vacuum u.v. monochromator, they can be used for qualitative determination of u.v. radiation. There is a pressing need to make further development of u.v. detectors which are both sensitive over a wide range of the spectrum and stable, because most available detectors have either limited range or no wavelength linearity. Although photomultipliers coated with sodium salicylate have been found to yield reproducible data by several investigators (40, 209, and 226-229) they are much more sensitive to visible and near u.v. than to shorter wavelength radiation. Photographic plates have the same disadvantages, and moreover, they appear to be less reliable for quantitative spectrophotometry.

Detectors which are sensitive only to vacuum u.v. radiation will minimize the difficult problem of scattered

or stray light, when a photomultiplier or photographic plate is in use.

It should be emphasized that the detection process here is triggered by photoionization, and in fact the long wavelength limit of sensitivity of this detector is set by the ionization potential of the gas molecule used

The efficiencypeak height of the signal of this detector apparently depends on the pressure of the gas used, but relatively low pressures (3 - 5 microns of acetone) would be more desirable for a sensitive detector. As the pressure increases the peak height increases and then decreases after passing a maximum at about 30 microns. The decrease was probably due to collision and loss of ions. The efficiency was also found to be increased with the number of photons.

When the capacitor discharge flash light source was used, no saturation - in the limit of applied voltage - in the ion current due to high incident intensity photons was noticed. The efficiency also showed a dependence with respect to the frequency of incident photons. This dependence was expected because the photoionization efficiency of a gas is known to vary with the wavelength.

However, since no quantitative studies were carried out to investigate the characteristics of this type of detector for the u.v. radiation, it would be necessary

to make a further development and exploratory work on this subject before any comment.

5. Identifying the overlapping orders of a concave grating in the far and extreme ultra-violet region:

when working in the higher orders of a grating spectrograph it is usually necessary to identify and separate the overlapping orders to avoid errors. In the visible and near ultra-violet region this separation can readily be accomplished by filters. In the vacuum ultra-violet it is much more difficult to separate the orders and in spite of the need for high resolution much of the vacuum ultra-violet work has been done in the first order. It therefore seems useful to devise a new technique in order to obtain high resolution at the shorter wavelength.

The technique included introduction of several gases (or compounds) having different ionization potentials, to the ionization chamber, then by scanning the grating spectrum in the required wavelength range for each gas, and looking at its parent ion one can tell the order of the spectral line.

Most of the spectral lines used in this work were of the second order because they were stronger (see 3.1.1.6B and Fig. 8 and 9).

5. MATERIALS

The organic compounds investigated were:

a) Acetone; methyl-ethyl ketone; methyl-n-butyl ketone; acetaldehyde; benzene; monobromobenzene and mono-iodo-benzene.

These compounds were reagent grade and were all distilled, the first fraction was discarded and the middle fraction collected in a dry nitrogen atmosphere. All refractive indexes and boiling points agreed with literature values.

b) n-Propane and n-Butane were prepared by Grignard's reaction (230). n-Propane from n-propylbromide and n-butane from n-butylbromide. Magnesium turnings (6 gm.) and n-propylbromide or n-butylbromide (26.7 c.c.) were used in sodium dried tetrahydrofurane (50 c.c.). The product was decomposed by diluted sulphuric acid. The evolved n-propane or n-butane passed through concentrated sulphuric acid (to dry it and to get rid of olefins) and then trapped in a sample tube cooled by solid carbon dioxide in methylated spirit. Fractional distillation was carried out several times until the volatile material pumped out and a pure hydrocarbon was obtained. The purity was assessed by examining their n.m.r. spectra. Lines associated with olefinic protons or proton adjoint to, or on, Br were absent.

The sample compound was degassed by several cycles of freezing and pumping on the all-glass vacuum line before introduction into the storage section of this line, then through a vernier control needle valve to the ionization chamber. All taps were of the diaphragm valve type, the diaphragms being made from neoprene rubber and the whole valve was bakeable up to 150°C.

The samples were introduced to the ionization chamber in such quantity as to give the desired pressure. The gas pressure in the ionization chamber was determined by means of a Pirani gauge type 6A, attached to the gas line at a point about 23 centimeters up stream from the ionization chamber. A pressure of 5 microns was maintained in the line throughout the experiments. This gives about 3 microns in the ionization chamber because of the differential pumping at the exit slit.

At three microns pressure at room temperature 23°C, the number of molecules per cm^3 is 9.8×10^{13} and the mean free path (L) for CH_3CO^+ m/e = 43 a.m.u. is 2.1 cm. between collisions. The collision frequency then will be 1597 collisions per second. Because the life-time of the particle is relatively short, the system would be considered as a collision free region at that pressure.

PART B

RESULTS AND DISCUSSION

1. THEORETICAL CALCULATIONS

1.1. EXCESS KINETIC ENERGY OF FRAGMENT IONS

Often molecular ions are formed in an unstable state then dissociate. The possibility exists that some of the resulting fragment ions separate with a considerable range of kinetic energies. This fact was first demonstrated experimentally in the ion source of the magnetic deflection mass spectrometer by Bleakney and Tate(231). However, the knowledge concerning initial kinetic energy of framment ions from polyatomic molecules is still rather limited.

The initial energy of fragment ions are important for these reasons:

1. It must be taken into account in calculating heats of formation from appearance potential measurements, and in this case the kinetic energy is measured just above the threshold.
2. To eliminate initial energy as a source of error.
3. The kinetic energy is of interest itself, and would be a valuable means to insight into the process of dissociation of ionic species.

Normally the initial or excess kinetic energy may be determined by

a) A retarding potential field in front of the ion collector plate and recording the ion current as a function of retarding potential (233, 234 and 80).

b) Peak shape analysis: The excess kinetic energy causes the shape of the ion peak to be asymetric and broader than that for a normal peak. This alteration of the peak shape has been studied in detail and can be used to give a measurement of the initial kinetic energy of fragment ions (235).

c) Applying special energy selector (129).

d) Deflection method (236 and 237).

e) A rather new technique has been followed in this work. It includes retaining the ions in the ionization chamber by introducing a variable time delay between ionization and acceleration into the drift tube-analyzing section. The ion dissociation kinetic, or ion decay may be followed from time zero to 3000 microseconds after ionization. By comparing the experimental rate of decay at room temperature (300 K^{o}) with those calculated at different temperatures i.e. at different excess kinetic energy, then one can tell whether the fragment ions have excess or initial kinetic energy or not.

1.2. MECHANISM OF FORMATION OF HIGH KINETIC ENERGY IONS DURING DISSOCIATION

It has long been known that fragment ions from diatomic and polyatomic molecules formed by Electron Impact often have appreciable amounts of kinetic energy, but no information has been available so far that deals with high kinetic energy ions formed during dissociation by photoionization.

The formation and distribution of kinetic energies among the fragment ions formed from diatomic molecules of a given species in a relatively collision-free region such as the ionization chamber of this spectrometer can be explained satisfactorily on the basis of potential energy diagrams of the normal ground-state and of various ionized states involved using the Franck-Condon Principle (80).

Fragment ions from polyatomic molecules have not been so thoroughly studied even by electron impact as those from diatomic molecules, since the potential energy diagrams for polyatomic molecules are (N+1) dimensional where N is the number of oscillators in the polyatomic molecule. This makes the pictorial representation of such diagrams extremely difficult, if not impossible. However, one can display examples of the various types of processes leading to molecular fragmentation for the two-dimensional diagrams

representing the states of diatomic molecules. Although the diagrams for polyatomic molecules are considerably more complex and the number of possible modes of fragmentation correspondingly greater, the types of processes that may occur are probably alike for diatomic and polyatomic molecules.

1.2.1. Diatomic Molecules

In Fig. 13 is shown a set of potential energy curves for the ground state and various ionic states of a theoretical diatomic molecule AB.

The system AB is represented here as a particle moving about the plane of this paper surface, but is constrained to move in certain specified ways depending on the state of the system.

In the absence of any external force, which may impart some energy to the system, e.g. inter-molecular collision, electron, photon or secondary process (it is supposed that the molecule is in a collision free region), the particle is constrained to move along a line of constant total energy (law of conservation of energy). In addition it is constrained to remain always above the curve describing the potential-energy curve of the state in which it exists, that is to maintain at all times a positive kinetic energy. Thus, in the absence of external force the particle representing the system will oscillate along the line representing

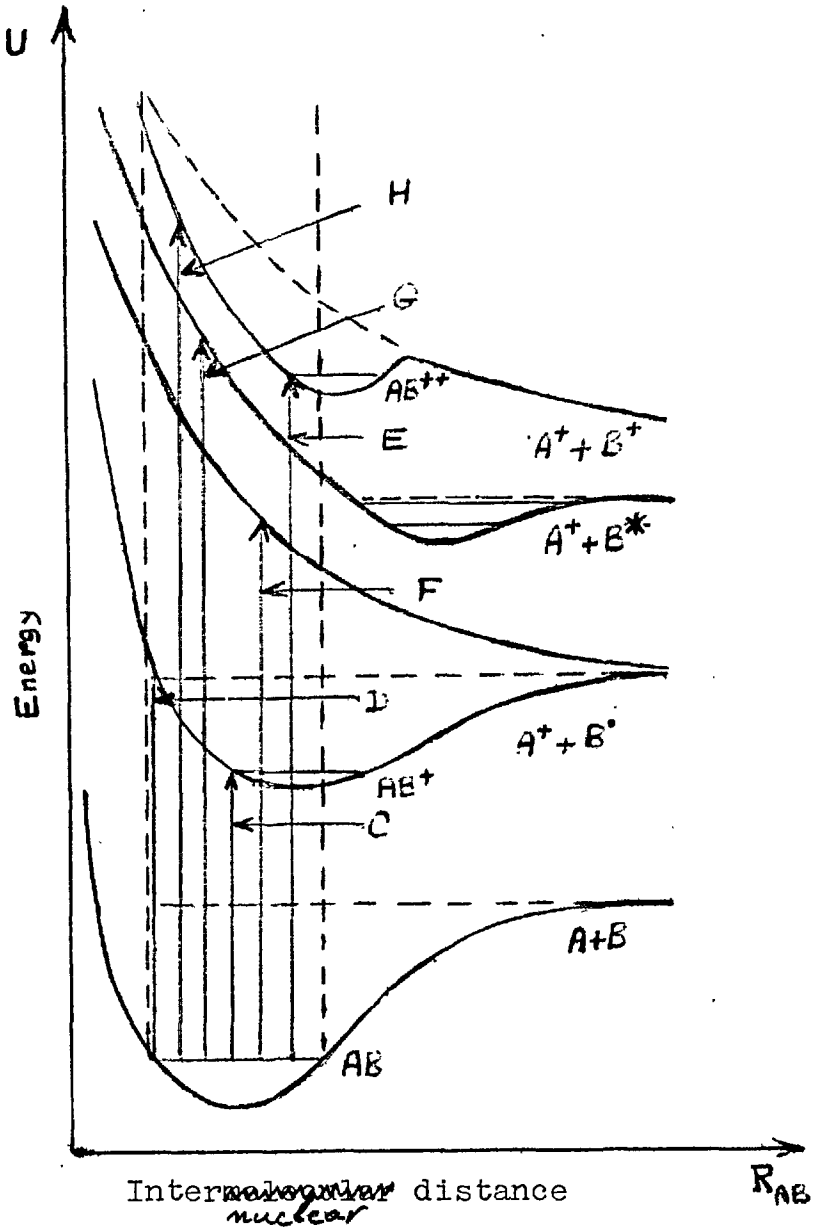


Fig. 13: Potential-energy curves for the ground state and some ionized states of the theoretical diatomic molecule AB. The vertical dotted lines show the classical limits of the Franck-Condon transition region.

the ground state energy of the molecule, between the limits imposed by the potential-energy curve.

If now a photon interacts with or an electron impinges upon the system, the constant-energy constraint is modified to the extent that the photon or electron can transfer some or all of its energy into the AB system, by moving the particle to some other energy level. There are several restrictions on such energy transfers.

1. Since the transfer of energy takes place in a very short time, then the inter-molecular distance cannot change significantly during the transition, and in terms of the diagram all energy transfers by photoionization or electron impact are to be vertical according to the Franck-Condon-Principle.

2. Since each transition state may be represented by a wave function, the probability of transition occurring between any two points or two levels is dependent on the overlap integral of the wave function representing the system at these points:

$$\int \psi_i \cdot r \cdot \psi_f \, d\tau \qquad (1)$$

where ψ_i and ψ_f are the eigenfunctions of the initial and final states of the transition under consideration, dr the inter-molecular separation. ~~and $d\tau$ the molecular volume element~~.

From this it follows that there is a large transition probability only between those overlapping points - or rather the combining states whose eigenfunctions have maxima for the same inter-molecular separation - hence there is a higher probability of finding the moving system. The character of the wavefunction is such that the transitions between points near the edges of potential energy curves (i.e. the point at which the kinetic anergy of the system is small) are the only probable ones[*].

The transitions representing these constraining conditions are shown as vertical lines in Fig. 13.

Transition C, D, and E are typical of processes leading to ions of thermal kinetic energies; process C leading to the production of the molecular ion AB^+, process D leading to the production of a fragment ion A^+ and a neutral radical B', the process E leading to the doubly charged ion AB^{++}. The transitions represented by F, G, and H, on the other hand, produce ions possessing kinetic energy. The amount of such kinetic energy is given by the vertical separation at $R = \infty$, between the dotted line denoting the total energy of the system and the solid line in the figure giving the potential energy of this system.

---

[*]The ground vibrational level of a bound state is an exception because the probability function is greatest in the centre of potential well (curve minimum) where the kinetic energy is also the greatest.

The total kinetic energy must be partitioned between the two fragments inversely proportional to their respective masses. Process F represents excitation to a bound-state energy curve at an energy well above the dissociation limit for the products A^+ and $B^\cdot$. Process G represents an excitation to a repulsive-state curve leading to the same products, and process H represents an excitation to a potential-energy curve for the doubly charged ion AB^{++} at an energy equal to or greater than the dissociation energy.

It will be noted that there is no way in which the parent ions AB^+ or AB^{++} can be formed with excess kinetic energy, although there are many possible excitation processes that lead to the formation of these ions with a varying amount of excess vibrational energy.

It should be remarked and emphasized that the energy curves shown in Fig. 13 in no way represent all the processes that can lead to production of fragments. Two types of processes in particular have not been mentioned in the diagram, since: One of these (1) is an excitation not involving ionization, which can lead to excited states of the parent molecule, thermal radical, or kinetic energy radical. This type of process has not been indicated, since the main interest in the present work is focussed on ions rather than radicals.

The second process (2) is the one that involves level transfer either through emission of radiation or through energy level crossing, or the possibility of the system's transferring from one level to another at the crossing point. Although such processes have the effect of permitting the products to be formed with a variety of energy distributions, the general types of these products formed are the same as those arising from processes shown in Fig. 13. Chupka has considered such processes (123).

However, when the above treatment is extended to polyatomic molecules, the major difference is the increased number of available energy states and the more modes of fragmentation possible.

The majority of all ions usually observed in a mass spectrometer are the result of processes of the type C, D, and E or of a process involving inter-energy-level transition.

Fragment ions produced from these processes are expected in general to be formed with small amounts of kinetic energy, because the investigations carried out by Taubert (237), Monahan and Stanton (242), indicated a very large number of the fragment ions formed from hydrocarbons have excess kinetic energies in slight excess of that thermal energy that the ions naturally possess. Processes of the type D almost always impart to the fragment ions some kinetic energy, since it is rather unlikely

that the limit of the region of allowable excitation processes will intersect the potential-energy-curve at precisely the energy of dissociation of that curve.

A question which now arises regarding the ions formed with large amount of excess kinetic energy is:

Which one of the three processes F, G or H is the dominant process leading to formation of these ions?

Processes F and G are the same or indistinguishable unless detailed and advanced knowledge concerning the shapes of their potential energy curves is made available, but the process type H giving rise as it shows to a pair of ions may be experimentally distinguished from the other processes.

1.2.2. Polyatomic molecules:

It has earlier been mentioned that fragment ions from polyatomic molecules have not been so thoroughly studied as those from diatomic molecules, and all the knowledge concerning the kinetic energy ions is derived from electron impact methods.

High kinetic energy ions formed from the dissociation of polyatomic molecules have been interpreted in previous studies (243, 244) as arising from processes type H. Hustrulid et al (243) have proposed that high kinetic energy ions result from the dissociation of doubly-charged ions — formed by electron-impact — into two singly charged

fragments. Mohler et al (244) supported this interpretation by computing the repulsive energies of various hydrocarbons on the assumption of Coulomb repulsion energies for doubly charged ions of these hydrocarbon compounds, and compared the total kinetic energies of fragmentation that Hustrulid observed.

The value of such a comparison is highly questionable, in view of two uncertainties involved in this comparison. In the first place, the calculated repulsion energy depends on the initial distance of separation between the two charges which must be estimated.

Mohler et al based their calculations on the greatest possible charge separation, associating the charges with protons attached to the end carbon. This is somewhat doubtful because for such a charge distribution the C-H bond would be considerably weakened. Hence one would expect such a configuration to give rise to fragmentation of a C-H bond rather than one of the C-C bonds.

A more realistic charge-separation distance would result from associating the charges with the end-carbon nuclei, Even then, the Coulomb energy could not be directly associated with the kinetic energy of the fragments, as can be seen from the upper potential energy curves in Fig. 13. The Coulomb repulsion curve is shown in the figure as a dotted line and the actual potential-energy

curve as a solid line. As the figure indicates - in general - the potential-energy curve for the doubly charged ion will deviate from the Coulomb repulsion curve, owing to the binding force exerted by the electrons remaining in the molecule. The extent of this binding will vary from molecule to molecule and from one configuration to another.

Hurley and Maslen (245) have carried out calculations of potential energy curves for doubly charged diatomic ions which indicates that the extent of binding for ions such as O_2^{++} and N_2^{++} is between 3 to 6 electron volts. For polyatomic molecules the probability for variation in binding energy may be considerably greater, particularly if excited states of the doubly charged ions are considered.

A test of the doubly charged-ion hypothesis involves the necessity that a pair of charged fragments be formed in any mechanism that results in the appearance of a singly charged ion, by looking at the analysis which has been carried out by Stanton (129), for propane molecule . Stanton concluded from his investigation of excess kinetic energy ions from propane that the reaction:

$$C_3H_8^{++} \rightarrow CH_3^+ + C_2H_5^+ \qquad (2)$$

must be rejected, because of the complete absence of excess kinetic energy $C_2H_5^+$ ions with CH_3^+ ion in the mass

spectrum of propane. An observation with which this research is nearly in agreement because $C_2H_5^+$ was only observed with small amount of kinetic energy, with the complete absence of CH_3^+ for photon energy up to 18 e.v.

Then process type H must be rejected according to Stanton's result, as the primary mechanism for high kinetic energy ion formation, and processes of type D, F or G must be the dominant mechanisms giving rise to the high kinetic energy ions.

It would be reasonable to assume that because the spectrometer was unable to ~~resolve~~ detect H or H_2 mass peak due to poor ~~resolving~~ sensitivity power, all the small possessed kinetic energy ions observed in this research arise out of cleavage of a C-C bond, as is the case for propane.

This is not to say that type H processes do not occur. Lozier (234) observed H^+ ions whose properties definitely characterized them as resulting from a type H process leading to the purely Coulombic-repulsive state H_2^{++}.

It would certainly be surprising if such processes occurred for organic molecules photoionized at 18 e.v. energy or less if they did not appear on bombardment with 50 or 70 e.v.

The conclusion one can reach, however, is that when irradiating organic molecules with photon at energy of

about 18 e.v. or even with electrons of 50 or 70 e.v. or less, the processes of type H are not nearly of such importance as sources of high kinetic energy ions as types 'D', 'F' or 'G' processes.

1.3. DECAY OF IONS IN THE IONIZATION CHAMBER

A major question arises when retaining the ions in the ionization chamber by applying a time delay between ionization and acceleration - mass analysis - why do some of the ions disappear?

Several modes for this loss or decay are possible, but the most important mode is the loss by thermal diffusion on to the repeller plate.

Ions formed in a field free region may diffuse out of that region as a result of their thermal velocities and collide with the repeller plate which is 3 mm. far from the photons' beam, or ionization region, and get lost.

Before doing the calculations we must assume:

1. The translation energies resulting from dissociation are negligible so that the ions have only the velocities initially possessed by the molecules.
2. All electrical fields are negligible so that the ions can be represented by a simple bunch of ions having a Maxwell-Boltzmann's velocity distribution.
3. The system is in a state of thermodynamic equilibrium.

The speeds of the molecules of a gas in a thermodynamic equilibrium are distributed according to Maxwell's distribution:

$$f(v)dv = \frac{dN}{N} = \left(\frac{m}{2\pi kT}\right)^{1/2} \cdot e^{-\frac{mv^2}{2kT}} dv \qquad (1)$$

Here $f(v)dv$ is the number of molecules (238) with speeds between (v) and (v + dv) cm/sec., m is the mass of molecule in grams; T is the absolute temperature in ^{o}K, and $k = 1.3806 \times 10^{-16}$ erg/^{o}K is Boltzmann's constant.

Evidently if N_t is the total number of molecules in the gas then:

$$\int_o^\infty f(v)dv = N_t \qquad (2)$$

The average velocity v_a is:

$$v_a = \frac{1}{N_t} \int_o^\infty vf(v)dv = \left(\frac{8kT}{\pi m}\right)^{1/2} \qquad (3)$$

and the r.m.s. velocity is:

$$v_r = \left[\frac{1}{N_t} \int_o^\infty v^2 f(v)dv\right]^{1/2} = \frac{3kT}{m} \qquad (4)$$

The most probable velocity v_p of the distribution is obtained by setting $df(v)dv$ equal to zero and solving for v then:

$$v_p = \left(\frac{2kT}{m}\right)^{1/2} \qquad (5)$$

By replacing the constants we have:

$$v_p = 12900 \sqrt{\frac{T}{m}} \text{ cm/sec.} \qquad (6)$$

$$v_a = 1.1284\ v_p \quad \text{cm/sec.} \tag{7}$$

$$v_p = 1.2248\ v_p \quad \text{cm/sec.} \tag{8}$$

For the ion CH_3CO^+ m/e = 43 a.m.u; T = 293°K, these velocities are:

$$v_a = 37698 \text{ cm/sec.} \tag{9}$$

$$v_p = 33540 \text{ cm/sec.} \tag{10}$$

$$v_r = 41053 \text{ cm/sec.} \tag{11}$$

Table 2 shows the distance travelled by this ion with time.

TIME DELAY IN MICRO-SECOND (t_D)	$x_1 = v_p x t_D$ = radius of sphere	$x_2 = v_a x t_D$ = radius of sphere	$x_3 = v_m x t_D$ = radius of sphere
1	0.0335 cm.	0.0376 cm.	0.0410 cm.
2	0.0670	0.0754	0.0821
3	0.1006	0.1131	0.1231
4	0.1341	0.1408	0.1642
5	0.1677	0.1885	0.2052
6	0.2012	0.2262	0.2463
7	0.2347	0.2639	0.2873
8	0.2683	0.3016	0.3284
9	0.3018	0.3393	0.3694
10	0.3354	0.3769	0.4105

The number of ions remaining in the ionization chamber as a function of time may be calculated as follows:

1. One dimension: At time t = 0, there are N_o molecule uniformly distributed with a linear density of $\frac{N_o}{a}$ along the distance a = 3 mm.

The fraction of the ions N_o still in the ionization region after t time is

a) $\frac{a-vt}{a}$ or $1 - \frac{vt}{a}$ if $-1 \leq \frac{vt}{a} < 1$

b) 0 if $\frac{vt}{a} \geq 1$

Because the ions may leave from either side of the ionization region. The number of ions in the region after time t is then:

$$N_t = \int_{\frac{v.t}{a} = -1}^{\frac{v.t}{a} = 1} (1 - \frac{vt}{a}) \cdot dN_v \qquad (12)$$

If we multiply and divide the quantity $\frac{vt}{a}$ by $v_p = (\frac{2kT}{m})^{1/2}$ then suppose that the quantity:

$$(\frac{m}{2kT})^{1/2} \cdot v = \alpha \qquad (13)$$

$$(\frac{m}{2kT})^{1/2} \cdot \frac{a}{t} = \alpha_o \qquad (14)$$

and $$(\frac{m}{2kT})^{1/2} \cdot dv = d\alpha \qquad (15)$$

By replacing these values in the probability function:

$$dN_{(\alpha)} = N_o \frac{1}{\sqrt{\pi}} e^{-\alpha^2} d\alpha \qquad (16)$$

we have

$$N_{(t)} = \int_{-\alpha_o}^{\alpha_o} (1 - \frac{\alpha}{\alpha_o}) N_o \frac{1}{\sqrt{\pi}} \cdot e^{-\alpha^2} d\alpha \qquad (17)$$

$$\text{or} \quad N_{(t)} = \frac{2N_o}{\sqrt{\pi}} \left[\int_o^{\alpha_o} e^{-\alpha^2} d\alpha - \frac{1}{\alpha_o} \int_o^{\alpha_o} e^{-\alpha^2} \alpha d\alpha \right] \tag{18}$$

If we suppose

$$A = \frac{2}{\sqrt{\pi}} \int_o^{\alpha_o} e^{-\alpha^2} d\alpha$$

$$B = \frac{2}{\sqrt{\pi}} \cdot \frac{1}{\alpha_o} \int_o^{\alpha_o} e^{-\alpha^2} d\alpha = \frac{1 - e^{-\alpha_o^2}}{\alpha_o \sqrt{\pi}}$$

and equation (18) finally becomes:

$$\frac{N_t}{N_o} = \frac{2}{\sqrt{\pi}} \int_o^{\alpha_o} e^{-\alpha^2} d\alpha - \frac{1 - e^{-\alpha_o^2}}{\alpha_o \sqrt{\pi}} \tag{19}$$

The value of term A and $e^{-\alpha_o^2}$ in term B are given directly in (239), and the evaluation of eq (19) can be made very easily by replacing the constants: a = 3 mm. and v_p = 33540 cm/sec. t = 0,1,2,..... 15 microseconds T = 300K°.

Another method which was followed in the present work is to solve the equation by computer.

2. Three dimension system: Extending this mathematical treatment to the loss of ions in three dimensions we have for the number of ions with a velocity in the x direction of v_x and $v_x + dv_x$, and in the y direction of

v_y and $v_y + dv_y$, and in the z direction of

v_z and $v_z + dv_z$

Then:

$$dN = N\left[\frac{m}{2\pi kT}\right]^{3/2} e^{-\frac{m(v_x^2+v_y^2+v_z^2)}{2kT}} dv_x.dv_y.dv_z \quad (20)$$

At time t = 0 there are N_o molecules uniformly distributed in the volume x.y.z. with a volume density equal to $\frac{N_o}{x.y.z}$, and zero elsewhere.

After a delay time t, the fraction of molecules or ions still in the same volume is:

$$\frac{(x - v_x t)(y - v_y t)(z - v_z t)}{x.y.z}$$

following the same mathematical treatment as in the previous case we write:

$$N_t = 8N_o \int_o^{\frac{x}{t}} \int_o^{\frac{y}{t}} \int_o^{\frac{z}{t}} \frac{(x-v_x t)(y-v_y t)(z-v_z t)}{x\ y\ z} \cdot \left(\frac{m}{2\pi kT}\right)^{3/2} \cdot e^{-\frac{m}{2kT}(v_x^2+v_y^2+v_z^2)} \cdot dv_x.dv_y.dv_z \quad (21)$$

The factor 8 here arises from the integration over one octant.

Because the variables are independent they may be easily separated as

$$N_t = 8N_o \int_o^{\frac{x}{t}} \int_o^{\frac{y}{t}} \int_o^{\frac{z}{t}} \left(1-\frac{v_x t}{x}\right)\left(1-\frac{v_y t}{y}\right)\left(1-\frac{v_z t}{z}\right)\left(\frac{m}{2\pi kT}\right)^{3/2} \cdot e^{-\frac{m}{2kT}(v_x^2+v_y^2+v_z^2)} \cdot dv_x.dv_y.dv_z \quad (22)$$

$$\text{or } N_t = 8N_o \int_o^{\frac{x}{t}} \int_o^{\frac{y}{t}} \int_o^{\frac{z}{t}} \left(\frac{m}{2\pi kT}\right)^{3/2} \left(1 - \frac{v_x t}{x}\right) e^{-\frac{mv_x}{2kT}} \left(1 - \frac{v_y t}{y}\right) e^{-\frac{mv_y}{2kT}}$$

$$\cdot \left(1 - \frac{v_z t}{z}\right) e^{-\frac{mv_z}{2kT}} dx.dy.dz \qquad (23)$$

or

$$N_t = \frac{8N_o}{(\pi)^{3/2}} \left[\int_o^{\alpha_o} \left(1 - \frac{\alpha}{\alpha_o}\right) e^{-\alpha^2} d\alpha . \int_o^{\beta_o} \left(1 - \frac{\beta}{\beta_o}\right) e^{-\beta^2} d\beta . \int_o^{\gamma_o} \left(1 - \frac{\gamma}{\gamma_o}\right) e^{-\gamma^2} d\gamma \right.$$

where

$$\alpha = \left(\frac{m}{2kT}\right)^{1/2} v_x \; ; \quad \alpha_o = \left(\frac{m}{2kT}\right)^{1/2} \cdot \frac{a}{t} = \frac{x}{v_p t} \; ;$$

$$\text{and } d\alpha = \left(\frac{m}{2kT}\right)^{1/2} dv_x$$

$$\beta = \left(\frac{m}{2kT}\right)^{1/2} v_y \; ; \quad \beta_o = \left(\frac{m}{2kT}\right)^{1/2} \cdot \frac{y}{t} = \frac{y}{v_p t}$$

$$\text{and } d\beta = \left(\frac{m}{2kT}\right)^{1/2} dv_y$$

$$\text{and } \gamma = \left(\frac{m}{2kT}\right)^{1/2} v_z \; ; \quad \gamma_o = \left(\frac{m}{2kT}\right)^{1/2} \frac{z}{t} = \frac{z}{v_p t}$$

$$\text{and } d\gamma = \left(\frac{m}{2kT}\right)^{1/2} dv_z$$

then:

$$N_t = N_o \left[\frac{2}{\sqrt{\pi}}\left(\int_o^{\alpha_o} e^{-\alpha^2} d\alpha - \frac{1}{\alpha_o} \int_o^{\alpha_o} e^{-\alpha^2} \alpha d\alpha\right)\right] \cdot$$

$$\left[\frac{2}{\sqrt{\pi}}\left(\int_o^{\beta} e^{-\beta^2} d\beta - \frac{1}{\beta_o} \int_o^{\beta_o} e^{-\beta^2} \beta d\beta\right)\right] \cdot$$

$$\left[\frac{2}{\sqrt{\pi}}\left(\int_o^{\gamma_o} e^{-\gamma^2} d\gamma - \frac{1}{\gamma_o} \int_o^{\gamma_o} e^{-\gamma^2} \gamma d\gamma\right)\right] \qquad (25)$$

Equation (25) shows that the three dimensions case is a product of three one-dimensional cases given by equation (19).

This treatment may account for the decrease in the number of ions with time due to the collision with repeller plate, which is backing the photon beam-ionization region - and a = 3 mm. far from it. It does seem reasonable to conclude that this is actually the major mode of ions' decay in that short time.

2. PRESENT RESULTS

The results and discussion concerned with the design, construction and performance of the spectrometer are found in the previous sections, part A, while the results and discussion concerned with the behaviour of the organic compounds studied are treated in this part.

After the best instrumental operating procedure conditions had been determined according to the setting procedure discussed in the previous part, the mass spectra of some organic compounds were obtained at different values of photon energy, while the time delay between ionization and acceleration of ions was varied between zero and 15 microseconds in steps of one or two microseconds. The procedure was repeated several times for each of the compounds for various fixed time delay and different photon energy (10.57 - 18.07 e.v.) as well.

The results of this research work are presented in the form of parent (molecular) and fragment ions' decay curves given in Figures (14, 15, 17, 18, 20-23, 25-28, 30-32, 34, 36, 37-39, 41-42, 44, 46, 47), tables (3 to 12) and typical mass spectra, Figures (16, 19, 24, 29, 33, 36, 40, 43, 45). All were obtained from a series of oscilloscope photographs chosen to illustrate the range of processes which can be observed by this technique. All the photographs obtained were taken using the same condition. For the

tables the column headed exp. lists the experimental peak height or abundance of ions. The column headed calc. is the abundance of various fragment (F) or molecular (M) ions, as calculated from equation (18) in section 1.3 of this part, by computer.

TABLE 3. MOLECULAR AND FRAGMENT IONS PRODUCED BY PHOTOIONIZATION

and accelerated with constant momenta

Compound	m/e at = 18.07 e.v.	14.84 e.v.	10.57 e.v.	Probable Structure of ion
1.Acetone	58	58	58	$CH_3CO^+CH_3$
	43	43	-	$CH_3\ C\equiv O^+$
	28	-	-	CO^+
	15	-	-	$C\ H_3^+$
2.Methyl ethyl ketone	72	72	72	$C_2H_5CO^+CH_3$
	57	57	57	$CH_3CO^+CH_2$
	43	43	-	$CH_3\ C\equiv O^+$
	29	29	-	$CH_3\ C\ H_2^+$
	15	-	-	$C\ H_3^+$

Compound	m/e at = 18.07 e.v.	14.84 e.v.	10.57 e.v.	Probable ucture of ion
3.Methyl n-butyl ketone	71	71	72	$CH_3CO^+CH_2CH_2$
	58	58	58	$CH_3CO^+ CH_3$
	43	43	-	$CH_3 CO^+$
	29	29	-	$CH_3 \cdot C H_2^+$
4.Acetaldehyde	44	44	44	$CH_3 \cdot CHO^+$
	29	29	-	CHO^+
	15	15	-	$C H_3^+$
5.n-Propane	44	44	-	$CH_3C^+H_2CH_3$
	29	29	-	$CH_3 C H_2^+$
6.n-Butane	58	58	-	$C_4H_{10}^+$
	43	43	-	$CH_3CH_2C^+H_2$
	29	29	-	$CH_3 C^+H_2$
	15	-	-	$C H_3^+$
7.Benzene	78	78	78	$C_6H_6^+$
	51	51	-	$C_4H_3^+$
	39	-	-	$C_3H_3^+$
8.Monobromo-benzene	77	77	77	$C_6H_5^+$
9.Monoiodoben-zene	77	77	77	$C_6H_5^+$

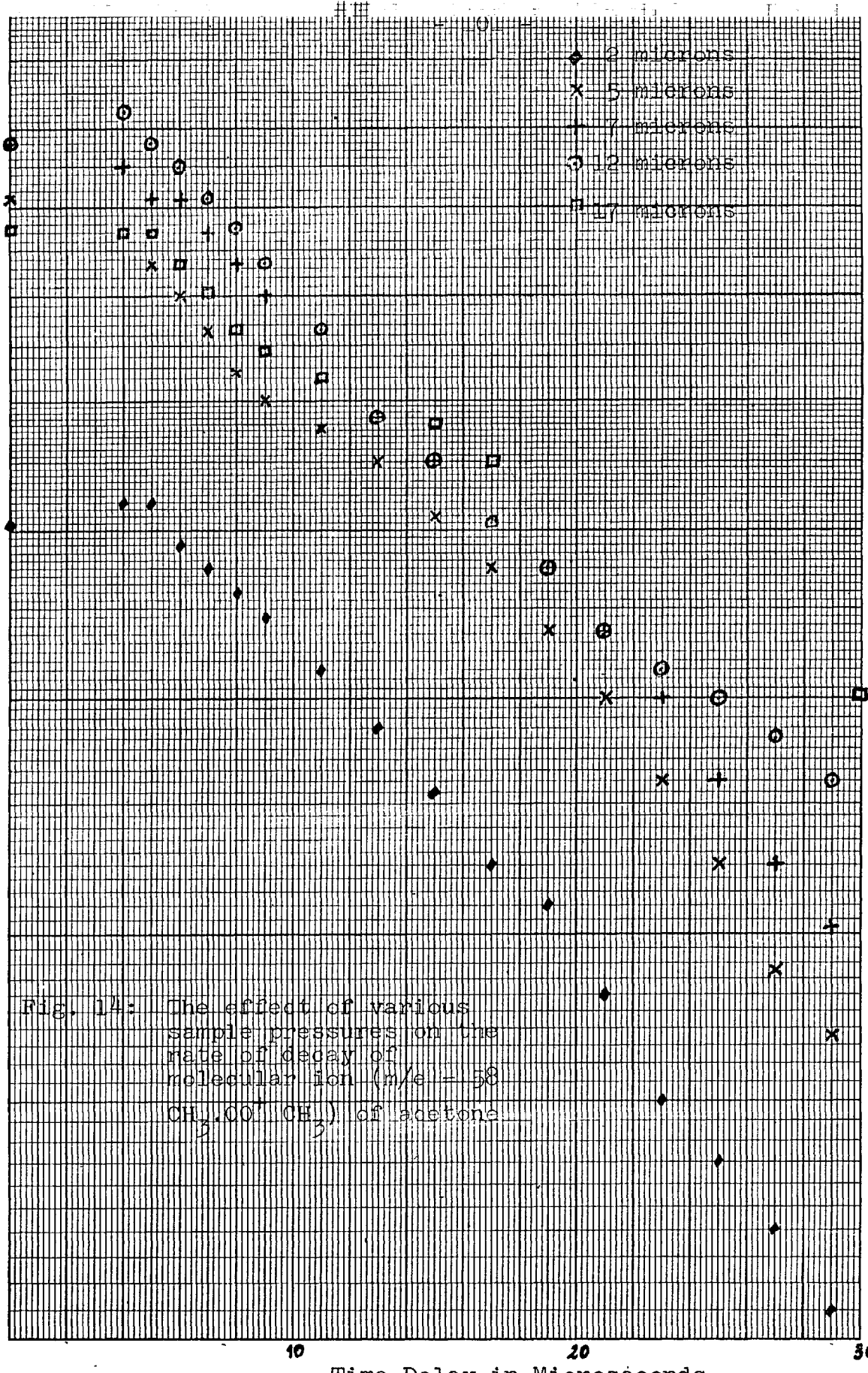
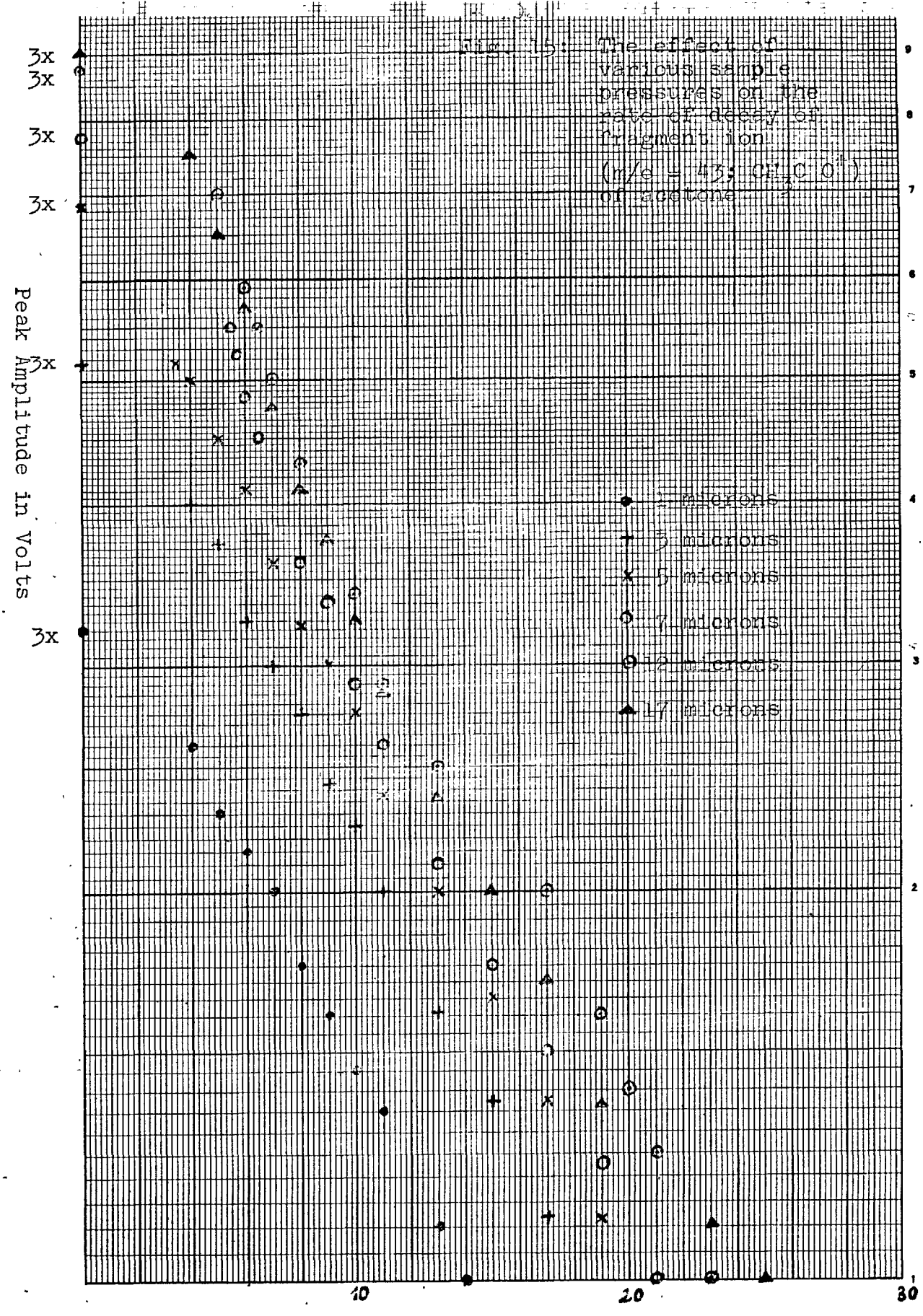


Fig. 14: The effect of various sample pressures on the rate of decay of molecular ion (m/e = 58 $CH_3.CO^+.CH_3$) of acetone


Fig. 15: The effect of various sample pressures on the rate of decay of fragment ion (m/e = 43; CH_3CO^+) of acetone
1 microns
3 microns
5 microns
7 microns
12 microns
17 microns
Peak Amplitude in Volts
Time Delay in Microseconds
10
20
30

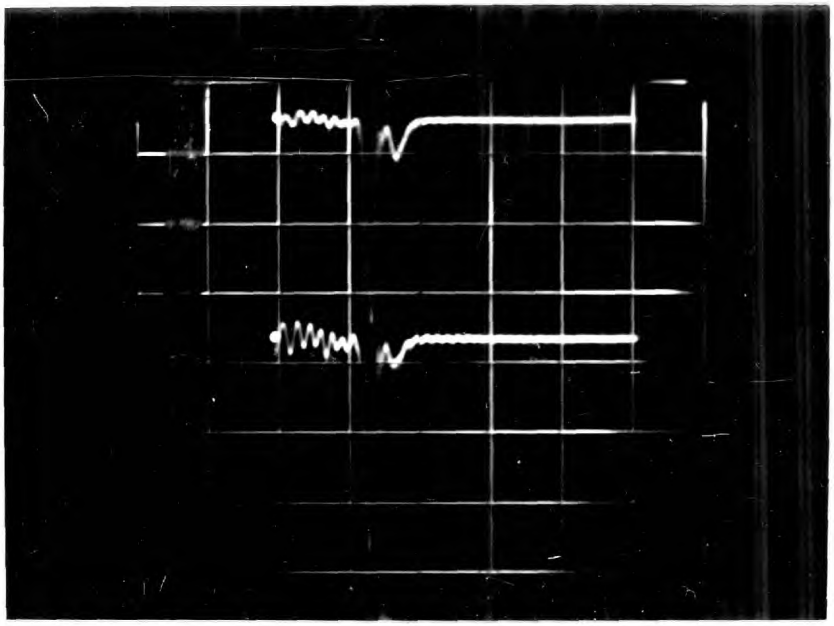


Fig. 16. Oscillogram of the mass spectrum of acetone at 14.84 e.v.; left to right masses, 43 and 58. The lower spectrum was obtained at delay time zero while the upper one was at one microsecond delay time.

TABLE 4. CHANGE OF THE RELATIVE ABUNDANCE OF IONS FROM ACETONE WITH DELAY TIME AT 14.84 e.v., (835.29 A°)

Delay time in Microseconds	Ion Peak at m/e =			
	EXP. 43(F)	CALC. 43(F)	EXP. 58(M)	CALC. 58(M)
	x3			
0	10	9.99	4.	9.99
1	-	9.36	-	9.44
2	-	8.71	-	8.89
3	-	8.07	-	8.34
4	9.33	7.43	6.	7.79
5	9	6.81	6.	7.24
6	8	6.22	6.	6.71
7	7.33	5.68	6.	6.20
8	6.33	5.20	5.75	5.74
9	5.66	4.78	5.5	5.31
10		4.41		4.94
11	4.66	4.08	5.25	4.60
12		3.80		4.30
13	3.66	3.55	5.	4.03
14		3.33		3.79
15	3.	3.13	4.80	3.57

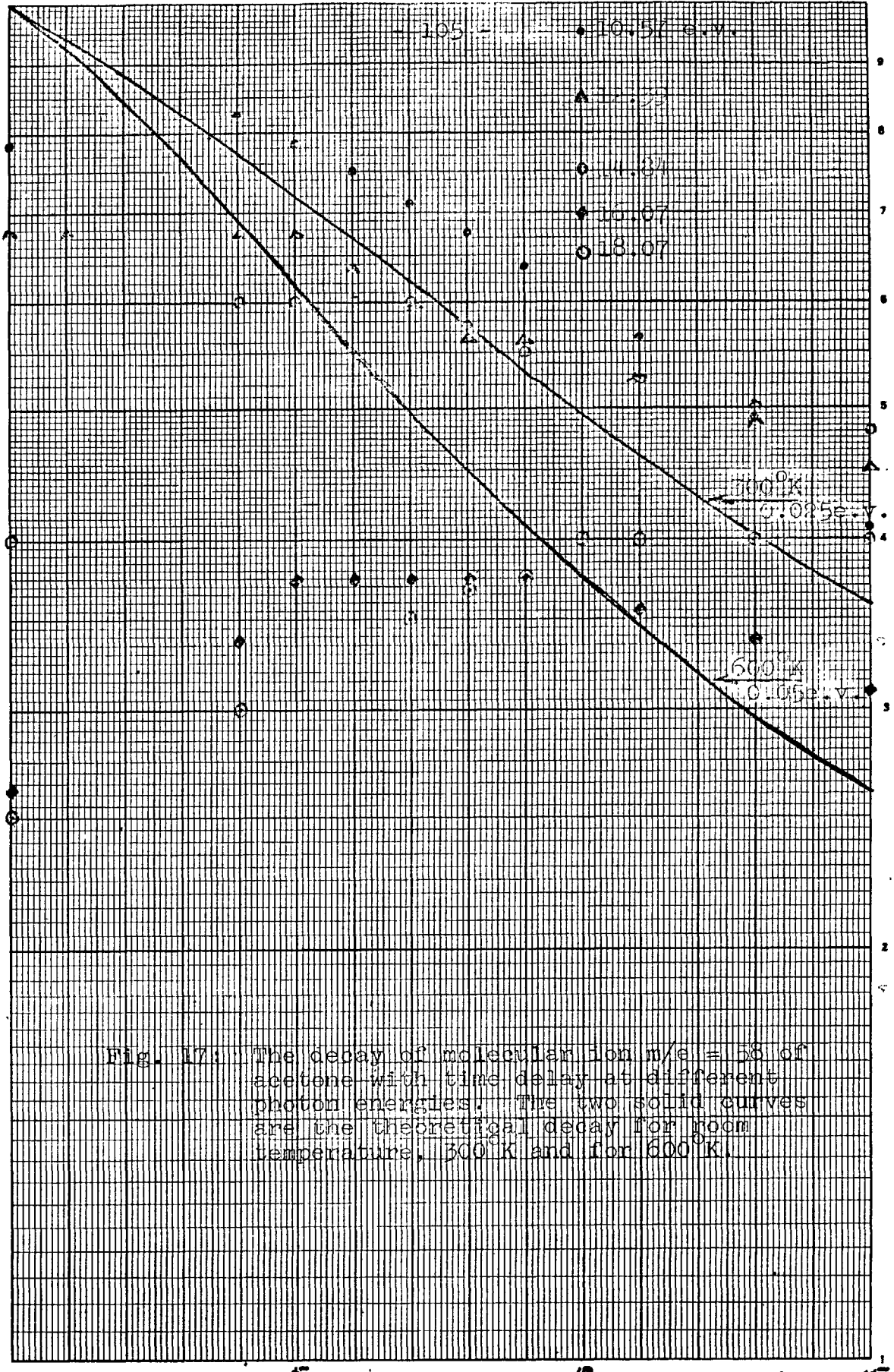


Fig. 17: The decay of molecular ion m/e = 58 of acetone with time delay at different photon energies. The two solid curves are the theoretical decay for room temperature, 300°K and for 600°K.

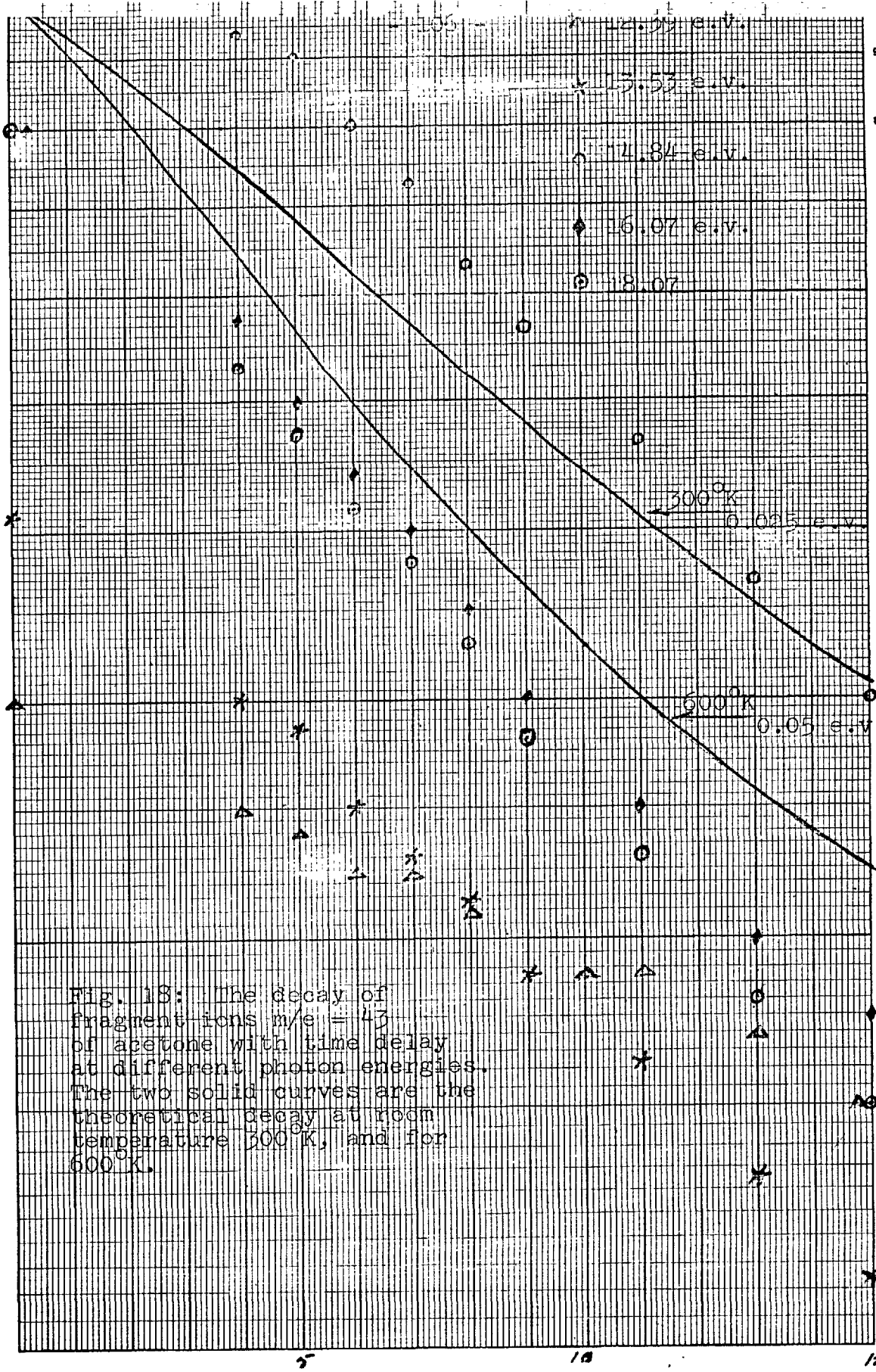


Fig. 18: The decay of fragment ions m/e = 43 of acetone with time delay at different photon energies. The two solid curves are the theoretical decay at room temperature 300°K, and for 600°K.

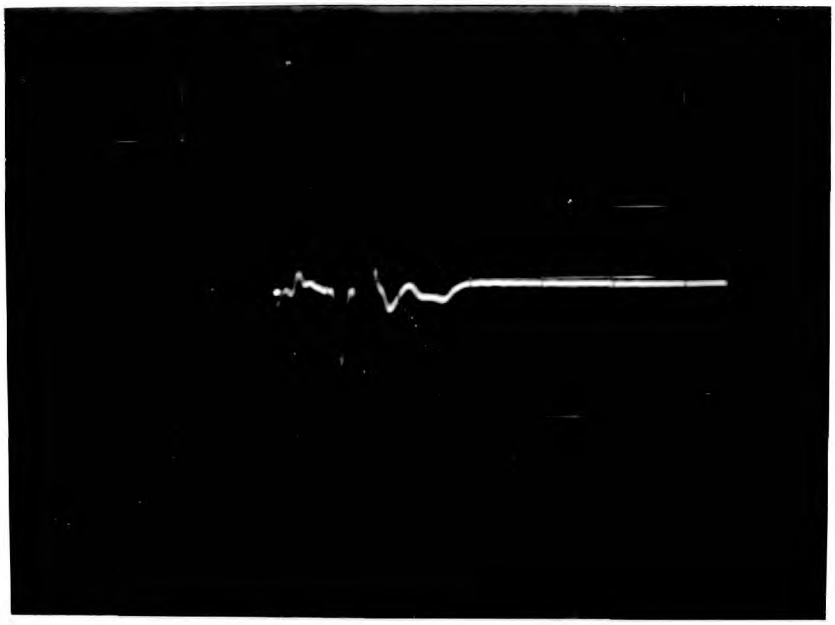


Fig. 19. Oscillogram of the mass spectrum of methyl-ethyl-ketone at 14.84 e.v.; left to right masses, 29, 43, 57 and 72.

TABLE 5. CHANGE OF THE RELATIVE ABUNDANCE OF IONS FROM METHYL-ETHYL KETONE WITH DELAY TIME AT 14.84 e.v. (835.29 A°)

Delay time in Microseconds	Ion Peak at M/e =							
	EXP. 29(F)	CALC. 29(F)	EXP. 43(F)	CALC. 43(F)	EXP. 57(F)	CALC. 57(F)	EXP. 72(M)	CALC. 72(M)
			3x					
0	7.12	9.99	10.25	9.99	2.62	9.99	1.5	9.99
1	6.37	9.21	10.	9.35	2.62	9.44	1.68	9.50
2	5.62	8.43	10.	8.71	2.43	8.88	2.25	9.00
3	4.89	7.65	9.75	8.07	2.43	8.33	2.25	8.51
4	4.5	6.89	9.25	7.43	2.38	7.77	2.25	8.01
5	3.75	6.17	8.75	6.81	2.25	7.22	-	7.52
6	3.37	5.53	7.5	6.22	2.1	6.68	-	7.03
7	3.	4.97	6.75	5.68	1.87	6.17	-	6.51
8	2.62	4.50	6.25	5.20	1.68	5.71	-	6.11
9	2.43	4.10	5.5	4.78	1.65	5.28	-	5.70
10	2.25	3.75	5.	4.41	1.50	4.90	-	5.32
11	1.87	3.46	4.5	4.08	1.42	4.57	-	4.98
12	1.5	3.20	4.	3.8	1.35	4.27	-	4.67
13	1.5	2.98	3.75	3.55	1.23	4.00	-	4.39
14	1.41	2.79	3.25	3.33	1.20	3.76	-	4.14
15	1.12	2.61	3.	3.13	1.12	3.54	-	3.91

EXP. = Experimental; CALC. = Calculated; F = Fragment; M = Molecular

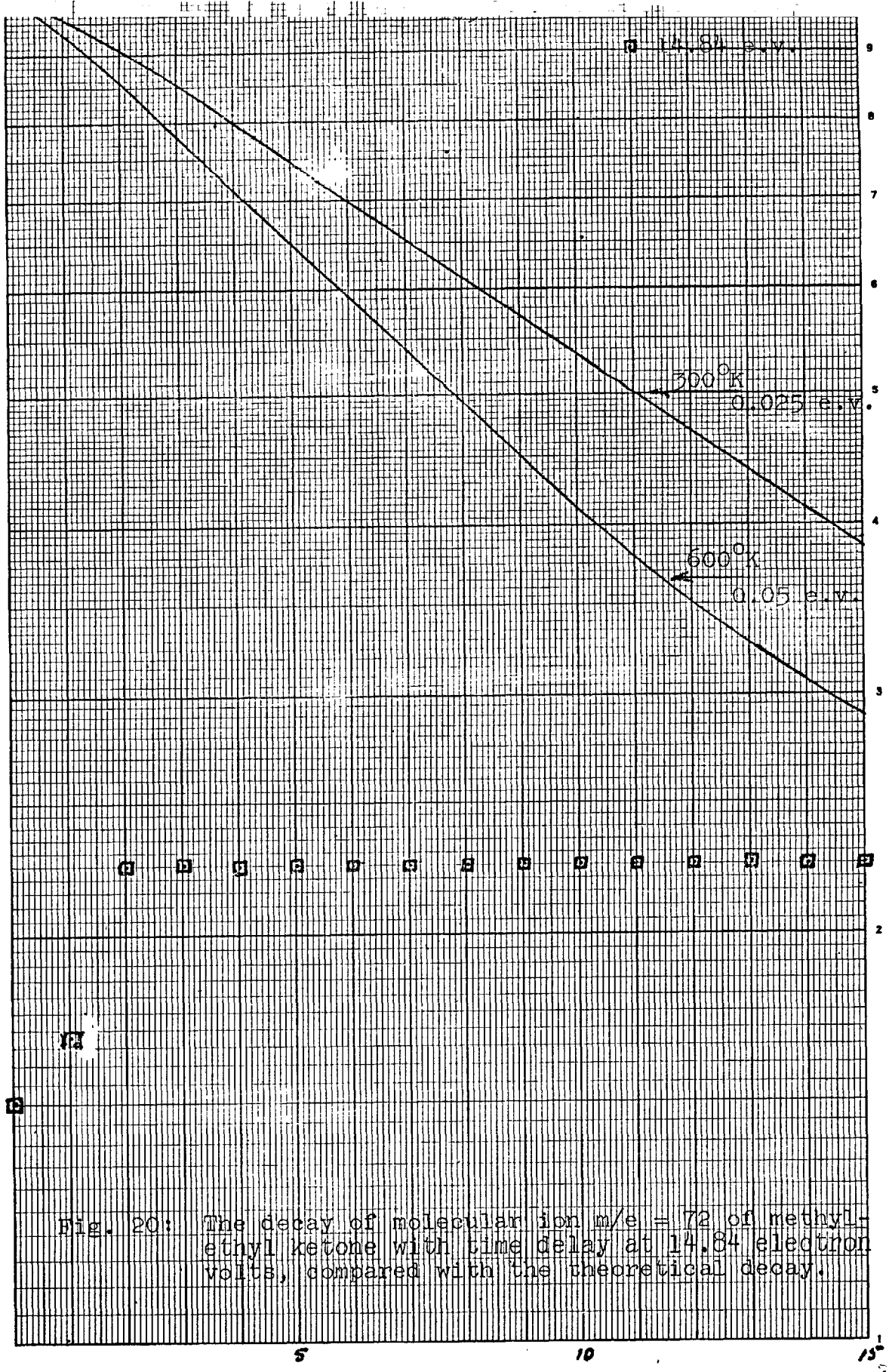


Fig. 20: The decay of molecular ion m/e = 72 of methyl-ethyl ketone with time delay at 14.84 electron volts, compared with the theoretical decay.

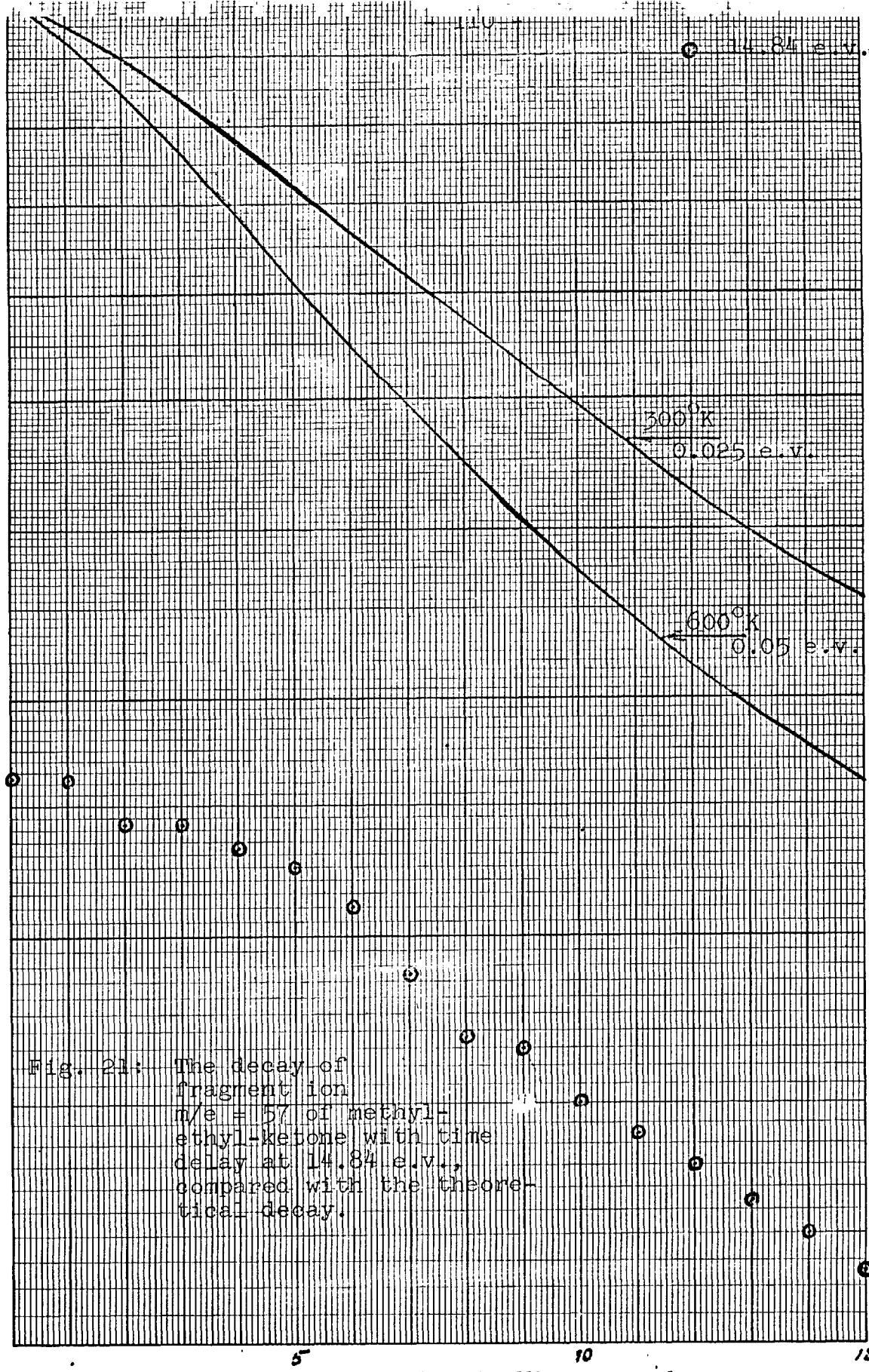


Fig. 21: The decay of fragment ion m/e = 57 of methyl-ethyl-ketone with time delay at 14.84 e.v., compared with the theoretical decay.

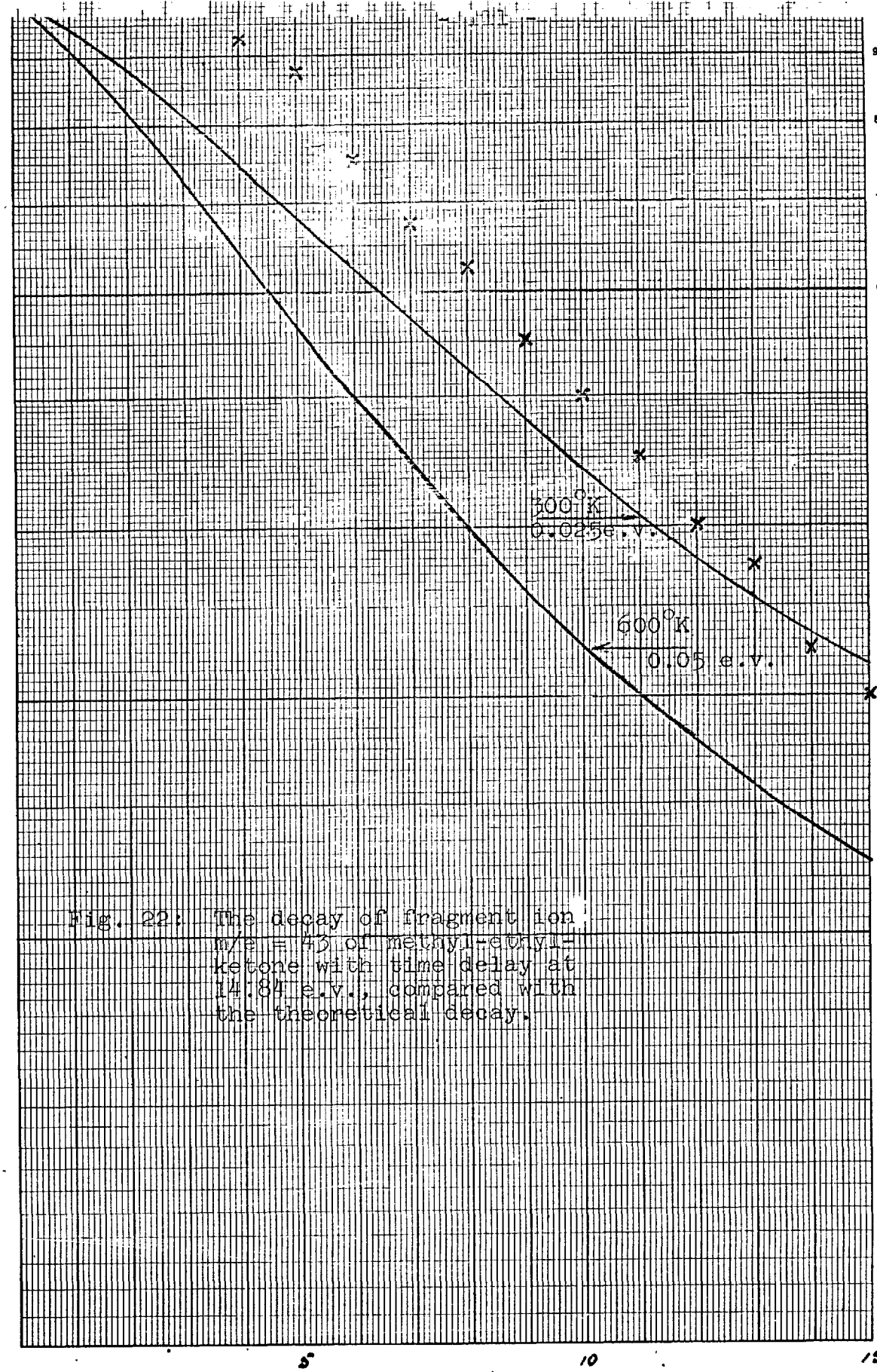


Fig. 22: The decay of fragment ion m/e = 43 of methyl-ethyl-ketone with time delay at 14.84 e.v., compared with the theoretical decay.

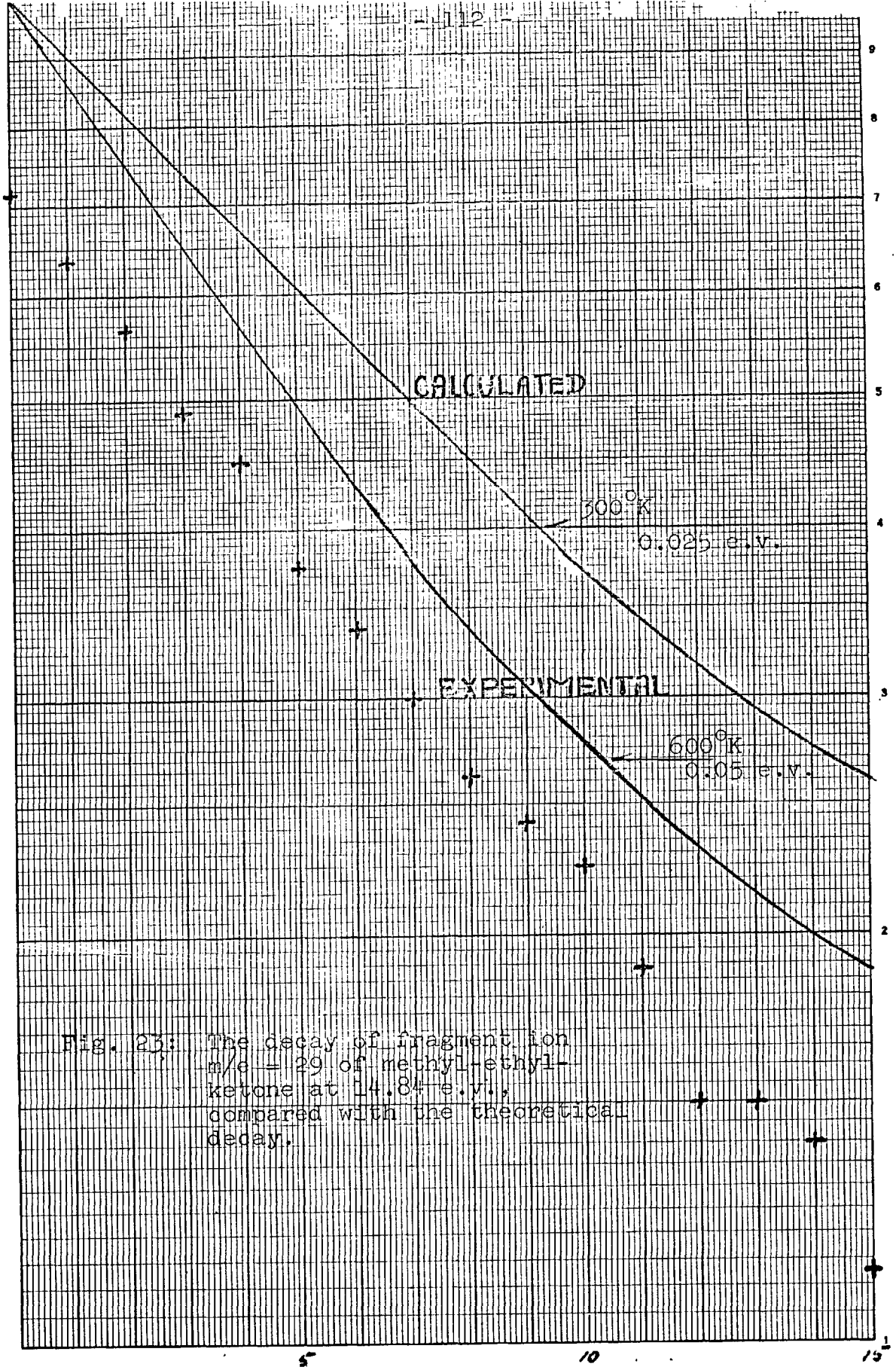


Fig. 23: The decay of fragment ion m/e = 29 of methyl-ethyl-ketone at 14.84 e.v., compared with the theoretical decay.

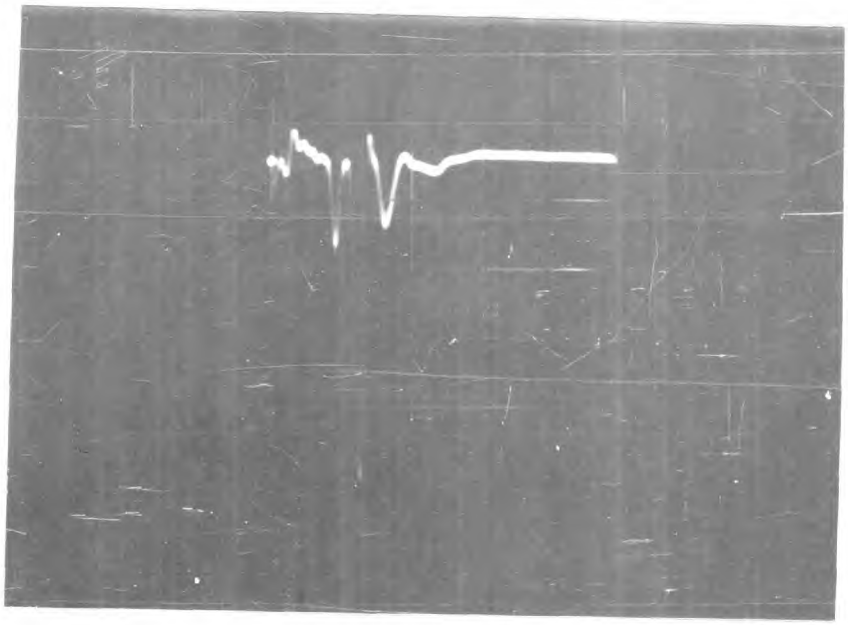


Fig. 24. Oscillogram of the mass spectrum of methyl-n-butyl ketone at 14.84 e.v. with zero time delay between ionization and acceleration; left to right masses 29, 43, 58 and 71.

TABLE 6. CHANGE OF THE RELATIVE ABUNDANCE OF IONS FROM METHYL-n-BUTYL KETONE WITH DELAY TIME AT 14.84. e.v.; (835.29 A°)

Delay time in Microseconds	Ion Peak at m/e =							
	EXP. 29F.	CALC. 29(F)	EXP. 43F	CALC. 43(F)	EXP. 58F.	CALC. 58(F)	EXP. 71F.	CALC. 71(F)
0	8.25	9.99	11.	9.99	1/10 x 7.5	9.99	2.25	9.99
1	7.5	9.21	11.	9.35	6.75	9.44	-	9.50
2	6.75	8.43	11.	8.71	6.75	8.89	-	9.00
3	5.85	7.65	10.5	8.07	6.	8.34	-	8.50
4	5.1	6.89	10.5	7.43	5.85	7.79	-	8.00
5	4.5	6.17	10.5	6.81	5.25	7.24	-	7.53
6		5.53		6.22		6.71		7.01
7	3.37	4.97	9.5	5.68	4.5	6.20	-	6.54
8		4.50		5.20		5.74		6.09
9	2.55	4.10	7.5	4.78	3.93	5.31	2.43	5.68
10		3.75		4.41		4.94		5.30
11	1.87	3.46	6.25	4.08	3.37	4.60	2.85	4.96
12		3.20		3.8		4.30		4.65
13	1.50	2.98	5.	3.55	3.0	4.03	3.0	4.37
14		2.79		3.33		3.79		4.12
15	1.12	2.61	3.75	3.13	2.75	3.57	3.0	3.89

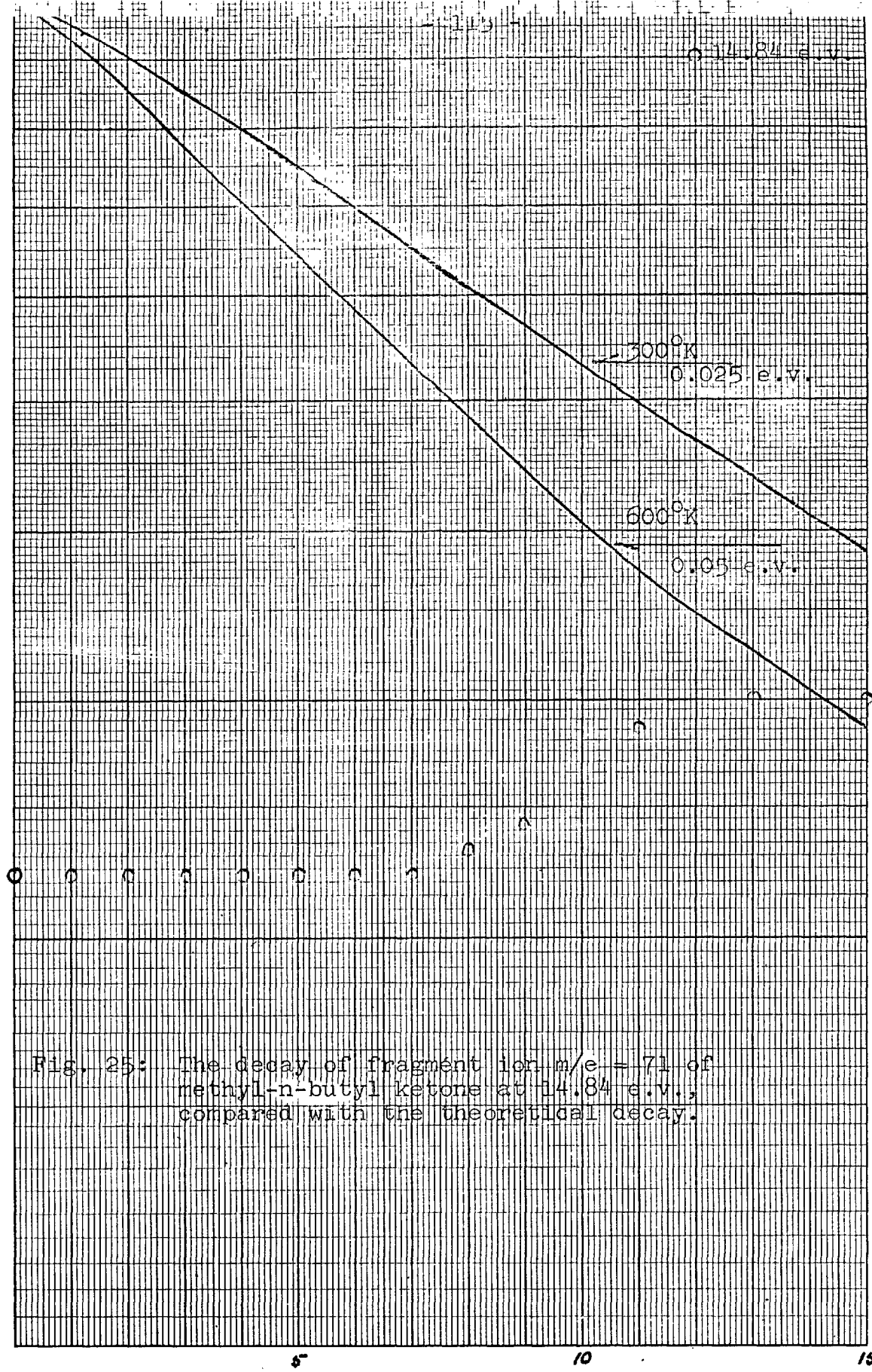


Fig. 25: The decay of fragment ion m/e = 71 of methyl-n-butyl ketone at 14.84 e.v., compared with the theoretical decay.

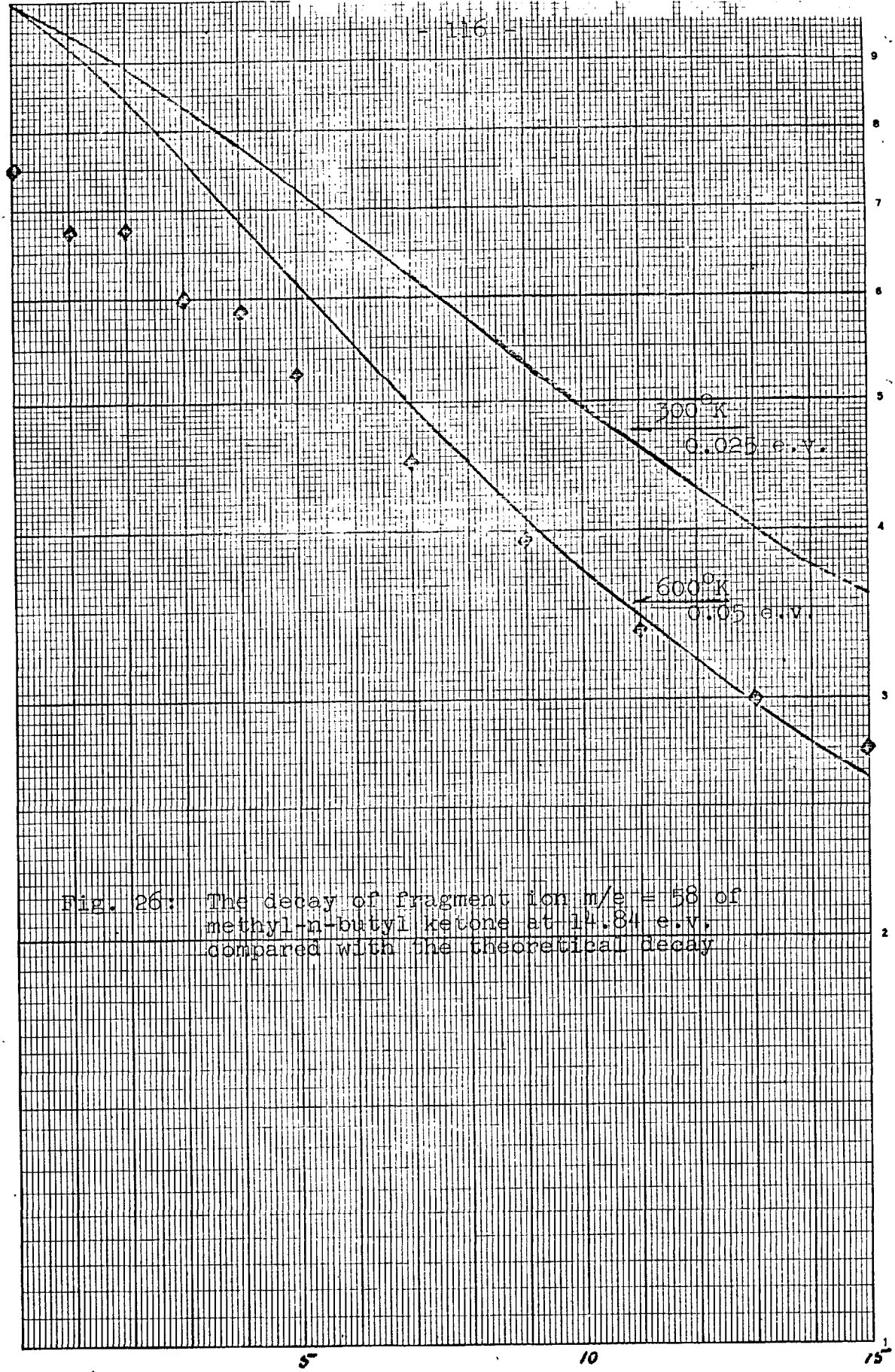


Fig. 26: The decay of fragment ion m/e = 58 of methyl-n-butyl ketone at 14.84 e.V. compared with the theoretical decay

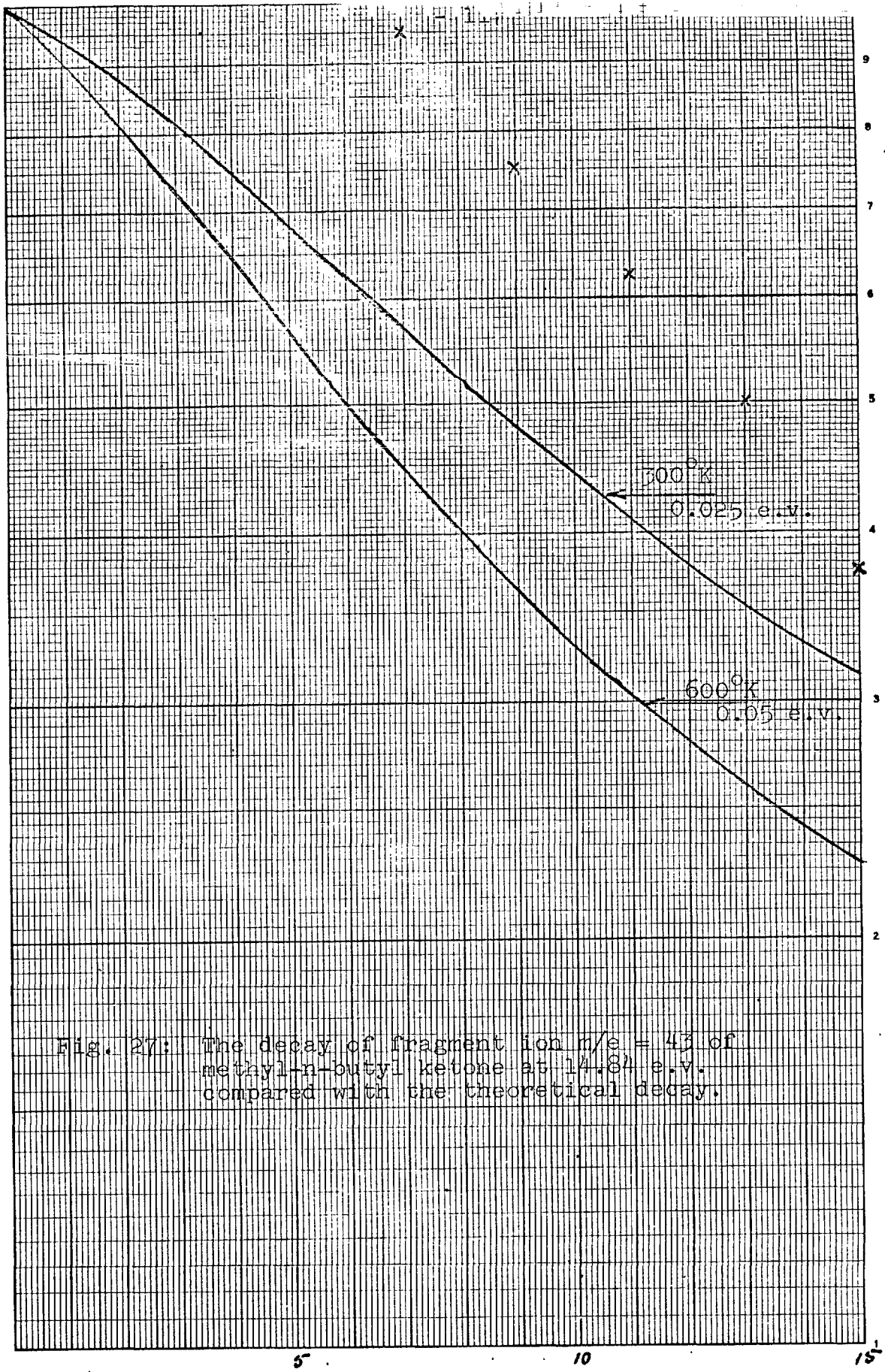


Fig. 27: The decay of fragment ion m/e = 43 of methyl-n-butyl ketone at 14.84 e.v. compared with the theoretical decay.

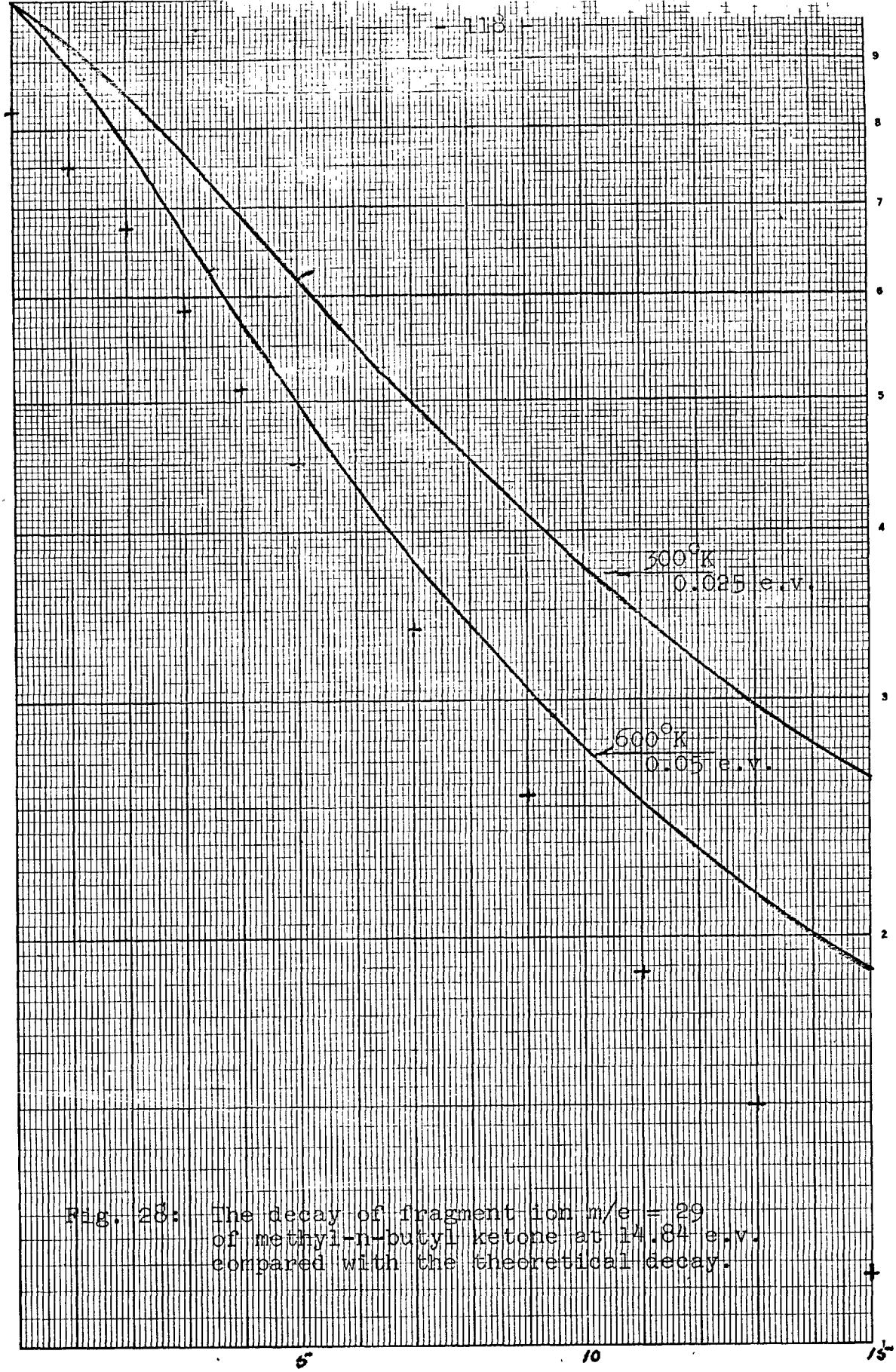


Fig. 28: The decay of fragment ion m/e = 29 of methyl-n-butyl ketone at 14.84 e.v. compared with the theoretical decay.

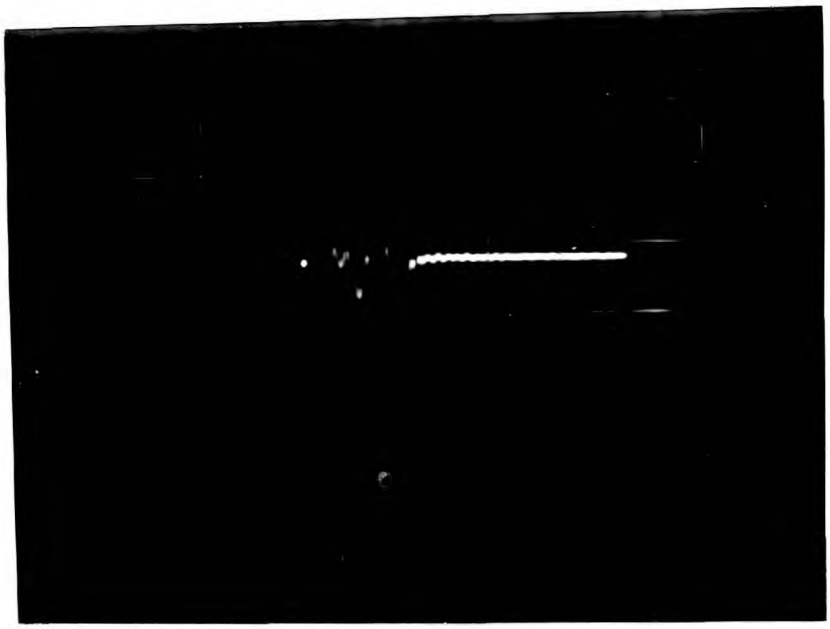


Fig. 29. Oscillogram of the mass spectrum of acetaldehyde at 14.84 e.v. with zero time delay between ionization and acceleration, left to right masses: 15, 29 and 44.

TABLE 7. CHANGE OF THE RELATIVE ABUNDANCE OF IONS FROM ACETALDEHYDE WITH DELAY TIME AT 14.84 e.v. (835.29 A°)

Delay time in Microseconds	Ion Peak at m/e =					
	EXP. 15(F)	CALC. 15(F)	EXP. 29(F)	CALC. 29(F)	EXP. 44M	CALC. 44(M)
			x3		x3	
0	3.9	9.99	8.0	9.99	6.00	9.99
1	3.6	8.91	7.12	9.21	6.25	9.36
2	3.187	7.83	6.5	8.43	6.50	8.73
3	2.7	6.76	5.75	7.65	6.75	8.09
4	2.25	5.80	4.62	6.89	7.	7.46
5	1.87	5.00	3.87	6.17	6.75	6.84
6	1.50	4.35	3.25	5.53	6.50	6.26
7	1.2	3.84	2.62	4.97	6.25	5.72
8	0.937	3.42	2.12	4.50	6.	5.24
9	-	3.08	1.87	4.10	5.75	4.82
10	-	2.80	1.5	3.75	5.5	4.45
11	-	2.57	1.25	3.46	5.25	4.12
12	-	2.37	1.0	3.20	5.	3.84
13	-	2.19	-	2.98	4.75	3.58
14	-	2.04	-	2.79	4.62	3.36
15		1.91		2.61	4.5	3.16

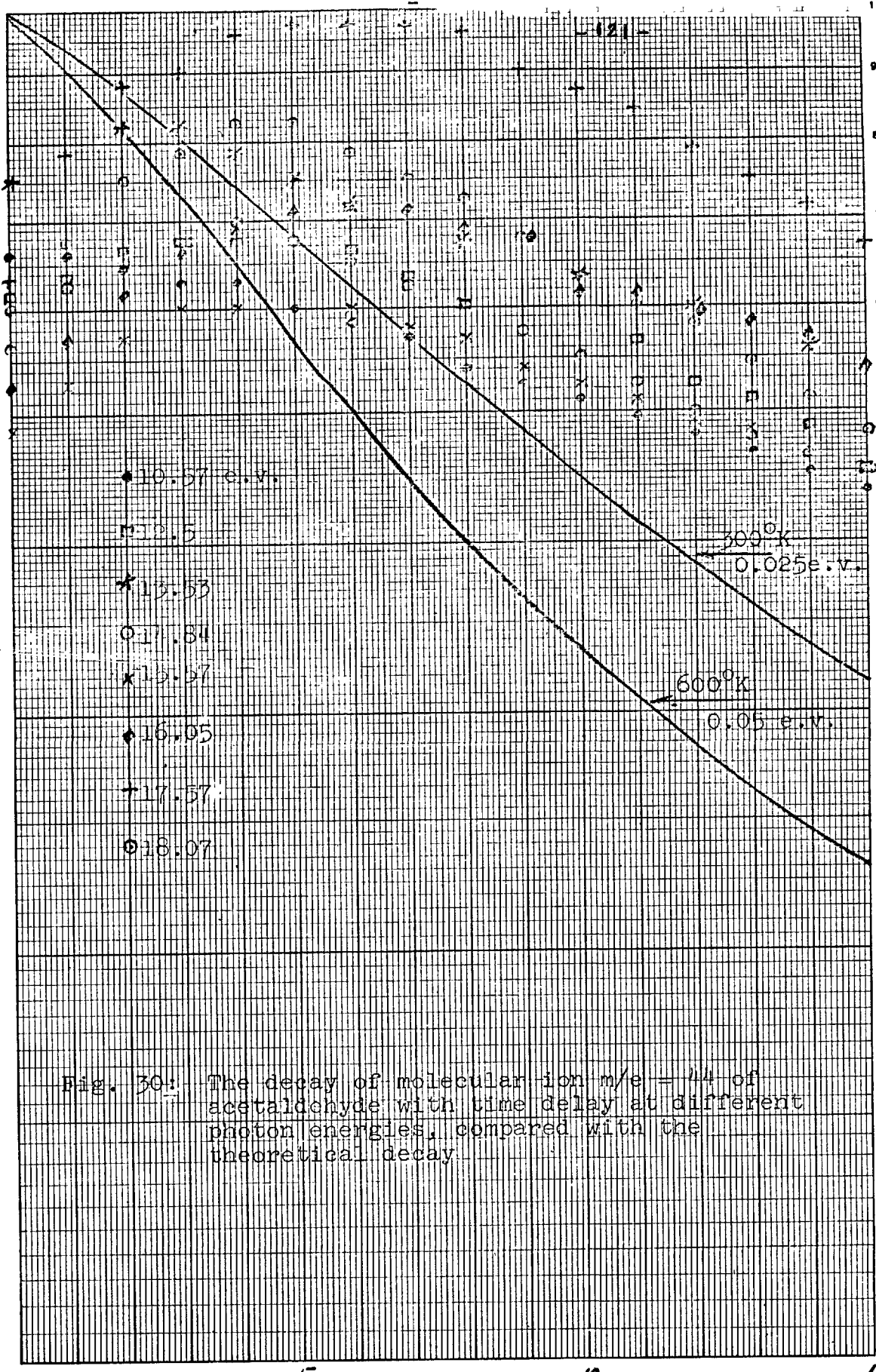


Fig. 30: The decay of molecular ion m/e = 44 of acetaldehyde with time delay at different photon energies, compared with the theoretical decay.

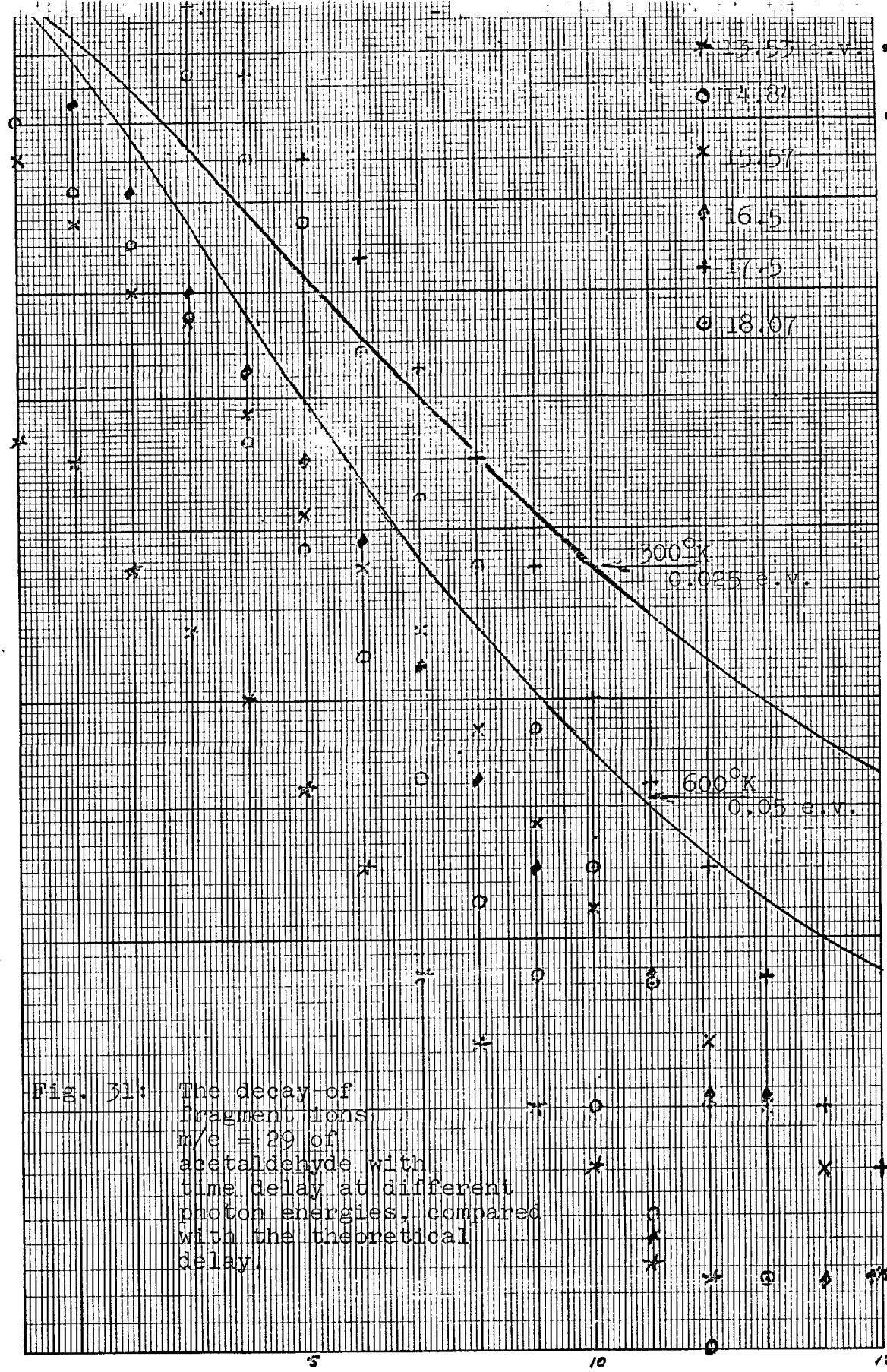


Fig. 31: The decay of fragment ions m/e = 29 of acetaldehyde with time delay at different photon energies, compared with the theoretical delay.

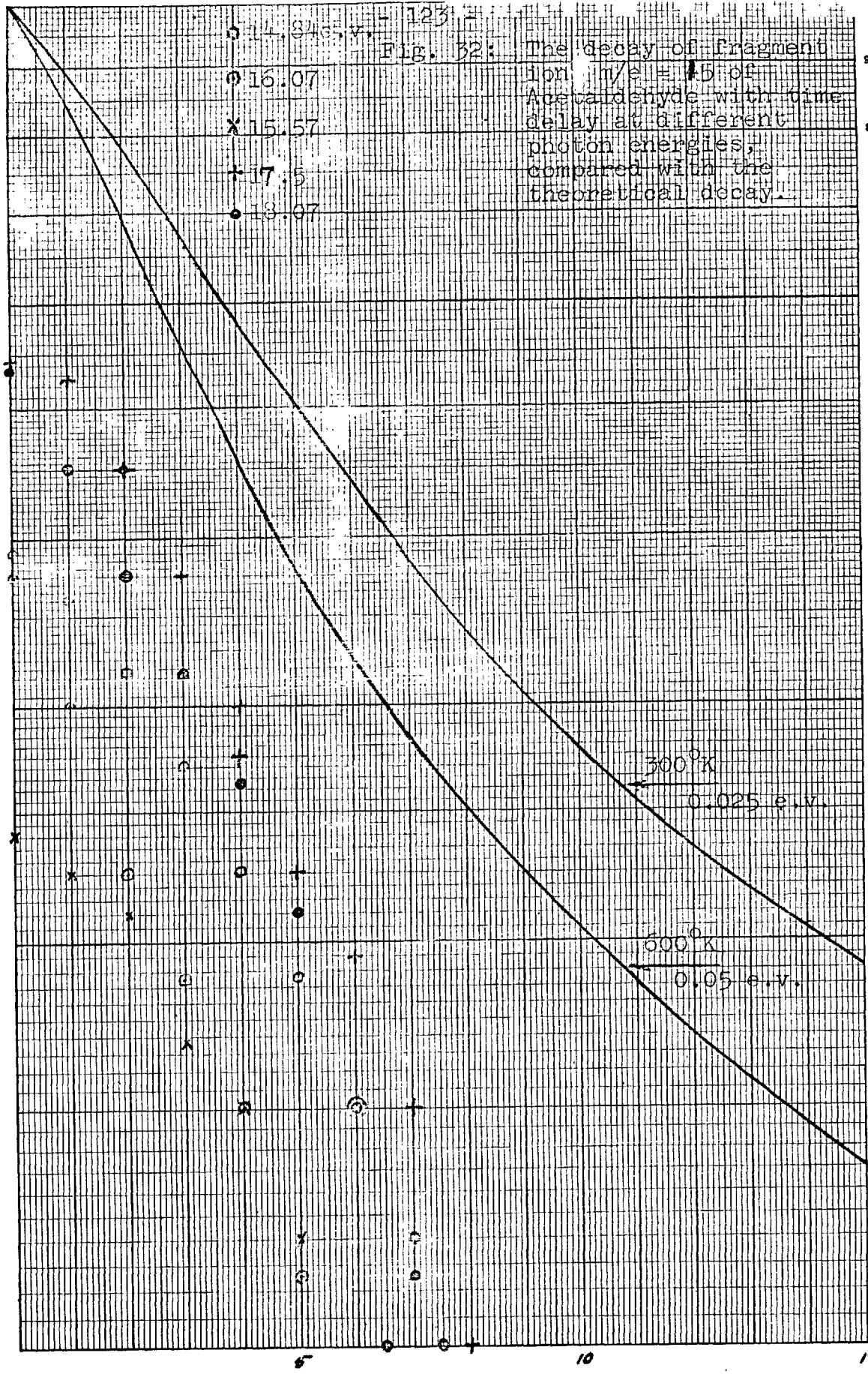


Fig. 32: The decay of fragment ion m/e = 45 of Acetaldehyde with time delay at different photon energies, compared with the theoretical decay.

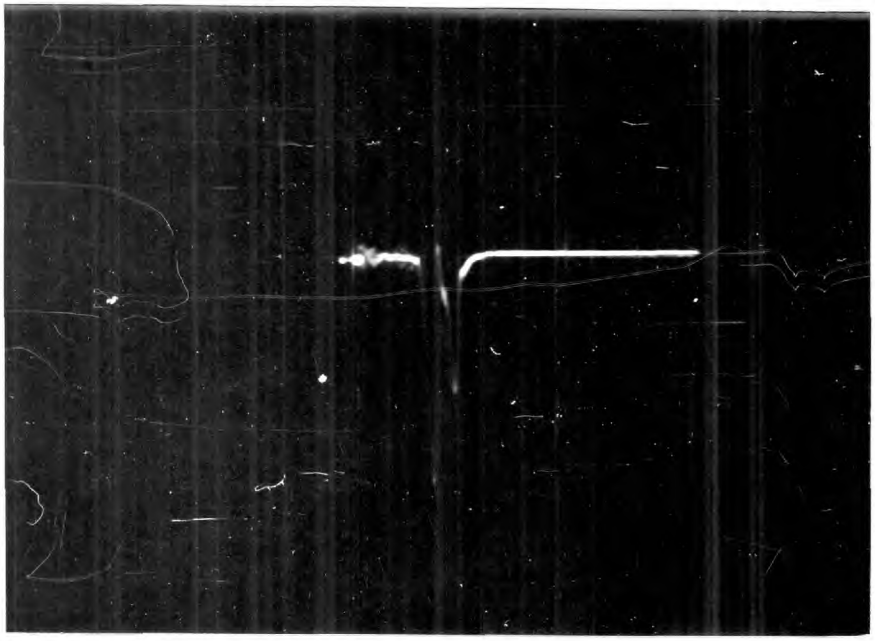


Fig. 33. Oscillogram of the mass spectrum of n-propane at 14.84 e.v. with zero time delay between ionization and acceleration, left to right masses, 29 and 44

TABLE 8. CHANGE OF THE RELATIVE ABUNDANCE OF IONS FROM n-PROPANE WITH DELAY TIME AT 14.84 e.v.(835.29 A°)

Delay time in Microseconds	Ion Peak at m/e =			
	EXP. 29(F)	CALC. 29(F)	EXP. 44(M)	CALC. 44(M)
	x3			
0	9.6	9.99	9.75	9.99
1	9	9.21	10.5	9.36
2	8.4	8.43	10.12	8.73
3	7.8	7.65	10.12	8.09
4	7.5	6.89	9.75	7.46
5	6.9	6.17	9.75	6.84
6	6.	5.53	9.	6.26
7	5.4	4.97	8.85	5.72
8	4.8	4.50	8.62	5.24
9	4.2	4.10	8.25	4.82
10	4.05	3.75	7.87	4.45
11	3.6	3.46	7.57	4.12
12	3.3	3.20	7.12	3.84
13	3.	2.98	7.12	3.58
14	2.7	2.79	6.75	3.36
15	2.55	2.61	6.375	3.16

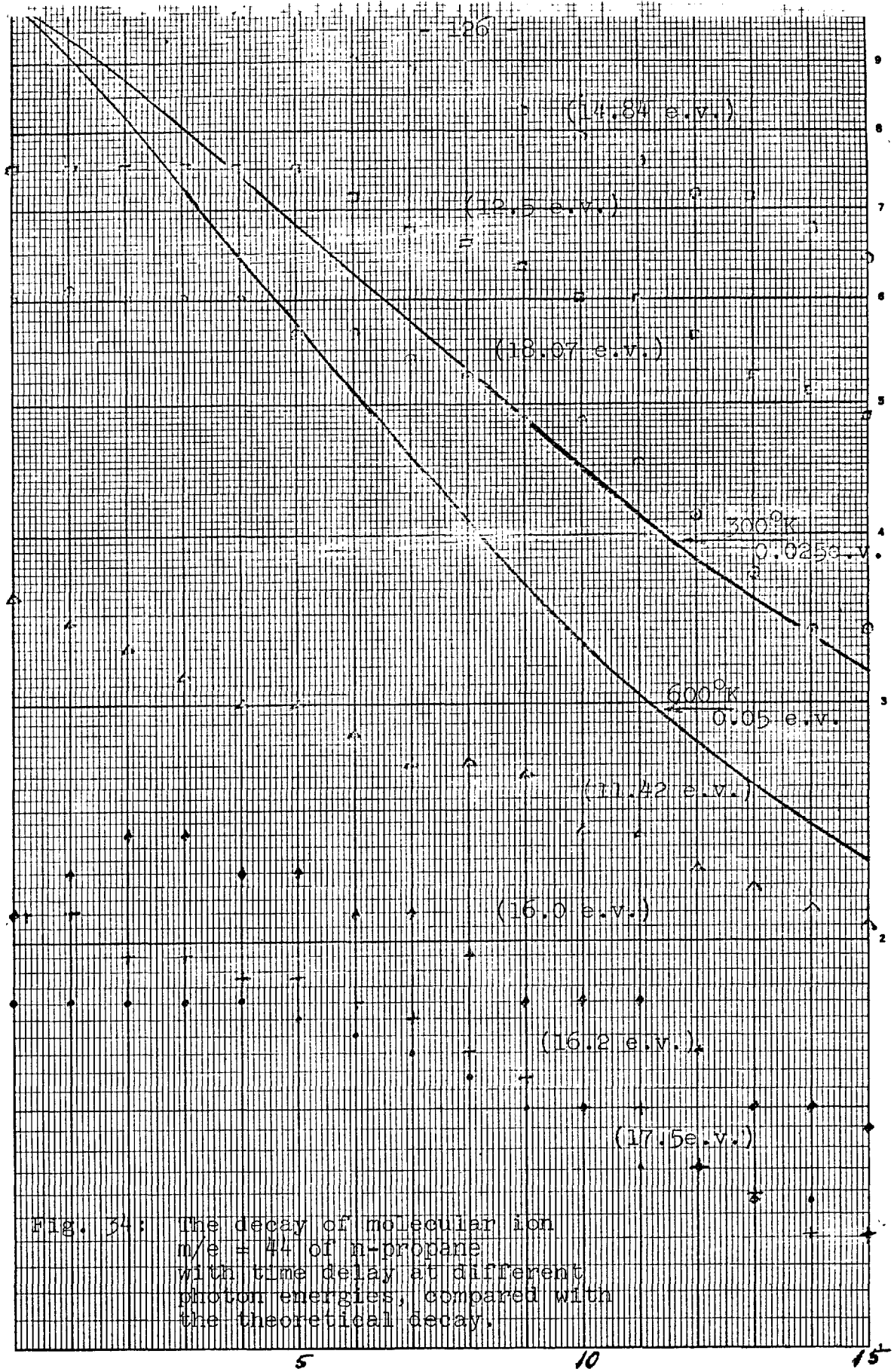


Fig. 54: The decay of molecular ion m/e = 44 of n-propane with time delay at different photon energies, compared with the theoretical decay.

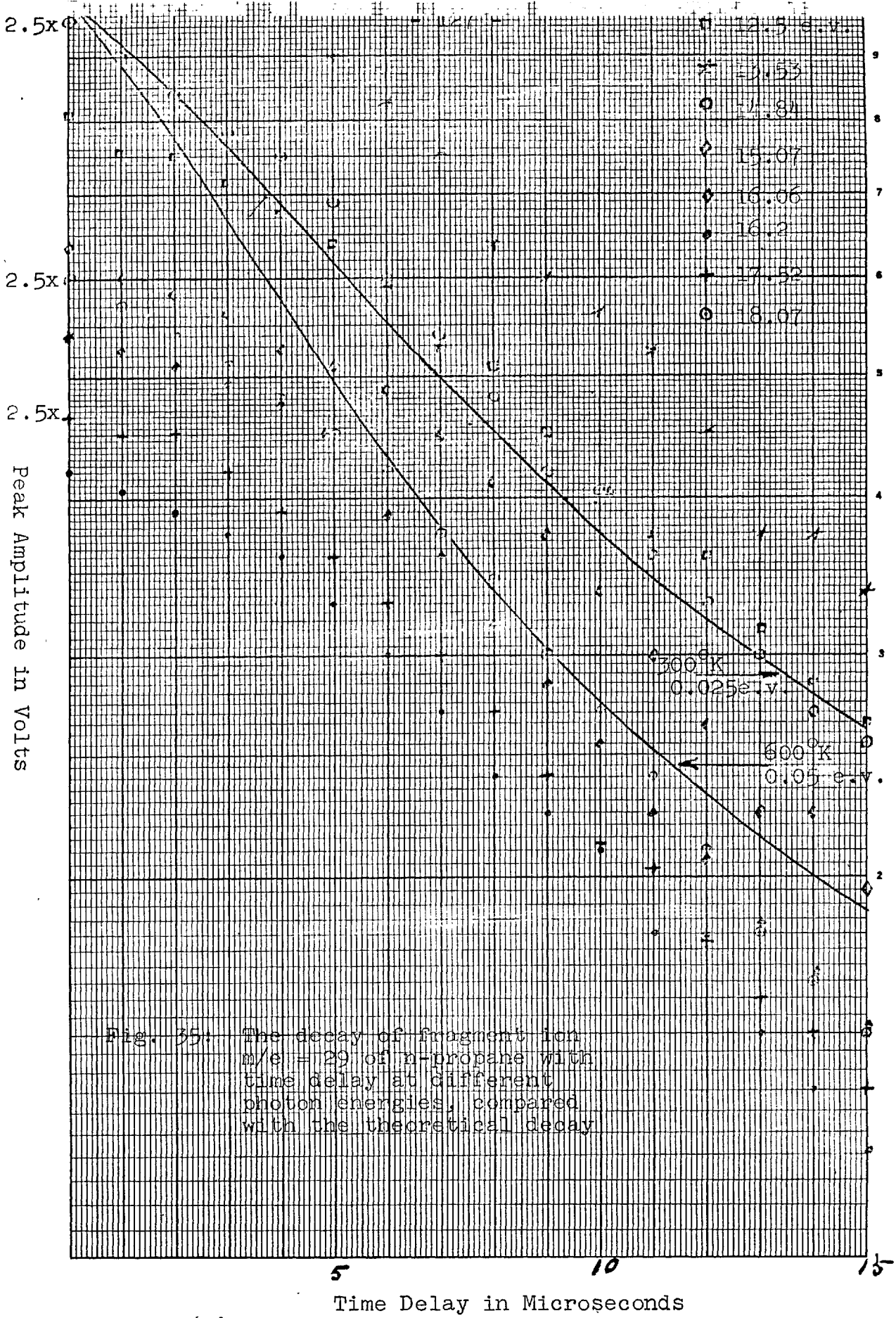


Fig. 35: The decay of fragment ion m/e = 29 of n-propane with time delay at different photon energies, compared with the theoretical decay

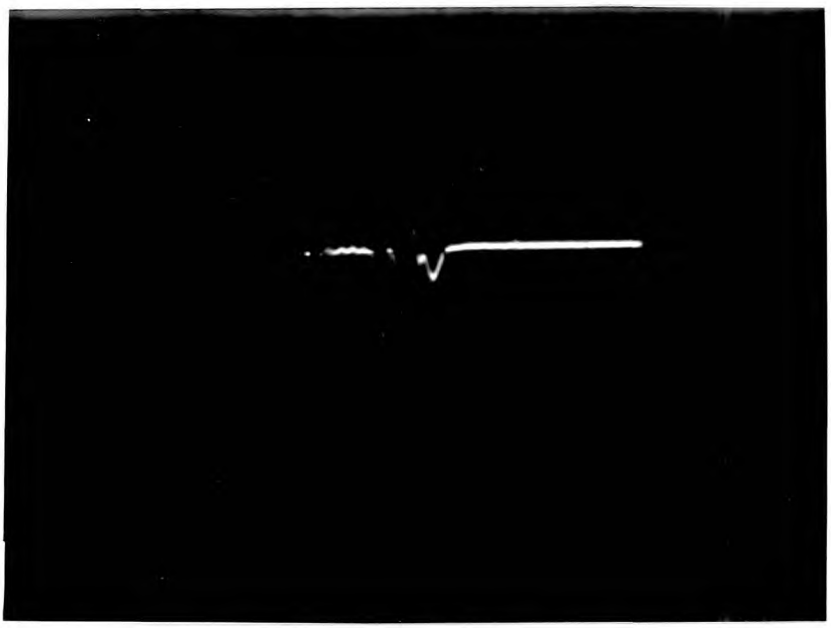


Fig. 36. Oscillogram of the mass spectrum of n-butane at 14.84 e.v. with zero time delay between ionization and acceleration, left to right masses: 27, 43 and 58

TABLE 9. CHANGE OF THE RELATIVE ABUNDANCE OF IONS FROM n-BUTANE WITH DELAY TIME AT 14.84 e.v.(835.29 A°)

Delay time in Microseconds	Ion Peak at m/e =					
	EXP. 29(F)	CALC. 29(F)	EXP. 43(F)	CALC. 43(F)	EXP. 58(M)	CALC. 58(M)
			x10			
0	13	9.99	3.5	9.99	5.	9.99
1	14	9.21	3.5	9.36	6.	9.44
2	13	8.43	3.4	8.71	6.	8.89
3	12.	7.65	3.3	8.07	6.	8.34
4	11	6.89	3.3	7.43	5.8	7.79
5		6.17		6.81		7.24
6	10	5.53	3.1	6.22	5.2	6.71
7	8	4.97	2.9	5.68	5.	6.20
8	7	4.50	2.6	5.20	5.	5.74
9	6	4.10	2.4	4.78	4.5	5.31
10	5	3.75	2.2	4.41	4.3	4.94
11	4.5	3.48	2.	4.08	4.2	4.60
12	4	3.20	1.7	3.80	4.	4.30
13	3.5	2.98	1.6	3.55	3.8	4.03
14	3	2.79	1.4	3.33	3.8	3.79
15	2.5	2.61	1.3	3.13	3.5	3.57

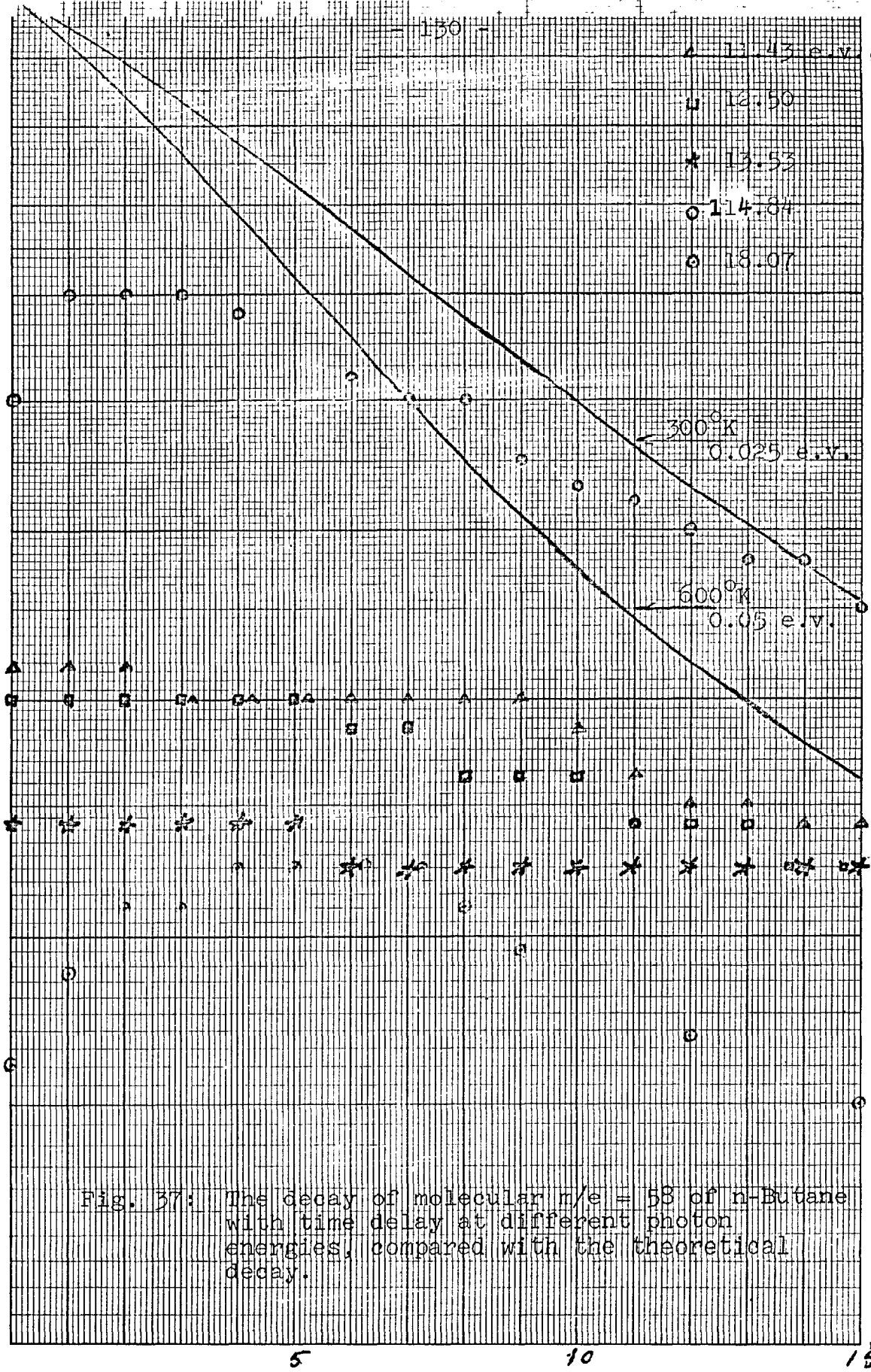


Fig. 37: The decay of molecular m/e = 58 of n-Butane with time delay at different photon energies, compared with the theoretical decay.

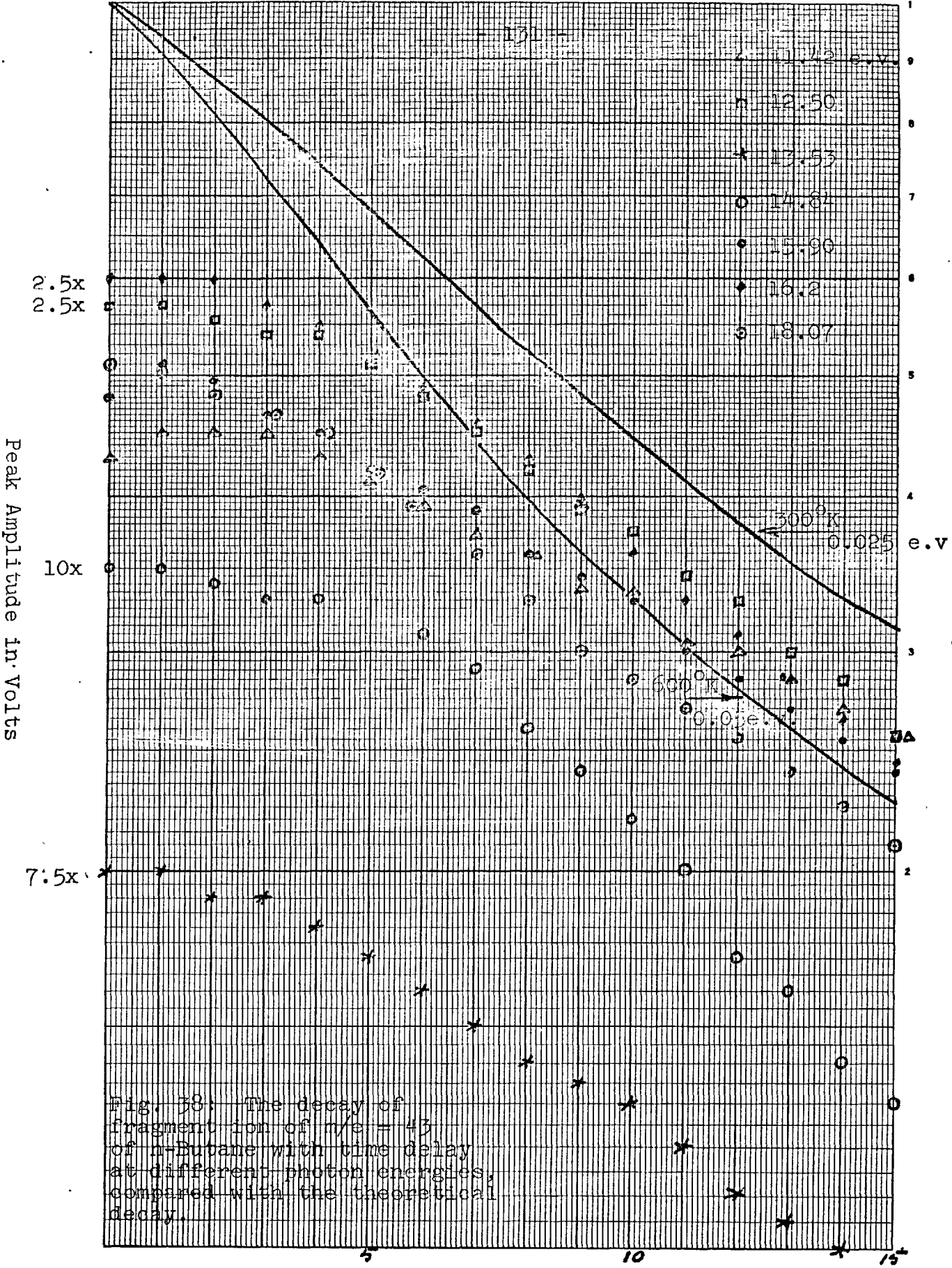


Fig. 38: The decay of fragment ion of m/e = 43 of n-Butane with time delay at different photon energies, compared with the theoretical decay.

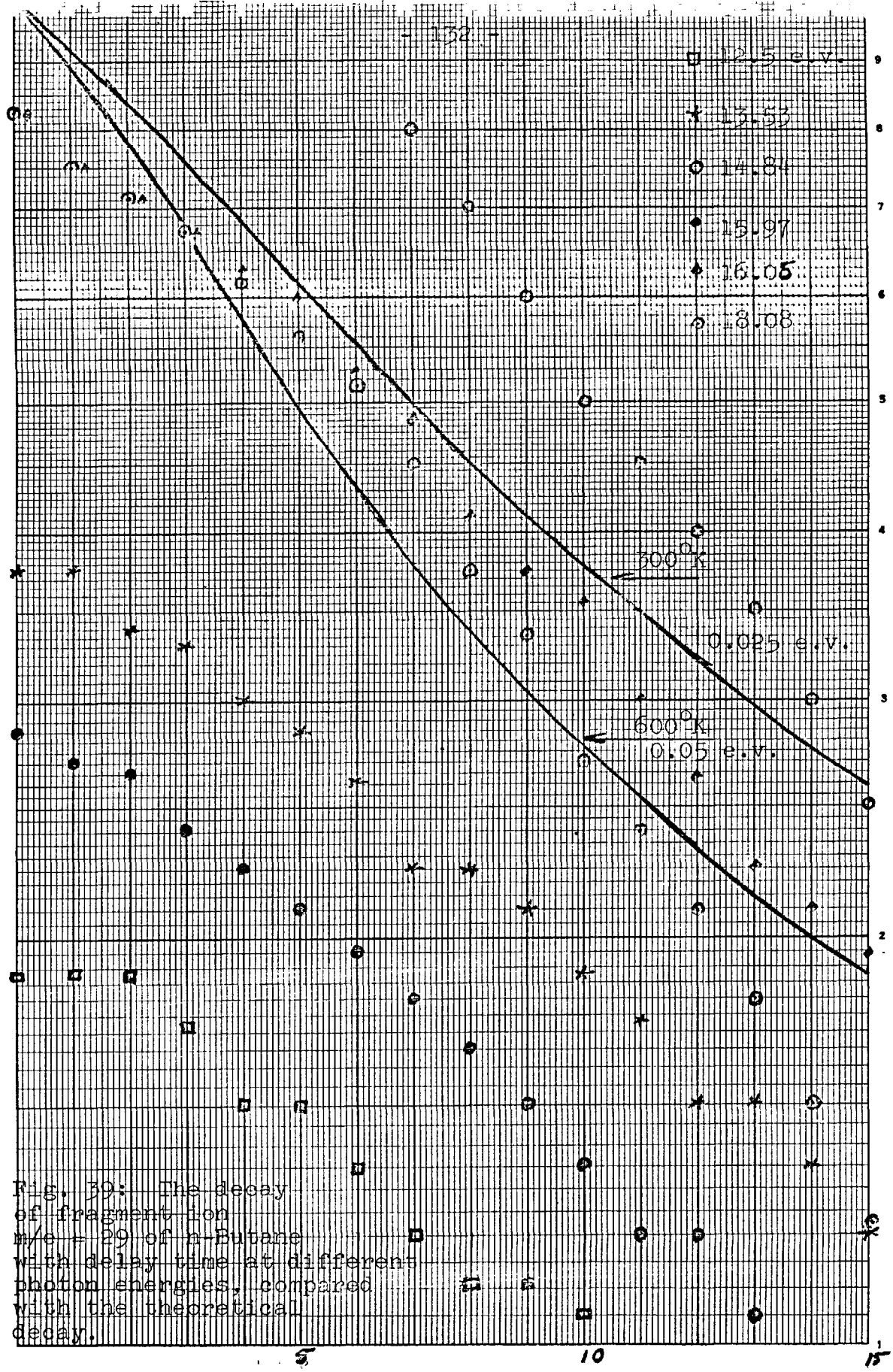


Fig. 39: The decay of fragment ion m/e = 29 of n-Butane with delay time at different photon energies, compared with the theoretical decay.

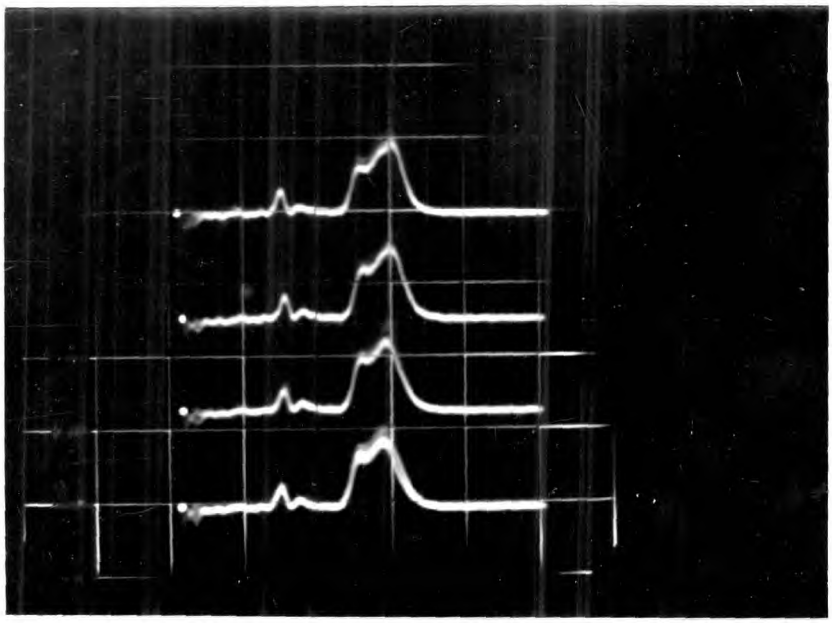


Fig. 40. Oscillogram of the mass spectrum of benzene at 14.84 e.v.; left to right masses: 51 and 78: down to up 0; 1; 2 and 3 μ second time delay

TABLE 10. CHANGE OF THE RELATIVE ABUNDANCE OF IONS FROM BENZENE WITH DELAY TIME AT 14.84 e.v.(835.29 A°)

Delay time in Microseconds	Ion Peak at m/e =			
	EXP. 51(F)	CALC. 51(F)	EXP. 78(M)	CALC. 78(M)
0	1.5	9.99	6.	9.99
1	1.5	9.41	6.	9.52
2	1.5	8.82	6.15	9.04
3	1.5	8.23	6.37	8.57
4	0.937	7.64	6.37	8.09
5	0.825	7.06	6.37	7.62
6	0.825	6.05	7.12	7.15
7	0.825	5.98	7.12	6.69
8	0.825	5.51	7.5	6.25
9	0.825	5.08	7.5	5.84
10	0.75	4.71	7.5	5.47
11	0.75	4.37	7.85	5.12
12	0.75	4.08	7.87	4.81
13	0.75	3.82	7.87	4.53
14	0.75	3.58	7.5	4.27
15	0.75	3.37	7.5	4.04

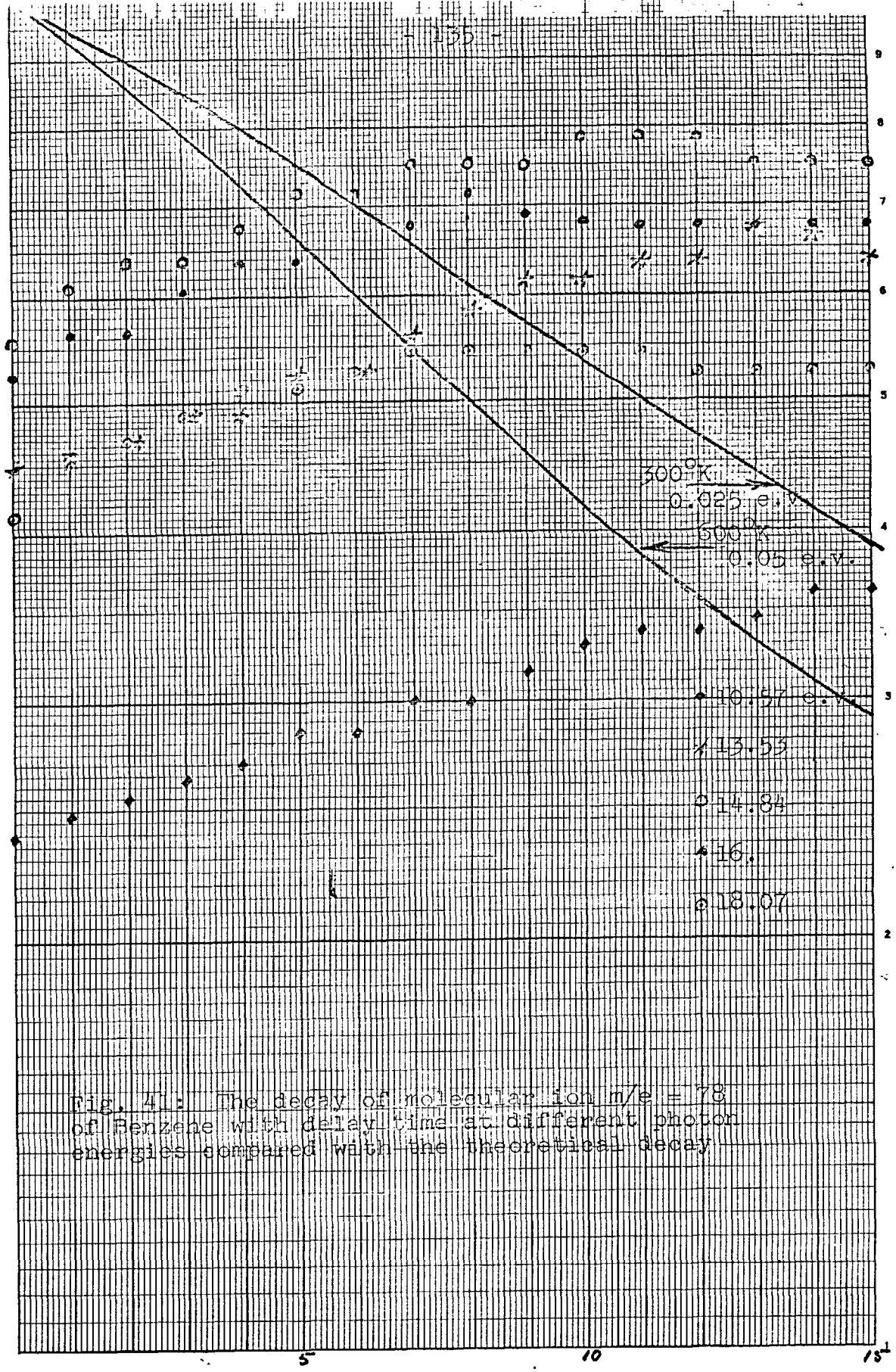


Fig. 41. The decay of molecular ion m/e = 78 of Benzene with delay time at different photon energies compared with the theoretical decay

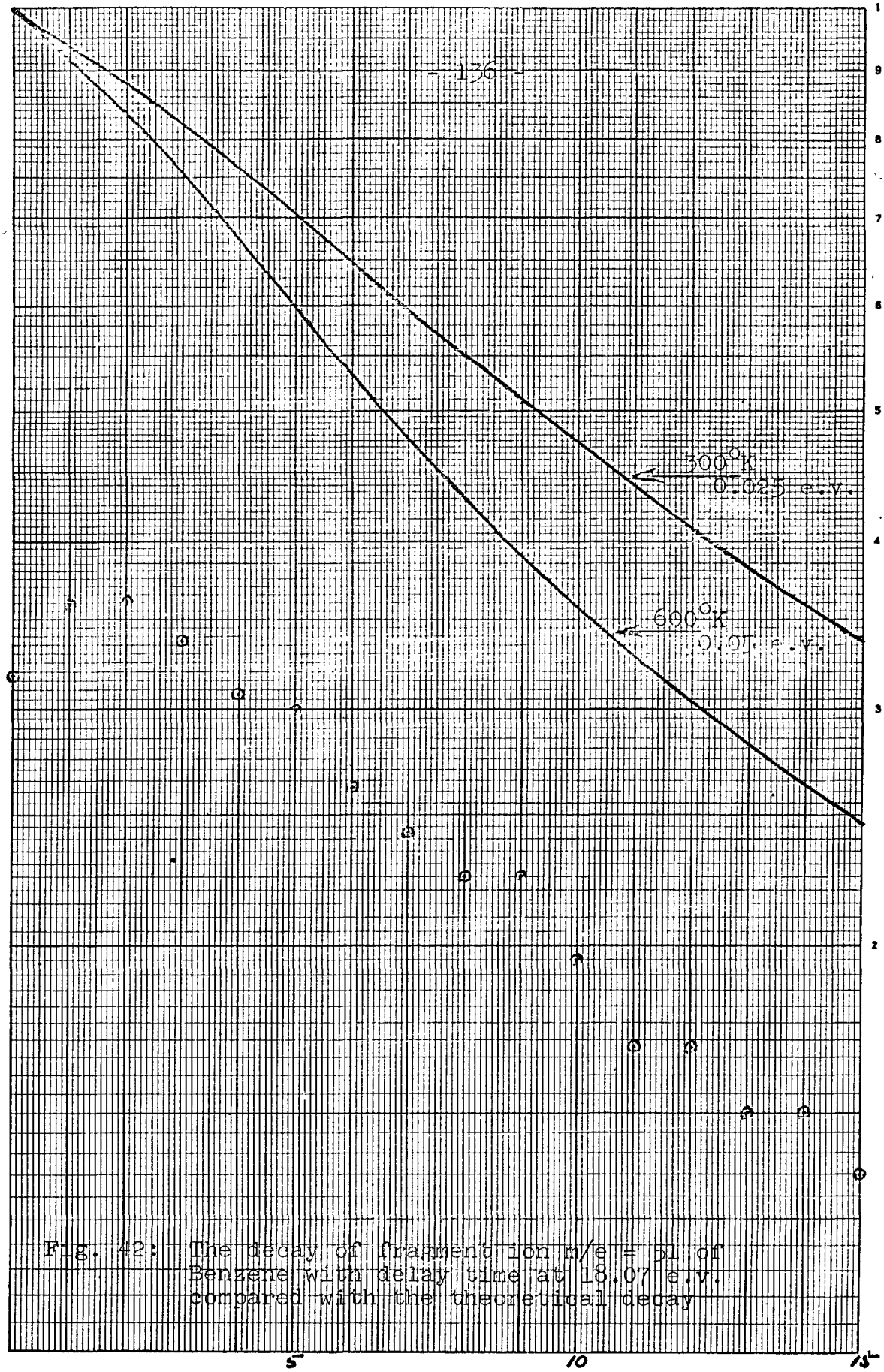


Fig. 42: The decay of fragment ion m/e = 51 of Benzene with delay time at 18.07 e.v. compared with the theoretical decay

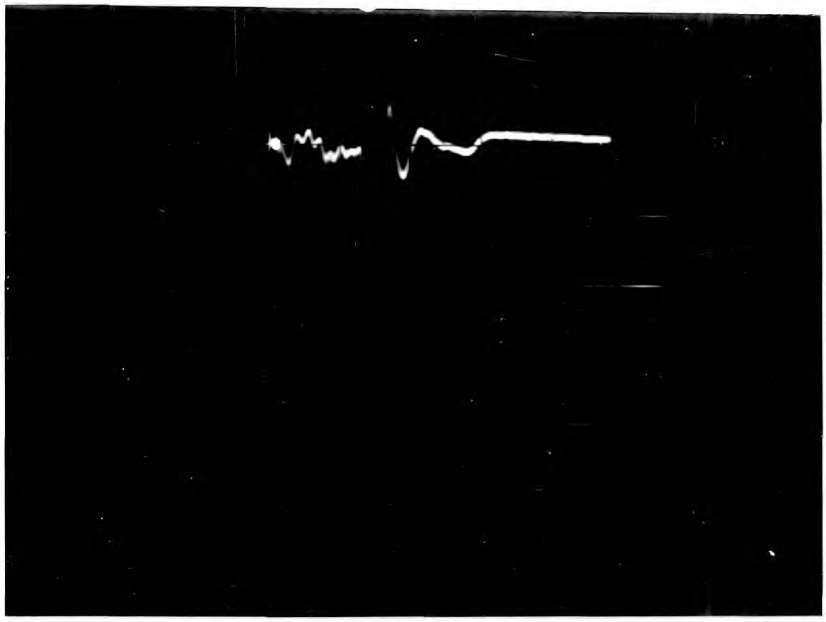


Fig. 43. Oscillogram of the mass spectrum of monobromobenzene at 14.84 e.v., with zero time delay between ionization and acceleration; left to right masses, 28, 43, 58 and 77; the peak at 28, 43 and 58 were caused by acetone trace in the ionization chamber.

TABLE 11. CHANGE OF THE RELATIVE ABUNDANCE OF IONS FROM BROMOBENZENE WITH DELAY TIME AT 14.84 e.v. (835.29 A°)

Delay time in Microseconds	Ion Peak at m/e =	
	EXP. 77(F)	CALC. 77(F)
0	2.3	9.99
1	2.3	9.52
2	2.25	9.04
3	=	8.56
4	=	8.08
5	2.2	7.60
6	2.	7.13
7	1.87	6.67
8	-	6.23
9	1.5	5.82
10	1.35	5.44
11	1.2	5.10
12	1.12	4.79
13	1.	4.51
14	1.	4.25
15	1.	4.02

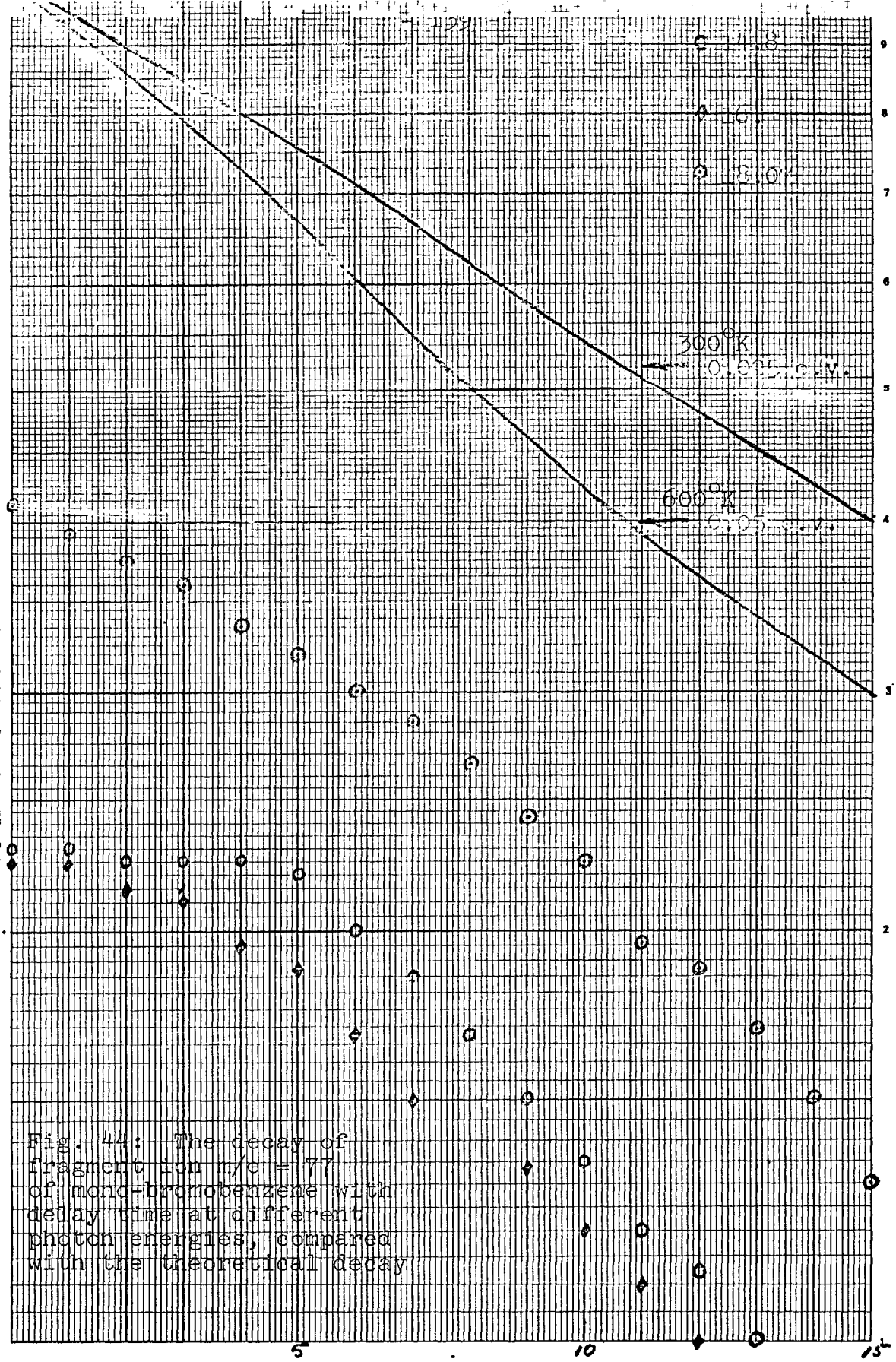


Fig. 44: The decay of fragment ion m/e = 77 of mono-bromobenzene with delay time at different photon energies, compared with the theoretical decay

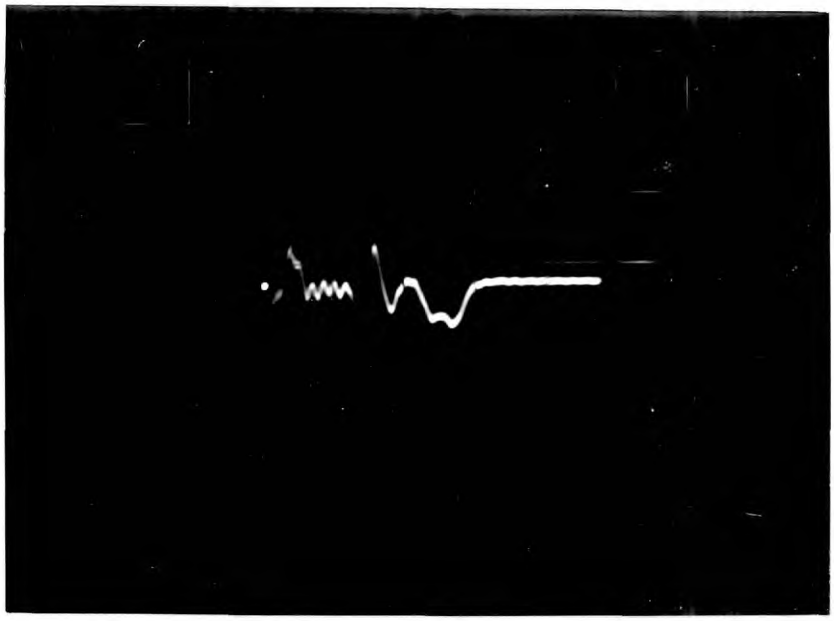


Fig. 45. Oscillogram of the mass spectrum of monoiodobenzene at 14.84 e.v. with zero time delay between ionization and acceleration; left to right masses: 28, 43, 58 and 77. The peak at 28, 43 and 58 were caused by acetone trace in the ionization chamber.

TABLE 12. CHANGE OF THE RELATIVE ABUNDANCE OF IONS FROM IODO-BENZENE WITH DELAY TIME AT 1 484 e.v. (835.29 A°)

Delay time in Microseconds	Ion Peak at m/e =			
	EXP. 51(F)	CALC. 51(F)	EXP. 77(F)	CALC. 77(F)
0	4.	9.99	6.5	9.99
1	4.	9.41	6.25	9.52
2	3.8	8.82	5.7	9.04
3	3.6	8.23	5.25	8.57
4	3.4	7.64	5	8.09
5	3.25	7.06	4.5	7.62
6	3.25	6.50	4.	7.15
7	2.9	5.98	3.8	6.69
8	2.9	5.51	3.5	6.25
9	2.6	5.08	3.2	5.84
10	2.6	4.71	3.	5.47
11	2.5	4.37	2.7	5.12
12	2.25	4.08	2.5	4.81
13	2.1	3.82	2.25	4.53
14	2.	3.58	2.	4.27
15	2.	3.37	2.	4.04

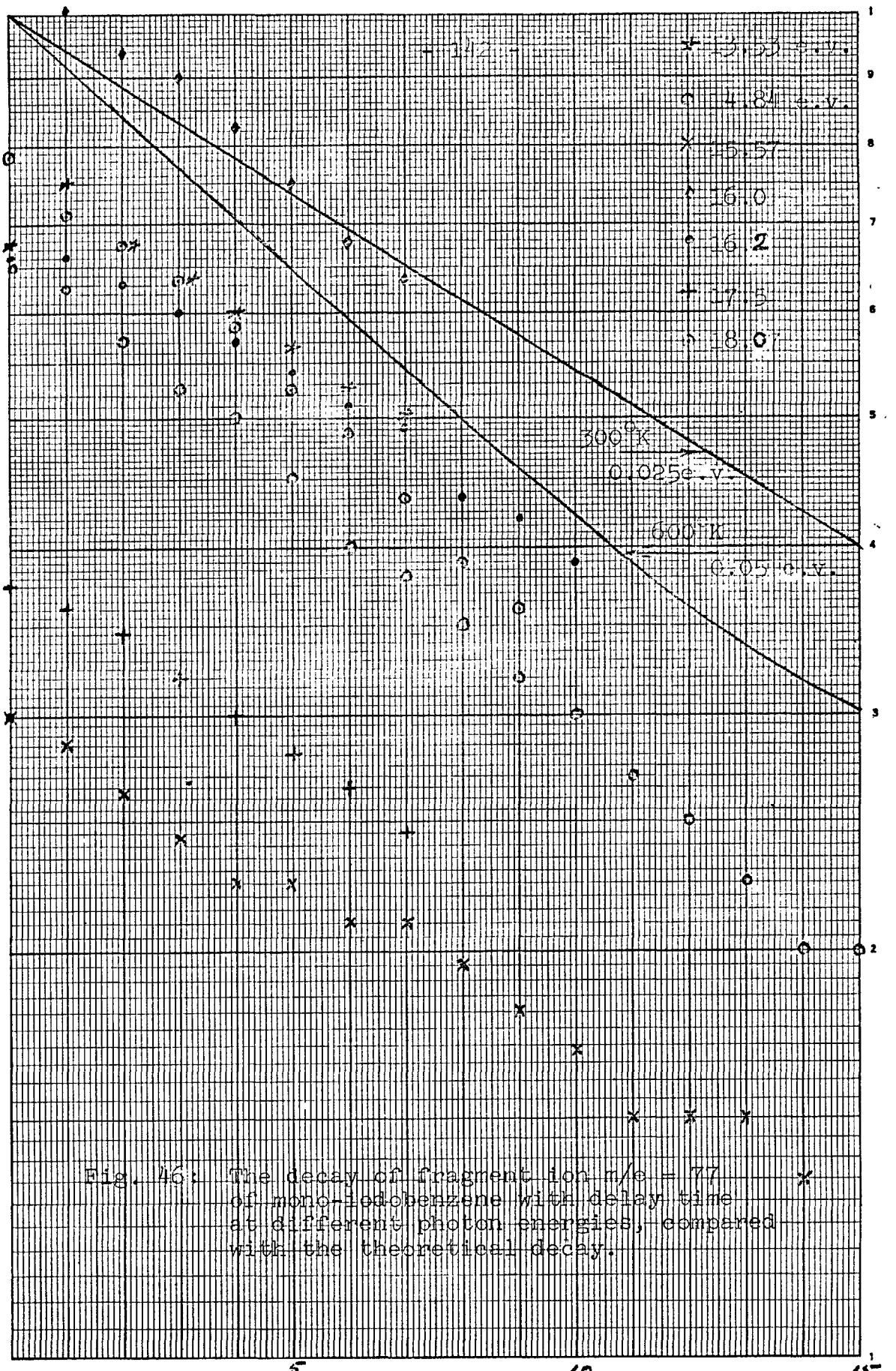


Fig. 46: The decay of fragment ion m/e = 77 of mono-iodobenzene with delay time at different photon energies, compared with the theoretical decay.

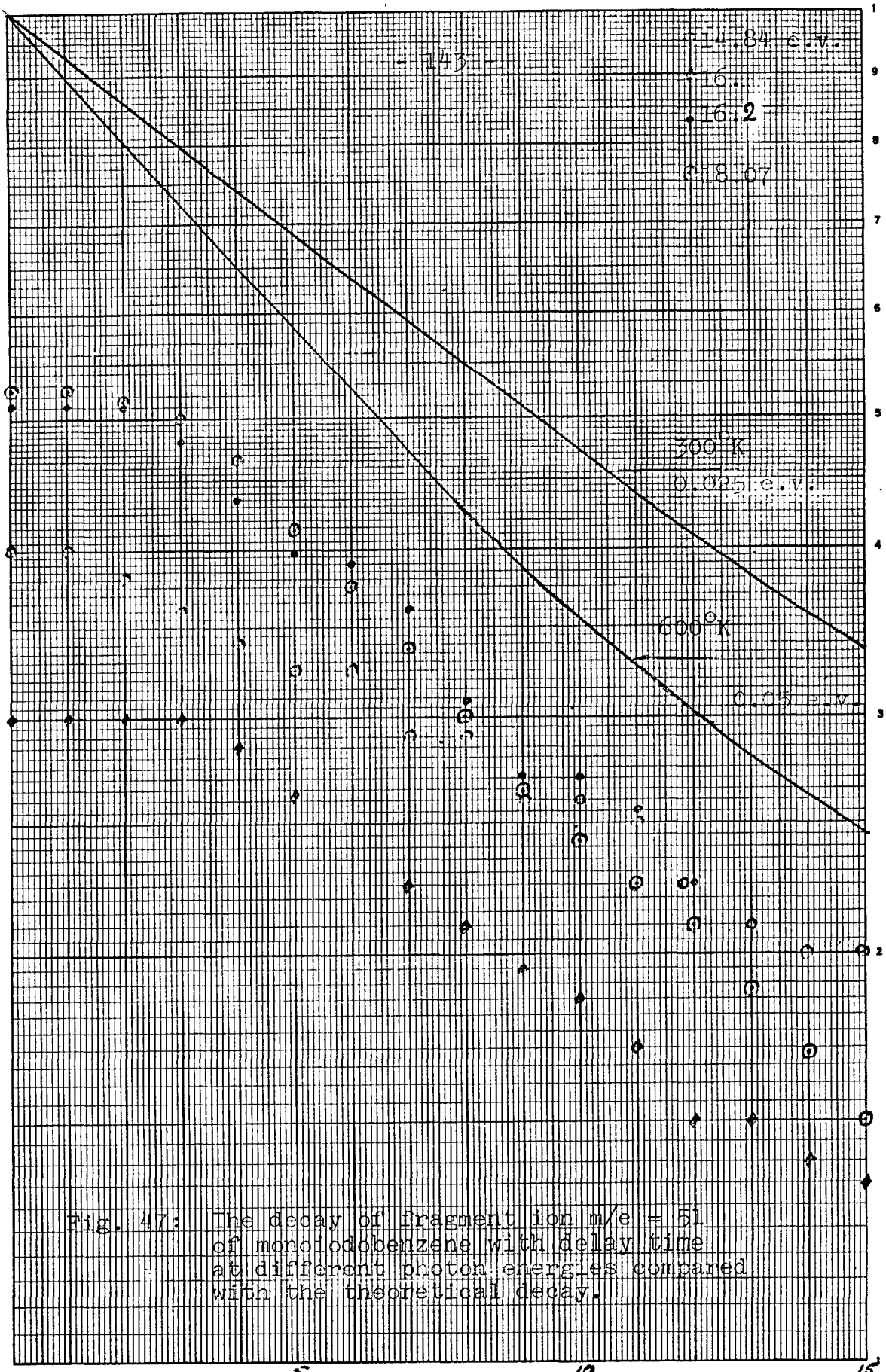


Fig. 47. The decay of fragment ion m/e = 51 of monoiodobenzene with delay time at different photon energies compared with the theoretical decay.

2.1 Effect of Pressure

A study was made to investigate the effect of sample pressure in the ionization chamber on the decay of ions. The results are shown in Figs. 14 and 15. The plot of the logarithm of the peak height *vs* delay time for both fragment and molecular ions at low pressures was linear up to seven microns. This was expected since all the ions are formed by a simple photon-molecule interaction.

At pressures higher than 7 microns - it was checked up to 17 microns only - the slope of the curve increases up to 10 microseconds, then decreases nearly linearly. The sharp decrease in peak height at high pressures must arise from ion-molecule collision in the ionization chamber and drift tube.

It was also observed that the spectrum peaks were broadened and a tail on the high mass side of intensity *vs* mass peaks. This must be due to collisions. Therefore about 3 microns gas pressure was used in the ionization chamber throughout the work to obtain a relatively collision free region.

2.2. Effect of Time Delay

The curves in figures (14, 15, 17, 18, 20-23, 25-28, 30-32, 34, 36, 37-39, 41-42, 44, 46, 47) were constructed to aid in the interpretation of data; to obtain decay constants (from half-life of the molecular and fragment ions) when appropriate. These experimental decay curves were all made at room temperature taken as 300K° but at different photon energies. Two theoretical curves are shown - solid lines - one for room temperature 300°K and the other for an elevated temperature, 600°K, but unfortunately for not all the fragment ions in table (3), especially those with small mass. In these cases decay curves could not be plotted because of the low intensity of their peaks. However, these fragments were relatively weak.

Several interesting points may be made concerning these decay curves:-

A. The apparent splitting in peak m/e = 78 of the benzene molecular ion Fig. 40 and the peak at m/e = 77 in the mass spectrum of monobromobenzene and monoiodobenzene Figs. 43 and 45, was probably associated with the poor resolving power of the instrument for masses heavier than 70 a.m.u., when operated with constant momentum, i.e. accelerating the ions by pulsed voltage (see 2.2).

It could also be caused by the negative going tail

of the accelerating voltage pulse since it has not properly rectangular positive shape (see Chapter 4 of part A and Appendix 4). This negative voltage tail will impart a negative momentum at the end of the positive momentum which could cause peak broadening and would have been the cause for the nonlinearity in TOF - m/e scale beyond 70 a.m.u.

B. In none of the spectra obtained was evidence found for any long lived metastable species. If there were any the resultant peaks were too small to be observed directly.

C. The rate of decay is greater as the mass of the fragment decreases. This was in good agreement with the theoretical calculations made in section 1.3 of this part, Fig. 48. This undoubtely was due to the greater migration or diffusion rate for ions with low mass than with larger ones. The rate of decay can be associated with the kinetic energy of dissociation, the smaller the mass of the fragment, the larger the amount of kinetic energy it possesses. This agrees with the principle of conservation of momentum, where the kinetic energy will be partitioned between the neutral (radical) and fragment ions in inverse proportion to their respective masses.

D. On inspection of the decay curves it will be noticed that few fragment ions appear to possess excess kinetic energy and for most fragment ions this was less than or

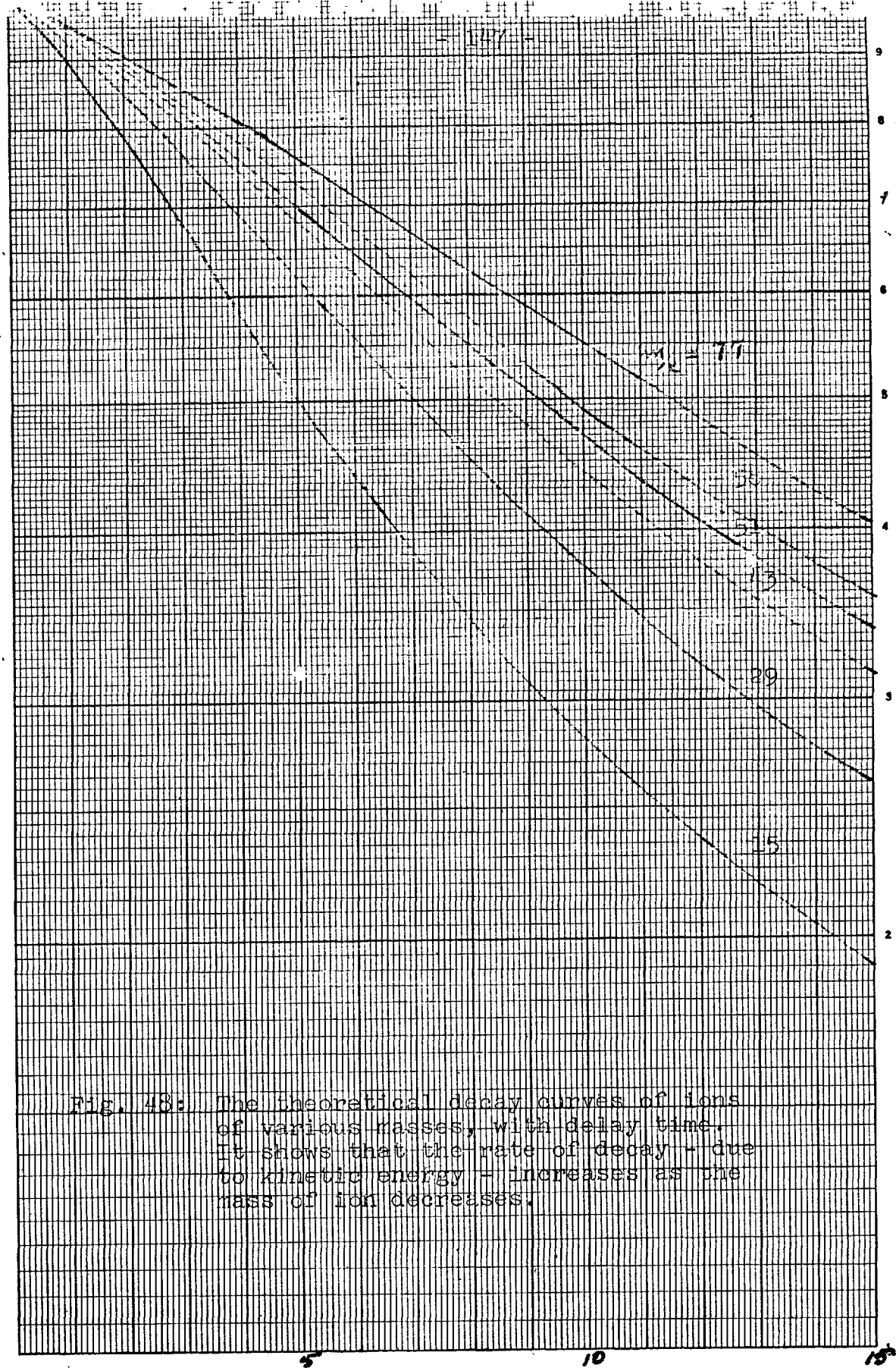


Fig. 48: The theoretical decay curves of ions of various masses, with delay time. It shows that the rate of decay - due to kinetic energy - increases as the mass of ion decreases.

equal to 0.05 e.v., except fragment ion m/e = 15 of acetaldehyde (Fig. 32) which had kinetic energy slightly above this level.

E. Similar fragment ions from different compounds have the same rate of decay such as m/e 29, or 43 Figs. 22 and 23, from methyl-ethyl ketone and from methyl-n-butyl ketone and m/e = 43 of acetone as well Figs. 18, 27 and 28. This indicates that the processes of formation of such ions are at least initially similar.

F. The rates of decay of fragment ions are different from those molecular ions having the same mass, e.g. m/e = 43, from acetone Fig. 18, and mass m/e = 44 from acetaldehyde Fig. 30, or propane Fig. 34. Similarly, the molecular ion of acetone m/e = 58 of methyl n-butyl ketone Figs. 17 and 26.

G. The slope of the decay curves of the parent ion sometimes increased slightly with the increase of photon energy. This indicates the rate constant for dissociation to be a function of the excess energy of the ion. As the photon energy was increased, the number of ions dissociating during a time shorter than one microsecond should also increase. This was noticed as a direct increase in the relative height of the fragment ions peaks as the photon energy increased.

In the case where the rate of decay does not increase

with excess photon energy that necessary to cause dissociation, the excess energy may remain as internal vibrational energy. This is the assumption made by numerous workers (240), that almost all excess energy of excitation or ionization - if not too large - appears as an internal vibrational energy of fragments and not as kinetic energy.

H. Molecular ions possess no kinetic energy due to primary ionization, except their initial thermal energy which is, according to the Boltzmann-Maxwellian's distribution,

equal at $300^{\circ}K$ to: $E = \frac{1}{2} m\, v_p^2 = k.T = 0.025$ e.v.

and $600^{\circ}K$ to 0.05 e.v.

where m is the mass of the molecule, v_p the most probable velocity and $k = 1.3806 \times 10^{-16}$ erg $/k^{\circ}$ is the Boltzmann's constant. Molecular ions don't possess excess kinetic energies since in the primary ionization the difference between the energy of incident photons and the ionization potential of one of the outermost electrons will be imparted as kinetic energy E to this ejected electron according to Einstein's equation:

$$h.\nu = e.\, V_i + E$$

or, more accurately, according to this equation:

$$AB + h\nu = AB^{+} + e + I_p + E_{e.ion} + E_{k.ion} + E_{k.electron}$$

where e is the ejected electron, I_p the adiabatic ionization potential - the minimum energy required to remove the most

weakly bound electron with zero kinetic energy and the positive ion formed in the ground state - $E_{e.ion}$ is the excitation energy of the resulting molecular ion, $E_{k.ion}$ is the kinetic energy of the ion, and $E_{k.electron}$ is the kinetic energy of the ejected electron.

Even when the photon energy is several electron volts (or even higher than ten electron volts, as in the present work) higher than the ionization potential, the kinetic energy of molecular ion is very small and consequently can be neglected (60).

I. Molecular ion peak height sometimes remains constant for about ten microseconds Figs. 14 and 17, 15 microseconds Fig. 20 or more Figs. 25 and 41, but they mostly showed a definite increase with increasing delay time, then a decrease depending on the ion. This increment in peak height occurred within the first few microseconds of time delay showed a slight dependence on photon energy.

Three possible explanations for this phenomenon may be advanced:

1. The 'tail' of strong fragment peaks sometimes overlaps that of the parent and a part of the increase of the latter might result from interference between the two.

2. The increase in the molecular ion peak may be associated with a time delay focusing effect. The intro-

duction of a small time delay between ionization and ions acceleration can improve focusing the ion bunch (148). From the end of the photon pulse until the accelerating pulse applied the ions are free to move under the influence of their initial thermal velocities and kinetic energies of dissociation if possessed, as well as any stray fields - which have been discussed earlier in Chapter 5. These ions' motions tend to distribute the ions throughout the ionization chamber.

Plotting the values of time of flight (T-O-F) T versus the position of the ion x (Fig. 45) help in explaining this focusing phenomenon:

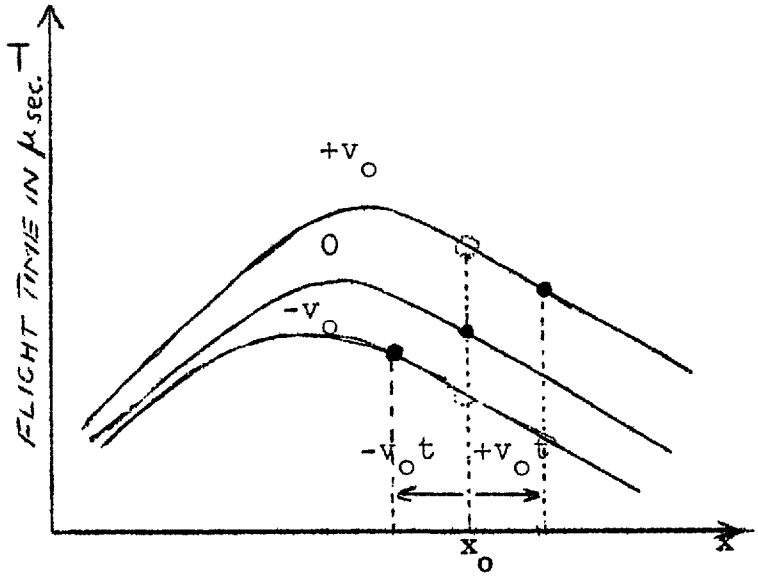


Fig. 45: Curves of · total flight time of an ion versus initial position of the ion in the ionization chamber

The middle curve represents ions with zero initial velocity, the upper and lower curves represent ions with initial velocities of $+v_o$ and $-v_o$ respectively. Supposing that $+v_o$ is for those ions travelling towards the drift tube and $-v_o$ is for those travelling towards the repeller plate.

During the short delay time period t, each ion moves a distance $\pm v_o t$ which produces a change in flight time T - which was given in equation (8) of section (2.1) or equation (15) of section (2.2) - of very nearly equal to $\pm \frac{dT}{dx} \cdot v_o t$. As the velocities remain the same each ion moves on its own trajectory to a new position indicated by a black circle. If the effect of the initial energy is to be eliminated - such as molecular ions - the change in flight time thus produced must compensate for the flight time difference with no delay time between ions with velocity zero and $\pm v_o$, and a focusing effect is produced.

This time difference at no time delay is approximately the time necessary for an ion travelling in the wrong or negative direction towards the repeller plate to be stopped. If the ion is travelling with initial velocity $(-v_o)$ in the accelerating field E, it will experience a force F equal to:

$$\vec{F} = e. \vec{E} = m. \vec{\gamma} = m. \frac{dv}{dt} \qquad (1)$$

and the time for the ion of mass m to stop is then given by:

$$t = \int_{-v_o}^{o} \frac{m}{eE}\, dv \qquad (2)$$

or

$$t = \frac{mv_o}{e.E} \qquad (3)$$

Thus the time spread introduced by the time delay (t) given in equation (3) will compensate for the time spread - of the ion bunch - due to the initial velocities if:

$$\frac{dT}{dx}\, v_o t + \frac{mv_o}{e\,E} = 0 \qquad (4)$$

or

$$t = - \frac{\frac{m}{e.E}}{\frac{dT}{dx}} \qquad (5)$$

It is apparent from equation (5) that the time delay focusing is possible only when $\frac{dT}{dx}$ is negative. This is verified in the region between the photon beam and repeller plate in the ionization chamber, where we can consider $\frac{dT}{dx}$ is negative, if the ionization region were the origin. But when $\frac{dT}{dx}$ is negative, this will violate the space focusing condition $\frac{dT}{dx} = 0$ (section 2.1) which has already been established in the present spectrometer.

However, if the delay time t is small, then $\frac{dT}{dx}$ must be large and gives poor focusing, but if it is too long the effect of the energy focusing $\frac{dT}{dx} = 0$ may be lost since

this quantity is not constant and some of the ions will travel too far into the region where $\frac{dT}{dx}$ is positive towards the drift tube and produce defocusing or broadening the mass peaks as the peaks' height decrease with increasing delay time.

With large values of delay time also, some of the ions - especially those with high energy such as fragments - will move towards the repeller plate impinging on it and are lost. This was the most probable cause for ions' decay in the ionization chamber and it was already treated in detail in part B section 1.3.

Thus as the time-delay varies from zero time, the peak height should go through a maximum then experience continuous decay. That was experimentally observed.

When one looks at equation (5) it is apparent that the time delay t required for focusing is independent of the initial ions velocity v_o, but is dependent and proportional to $m^{\frac{1}{2}}$ since $\frac{dT}{dx}$ (in equation 8 of section 2), is proportional to $m^{\frac{1}{2}}$. This means that fragment ions should show an increase in peak height like molecular ions with time delay focusing.

Actually this was not observed, except in one case, the fragment ion m/e = 51 of benzene Fig. 42 and that was probably due to experimental error. But if one looks at the decay curves of fragment ions it will be observed that there is a slow and constant decay during the first five

microseconds; while an increase was observed in the curves of Wahrhaftig (ref. 85) using electron impact technique.

However, this treatment may account for that increase in the molecular ion peak height which occurs in the first few microseconds of time delay. It may be however that by measuring peak area rather than height, the anomalous behaviour might be avoided since the number of ions produced in the ionization region in each pulse is proportional to the area recorded for ion peak rather than the height. This however could not be achieved in practice.

3. One last reason that might account for the increase is that the molecular ions may not be formed immediately as:

$$AB + h\nu \rightarrow AB^+ + e^-$$

but may arise indirectly thus:-

$$AB + h\nu \rightarrow AB^* \xrightarrow{slow} AB^+ + e \rightarrow A^+ + B^\cdot + e$$

The initially excited state must thus remain intact for a time. This period of time increases with excess photon energy, see Fig. 17 - sufficient for the excess photon energy (over the first ionization potential or some fraction of it) to become randomly distributed over the vibrational levels of molecule (240). Franck et al (246) have pointed out in general a polyatomic molecule

in an excited state will vibrate through a complex of 'Lissajous figures' before reaching an unstable configuration resulting in dissociation, and the life-time of this state depends on how long a path the polyatomic system travels within the potential energy surface (diagram) describing it before reaching a configuration leading directly to fragmentation and the rates of fragmentation of this molecule are determined by the probability of the energy randomly distributed over the molecular levels.

Unfortunately, since no similar research work has been reported so far (except ref. 85), this complication makes any quantitative or advanced discussion very difficult at this time.

PART C: APPENDICES - ELECTRONIC INSTRUMENTS

APPENDICES

ELECTRONIC INSTRUMENTS

1. PULSE GENERATOR AND MONITOR UNIT: This unit provided 180 volt square pulse of one microsecond duration, to trigger the microwave pulse generator (section 2 to follow) and has three time sharing signal measurement channels: 1) Sample (x), 2) Reference (y), 3) Stray light (z). These channels are linear in response up to 25 volts.

The unit also provided a 12.5 c/sec. square wave of 50 volts peak amplitude, which can be adjusted in frequency to rock the grating when required at its natural frequency 12 cycle per second. The complete circuit diagram of this unit is shown in Figure (47) and the component list in Fig. (48).

2. MICROWAVE PULSE GENERATOR: This unit was based upon military x-band radar transmitter. Major modifications were carried out on the circuit to work under laboratory conditions 230 volts/A.C. Full description is found in (3.1.1.6 a) and the complete circuit diagram is shown in Figure (49).

3. 10 K.V. POWER SUPPLY: The unit was a D.C/A.C. power supply. It provided the proper A.C. or D.C. potentials to the light source or to the magnetron of a microwave pulse generator (section 2). The voltage range was

adjustable between 0 - 10000 volts D.C. or A.C. Figure (7) shows the complete circuit diagram.

4. REPELLER VOLTAGE GENERATOR: The unit was already designed and constructed by Dr. D. W. Turner, later light modifications have been carried out on its circuit, Figure (50) to meet the instrument need. When triggered externally it provides reasonably square pulses of 2500 volts amplitude and 0.3 microsecond duration.

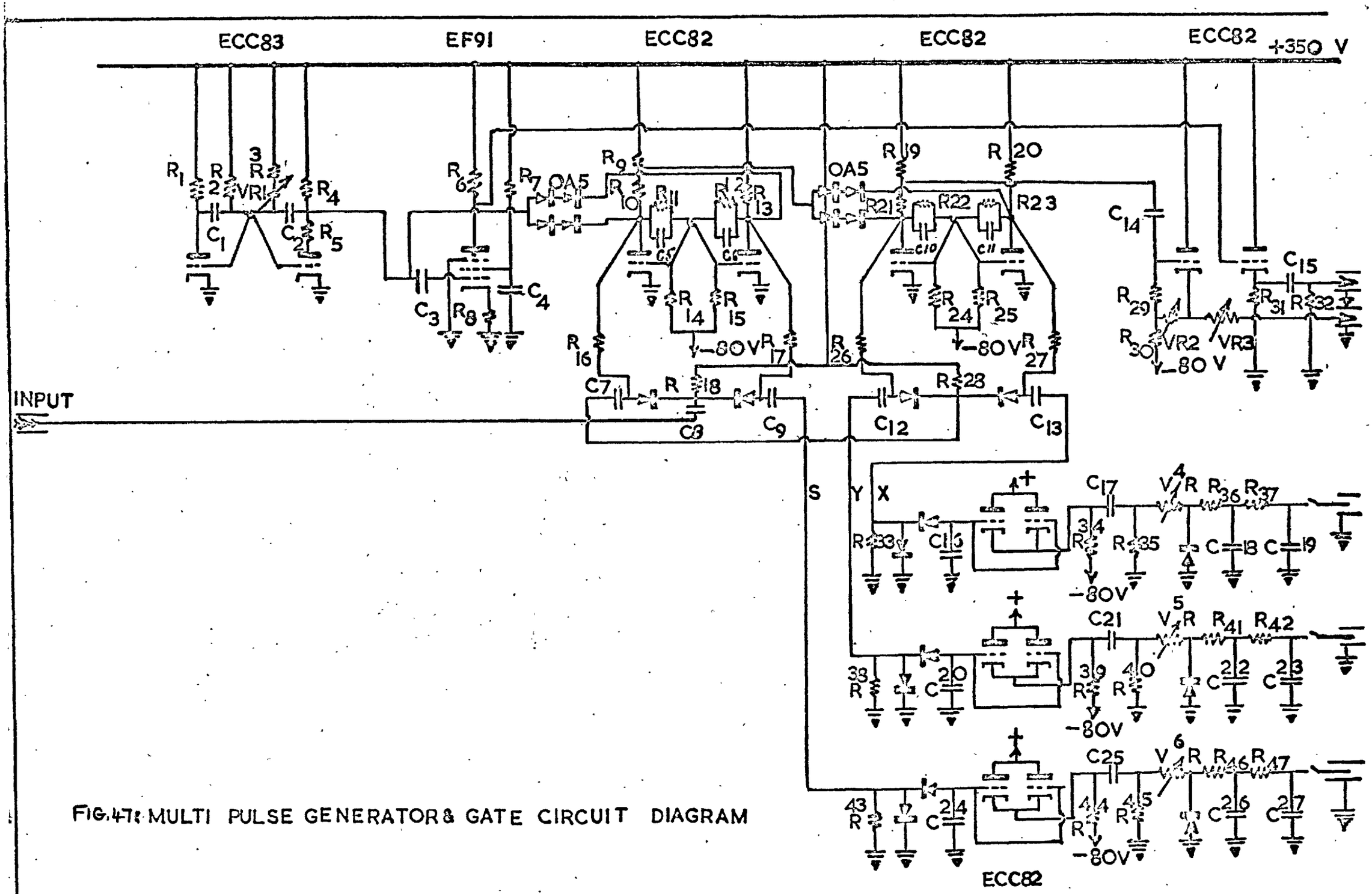


FIG.47: MULTI PULSE GENERATOR & GATE CIRCUIT DIAGRAM

FIG.48 : COMPONENT LIST

RESISTOR:

R8 = 100 Ω

R33,38,43. = 4600 Ω

R4,9,19,30 = 10K

R32 = 11 K

R5,10,21,34,39,44 = 33K

R1,13,20 = 47K

R31 = 68 K

R3,6,7,14,15,24,25 = 100K

R11,12,22,23 = 270K

R36,37,41,42,46,47 = 470K

R2,16,17,18,26,27,28,29,35,40,45 = 1 M

CONDENSER

C,3,5,6,16,20,24	= 100	pF
C,10,11	= 200	pF
C 4	= 0.0001	μF
C 7, 8, 9	= 0.001	μF
C 12,13	= 0.002	μF
C 2	= 0.025	μF
C 1	= 0.1	μF
C 14,15,17,18,19, 21 22 23 25 26 27	= 1	μF

OA5

VARIABLE RESISTOR:

VR,4,5,6	=	1 K
VR, 2,3	=	10 K
VR 1	=	100K

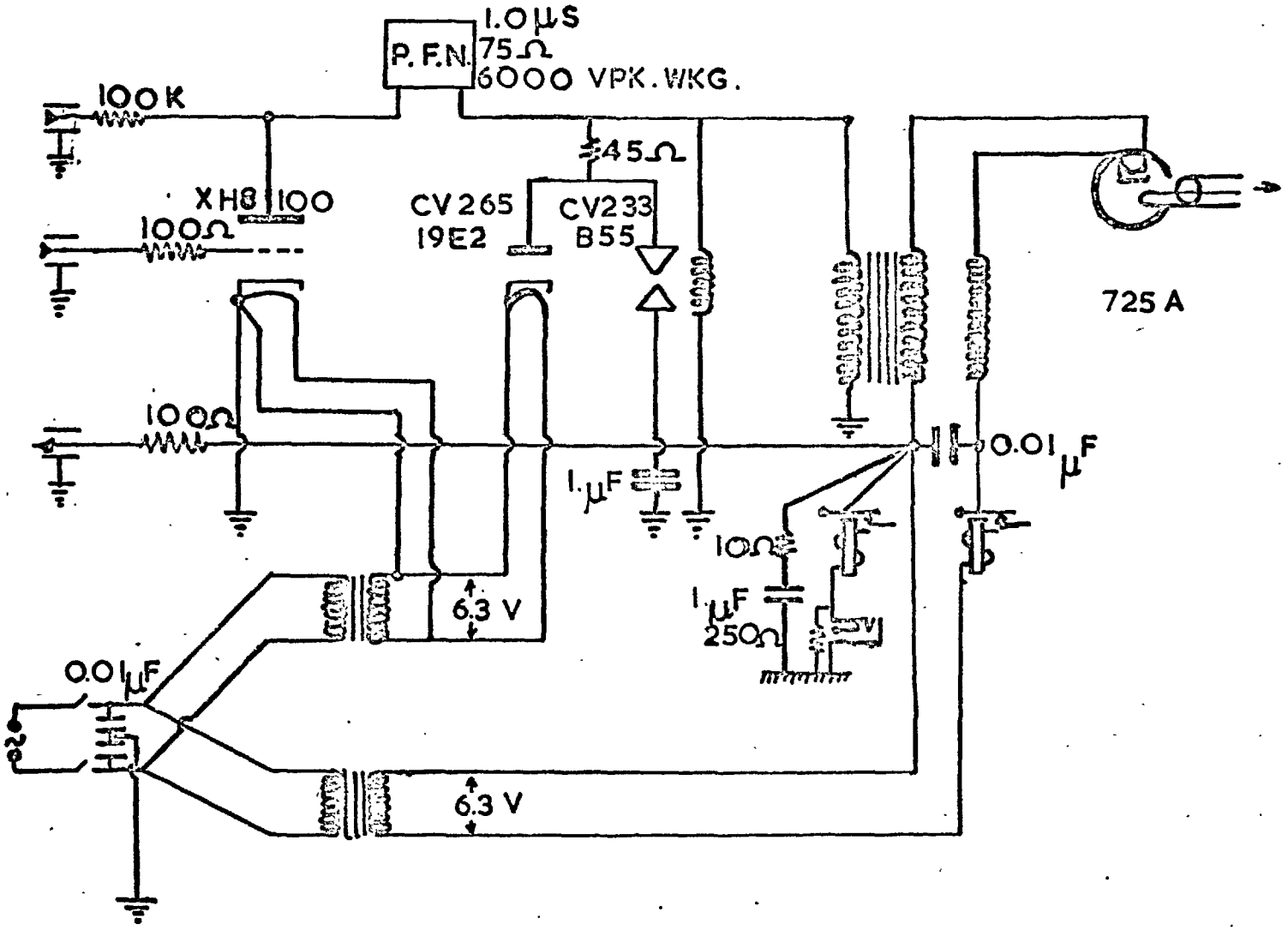


FIG. 49 : CIRCUIT DIAGRAM FOR PULSED MICROWAVE OSCILLATOR

- 162 -

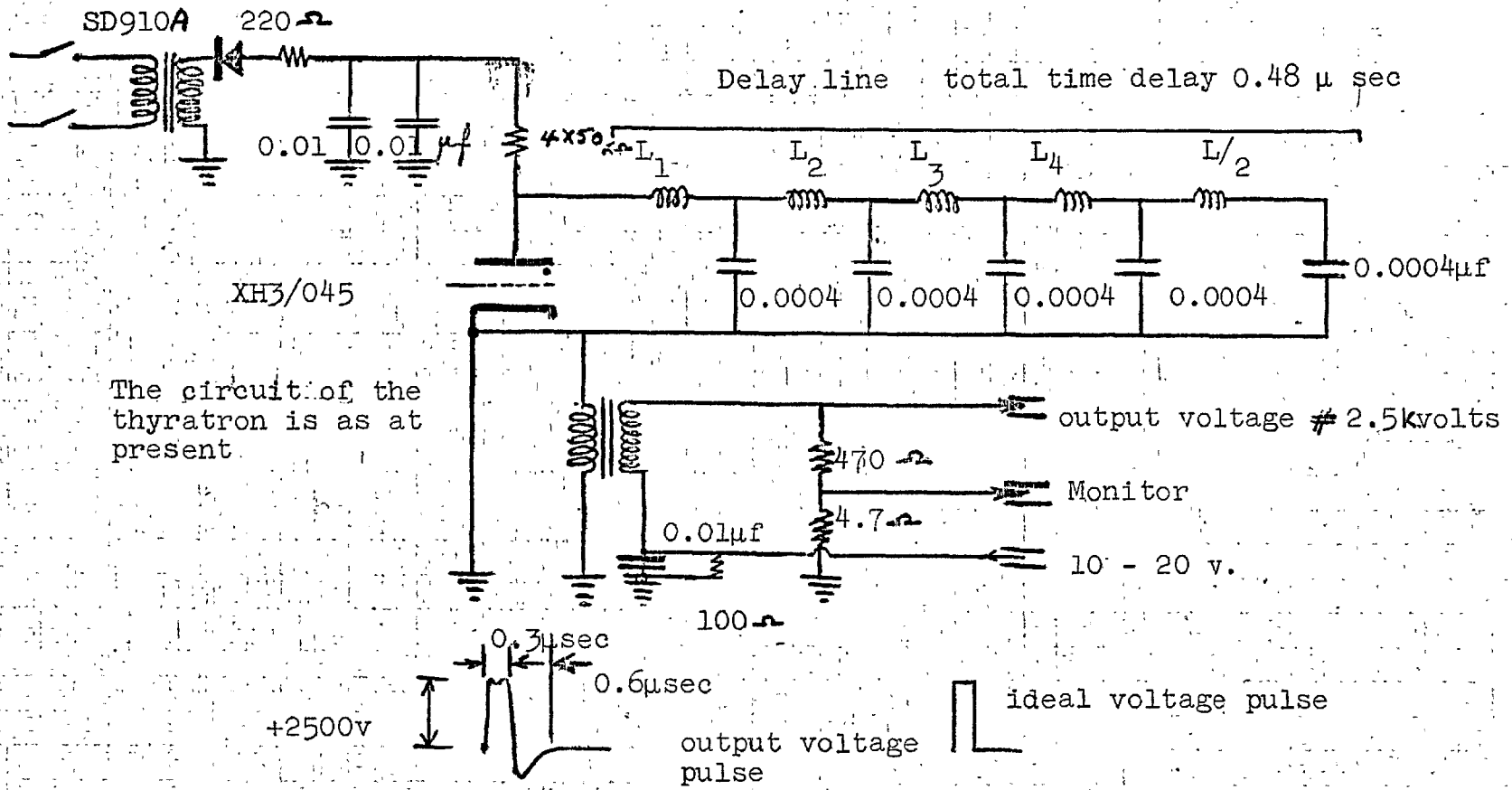


Fig. 50. Circuit diagram of the modifications carried out on the repeller voltage pulse generator and the shape of voltage pulse.

REFERENCES

REFERENCES

1. P. Lenard, Ann. d. Phys. 1, 486 (1900)
3, 298 (1900)
2. A. L. Hughes, Proc. Camb. Phil. Soc. 15, 483 (1910)
3. A. L. Hughes and L. A. DuBridge, 'Photoelectric Phenomena', McGraw-Hill, N.Y., 1932.
4. F. L. Mohler and P. D. Foote, Phys. Rev. 26, 195 (1925)
5. a. F. L. Mohler, P. D. Foote and R. L. Chenault, Phys. Rev. 27, 37 (1926)
b. F. L. Mohler, C. Boeckner and W. W. Coblentz, Science 69, 479 (1929)
c. F. L. Mohler and C. Boeckner, J. Res. Natl. Bur. Stand. 3, 303 (1929)
6. F. L. Mohler and C. Boeckner, J. Res. Ntl. Bur. Stand. 5, 186 (1930)
7. D. M. Parker and C. Lock, J. Opt. Soc. Am. 40, 264 (1950)
8. K. Watanabe, Phys. Rev. 83, 785 (1951)
9. R. Tousey, F. S. Johnson, J. Richardson and H. Toron J. Opt. Soc. Am. 41, 691 (1951)
10. K. Watanabe ,F. E. Marmo and E. C. Y Inn, Phys. Rev. 91, 1155 (1953)
11. N. Wainfan, W. C. Walker and G. L. Weissler, J. Appl. Phys. 24, 1318 (1953)
12. G. L. Weissler, 'Photoionization, Photoabsorption' in Proc. of the Third Int. Conf. on Ionization

Phenomena in Gases, Venice 1957.

13. G. L. Weissler, Photoionization and Photoionization-Induced ion-molecule reactions, 52pp, 1 Aug. 1963. Final Report, Dept. of Physics, Univ. of Southern California, Los Angeles, AFCRL 63877, March 5th, 1964, Unclassified AD 419548

14. G. L. Weissler, D. L. Judge and A. L. Morse, Report on Photoionization,V.U.V. Induced fluorescence diagnostic tool, 8pp, 28 Feb. 1964, Dept. of Phys., Univ. of Southern Calif. Los Angeles, AD 435601

15. K. Watanabe, J. Chem. Phys. 22, 1564 (1954)

16. ibid, J. Chem. Phys. 26, 542 (1957)

17. H. Sakai, J. W. Little and K. Watanabe, J. Chem. Phys., 26, 1335 (1957)

18. K. Watanabe, Photoionization and U.V. Absorption Processes, Hawaii Institute of Geophysics and Dept. of Phys., Univ. of Hawaii, Honolulu, Hawaii, Contract No. AF19 (604) - 4576 AFCRL Final Rept. Feb. 1962 19pp, NASA, N62-10947

19. K. Watanabe, T. Nakayama and J. Mottle, Final Report on Ionization potential of molecules by photoionization method. Contract No. DA-04-200-ORD 480 and 737 F.R. period March 1956 to Dec. 1959. Appeared in J. Quant. Spectrosc. Radiant Transfer 2, 369-382 (1962).

20. K. Watanabe, J.A.R. Samson, F.F. Marmo, J. Chem. Phys. 36, 783-786 (1962)

21. Ibid., J. Chem. Phys. 40, 553 (1964)

22. F. M. Matsunaga, 'Absolute Photoionization and Quantum Yields of Several Molecules in the Schumann Region', M.S. Thesis, Univ. of Hawaii, Dept. of Phys. Honolulu, June, 1960.

23. D. L. Ederer and D. H. Tomboulian, Phys. Rev. 133, A1525-1532 (1964).

24. D. L. Ederer, 'The Photoionization cross-section of Neon from 80 - 600 A^{o}', U.S. Office of Naval Research Contract No. 40137 Project NR17, 625, Rech. Rep. 10, June 1963.

25. D. L. Ederer, 'Photoionization of the 4d electrons in Xenon', Cornell Univ. Dept. of Phys. Ithaca, N.Y., Tech. Rep. No. 11, 32pp, Sept. 1964

26. J. A. R. Samson, J. Opt. Soc. Am. 54, 842 (1964)

27. Ibid J. Opt. Soc. Am. 54, 876 (1964)

28. Ibid J. Opt. Soc. Am. 54, 420 (1964)

29. G. R. Cook and P. H. Metzger, J. Opt. Soc. Am. 54, 968 (1964)

30. Ibid, J. Opt. Soc. Am. 55, 516 (1965)

31. Ibid, J. Chem. Phys. 41, 321 (1964)

32. Ibid, J. Chem. Phys. 41, 642 (1964)

33. A. J. C. Nicholson, J. Chem. Phys. 39, 954 (1963)

34. J. D. Morrison, Electron-molecules and photomolecule Collisions, pp.397-416 in Proc. of Inst. Int. de Chimie Douzieme, Conseil de Chimie tenu a l'universite Libre de Bruxelles 5 - 10 Nov. 1962, Bruxelles, Belgique, R. Stoops Ed.

35. R. W. Ditchburn, Proc. Conf. on Rocket Research in the upper Atmosphere, pp. 313, Pergamon Press, London 1954.

36. G. L. Weissler in Handbuch der Physik pp.304-382 vol.XXI (Flügge Ed.), Springer Verlag, Berlin, 1956

37. R. W. Ditchburn, Proc. Roy. Soc. A 236, 216 (1956)

38. R. W. Ditchburn, and Öpik in 'Atomic and Molecular Processes', pp.79 (D. R. Bates Ed.) Academic Press, N. Y., 1962

39. F. L. Mohler, 'Photoionization of Atoms and Molecules', N.B.S. Tech. Note 131, Jan. 1962.

40. K. Watanabe, Advances Geophys. 5, 153 (1958)

41. E. W. McDaniel, 'Collision Phenomena in Ionized Gases', pp.345, John Wiley and Sons, N.Y., 1964.

42. R. W. Kiser, Tables of Ionization Potentials, USAEC, TID-6142 (1960)

43. R. W. Kiser, Additions and Corrections to Tables of Ionization Potentials, USAEC, TID 6142 (1962)

44. L. B. Loeb, Basic Processes in Gaseous Electronics Chapter 9, p.801, Univ. of California Press, Berkeley, Calif. 1955

45. M. Nicolet in Handbuch der Physik, Vol. 11, Springer-Verlag, Berlin, 1958

46. M. Zelikoff, Ed. 'The Threshold of Space', Pergamon Press, Oxford, 1957

47. S. K. Mitra, 'The Upper Atmosphere' 2nd Ed. Hafner, N. Y.

48. R. A. Craig, 'The Upper Atmosphere' Academic Press, N. Y. and London, 1965

49. R. G. Fleagle and J ost A. Businger, 'An Introduction to Atmospheric Physics', Academic Press, N. Y. 1963

50. J. A. Ratcliffe, 'Physics of the Upper Atmosphere', Academic Press, N.Y., 1960

51. Report by P. J. Nawrocki and R. Popa, 'Atmospheric Processes', Prentice-Hall, Englewood Cliffs, N. J. 1962

52. G. P. Kuiper Ed. 'Solar Systems', vol. 2, The earth as a planet, Univ. of Chicago Press, Chicago, 1954.

53. G. Herzberg, 'Molecular Spectra and Molecular Stucture, 2nd ed., D. van Nostrand Co., N.Y. 1950.

54. D. W. Turner and M. I. Al Jobory, J. Chem. Soc. (London), Nov.(1963), 5141

55. Ibid, J. Chem. Soc. (London) Nov.(1964), pp.4434

56. D. W. Turner and T. N. Radwan, unpublished results.

57. T. N. Radwan, University of London, Thesis to be submitted (1966).

58. F. I. Vilesov, B. L. Kurbatov and A. N. Terenin, Soviet Phys. Doklady 6, 490, (1961)

59. Ibid, Soviet Phys. Doklady 6, 883, (1962.)

60. F. I. Vilesov and B. L. Kurbatov, Bulletin of the Acad. of Sciences of the U.S.S.R., Physical Series, 27, 1059, 1963, or Izvestiya Akademii Nauk SSSR, Seriya Fizicheskaya, 27, 1088, (1963).

61. A. N. Terenin and B. Popove, Physik Z. Sowjetunion 2, 299, (1932)

62. F. P. Lossing and I. Tanaka, J. Chem. Phys. 25, 1031, (1956)

63. R. F. Herzog and F. F. Marmo, J. Chem. Phys. 27, 1202, (1957). see also pp.124 of Rep. 46

64. E. Schonheit, Z. Physik, 149, 153, (1957)

65. H. Huzaier, M. G. Inghram and J. D. Morrison, J. Chem. Phys. 27, 313, (1957)
J. Chem. Phys. 28, 76, (1958)

66. F. I. Vilesov, B. L. Kurbatov and A. N. Terenin, Doklady Akad. Nauk SSSR, 94, 122, 1958

67. G. L. Weissler, J. A. R. Samson, M. Ogawa and G. R. Cook, 'Photoionization Analysis by Mass Spectroscopy', The U.S. Office of Naval Research Contract No. 228(11) Project No. NR-017-505

68. J. A. R. Samson, Mass Spectroscopic Determination of Different ions Produced by the Process of Photo-ionization, Univ. Microfilm, Ann Arbor, Mich. Library

of Congress card No. Mic 59-1862, 92 pp.

69. G. R. Cook, Photoionization induced ion-molecule reactions in a mass spectrometer, Univ. Microfilm, Ann Arbor, Mich., L.C. card No. Mic 59-3513, 117pp

70. G. R. Cook, J. A. R. Samson and G. L. Weissler, Photoionization induced ion-molecule reactions in a mass spectrometer, Univ. of Southern Calif, Dept. of Phys. Los Angeles, Calif. Contract AF19(604) 2049, (1/1), 1959, 88pp. abstracted in P.B. 145185 June 1960.

Several abstracts have also been reported by Cook and Samson on photoionization studies of N_2, N_2O, water vapor and ammonia. Experimental results are in the following references:

71. J. A. R. Samson and G. R. Cook, Bull. Am. Phys. Soc. (2), 3, 413, (1958)

72. Ibid, (2), 4, 454, (1959)

73. J. A. R. Samson, Univ. Microfilm Ann Arbor, Mich. L. C. card No. Mic 59-1862

74. F. I. Vilesov, M. E. Akopyan and A. N. Terenin, Soviet Physics, Doklady 6, 890 (1962). This is the English version of the original paper which appeared in 1961, Doklady Akad. Nauk, SSSR, 140, 1037, 1961

75. F. I. Vilesov, M. M. Akopyan and A. N. Terenin, Bull. of the Acad. of Sciences of the USSR, Physical Series, 27, 1054, (1963)

Izvestiya Akademii Nauk SSSR, Seriya Fizicheskaya, 27, 1083, (1963)

76. J. Momigny, Nature, 191, 1179, (1961)

77. V. H. Dibeler and R. M. Reese, J. Chem. Phys. 40, 2034, (1964)

78. V. H. Dibeler and R. M. Reese, J. Natl. Bur. Stand. (Phys. and Chem.), 68A, 409, (1964)

79. V. H. Dibeler, R. M. Reese, and Morris Krauss, J. Chem. Phys. 42, 2045, (1965)

80. H. D. Hagstrum, Rev. Modern Phys. 23, 185, (1951)

81. B. Steiner, C. F. Giese and M. G. Inghram, J. Chem. Phys. 34, 189, (1961)

82. M. B. Wallenstein, A. L. Wahrhaftig, H. M. Rosenstock and H. Eyring, 'Oberlin Symposium on Radiobiology', June 1950, John Wiley and Sons, Inc., N. Y. 1952

83. H. M. Rosenstock, M. B. Wallenstein, A. L. Wahrhaftig and H. Eyring, Proc. Natl. Acad. Sci. (U.S.), 38 667, (1952)

84. H. M. Rosenstock, A. L. Wahrhaftig and H. Eyring, J. Chem. Phys. 23, 2200, (1955)

85. A. L. Wahrhaftig, Ion-Dissociation Reaction in the Mass Spectrometer, pp.274 in Advances in Mass Spectrometry (J. D. Waldron, Ed.), Pergamon Press, Oxford 1959

86. L. Friedman, F. A. Long and M. Wolfsberg, J. Chem. Phys. 27, 714, (1957) J. Chem. Phys. 30, 1605, (1959) J. Chem. Phys. 31, 755, (1959)

87. J. D. Morrison and H. E. Stanton, J. Chem. Phys. 28, 9, (1958)

88. A. Kropf, E. M. Eyring, A. L. Wahrhaftig and H. Eyring, J. Chem. Phys. 32, 149, (1960)

89. W. A. Chupka and J. Berkowitz, J. Chem. Phys. 32 1546, 1960

90. E. J. Gallegos, R. W. Kiser, J. Am. Chem. Soc. 83, 773, (1961)

91. J. Collin, J. Chim. Physique pp.416 and 424, (1960)

92. Ibid, Bull. Soc. Chim. Belges, 69, 575, (1960)

93. Ibid, Bull. Soc. Chim. Belges, 69, 585, (1960)

94. Ibid, Colloq. Spectrosco International 9th (Lyons 1961), 3, 596, (1962)

95. Ibid, Bull. Soc. Chim. Belges, 71, 15, (1962)

96. Ibid, Bull. Soc. Roy. Sci, Liege, 32, 133, (1963)

97. J. Momigny, Bull. Soc. Chim. Belges, 70, 291, (1961)

98. E. L. Eliel , J. D. McCollum, S. Meyerson and P. N. Rylander, J. Am. Chem. Soc. 83, 2481, (1961)

99. S. N. Foner and R. L. Hudson, J. Chem. Phys. 36, 2676, (1962)

100. E. W. Godbole and P. Kebarle, Trans. Faraday Soc. 58, 1897, (1962)

101. R. Candano, Delfosse, J. M. and J. Steyaert, Ann. Soc. Sci. Bruxelles Ser. I, 76, 217, (1962)

102. I. Zlotowski and H. Wincel, Isotopen Tech. 2, 321, (1962)

103. F. N. Chelobov, S. S. Dubov and M. V. Tikhominov, Zh. Fiz. Khim. 37, 1500, (1963)

104. D. Van Raalte and A. G. Harrison, Can. J. Chem. 41, 2054, (1963)

105. J. A. Hipple and E. U. Condon, Phys. Rev. 68, 545, (1945)

106. J.A. Hipple, R. E. Fox and E. U. Condon, Phys. Rev. 69, 347, (1946)

107. J. A. Hipple, Phys. Rev. 71, 594, (1947)

108. N. D. Coggeshall, J. Chem. Phys. 37, 2167, (1962)

109. W. W. Hunt, Jr., R. E. Huffman and K. E. McGee, Rev. Sci. Instr. 35, 82, (1964)

110. W. W. Hunt, Jr. and K. E. McGee, J. Chem. Phys. 41, 2709, (1964)

111. H. M. Rosenstock, J. Chem. Phys. 42, 100, (1965)

112. E. Lindholm, Proc. Phys. Soc. (London) A66, 1068, (1953)

113. Ibid, Conference on applied mass spectrometry, Inst. of Petroleum, London, 1953

114. Ibid, Z. Naturforsch. 9a, 535, (1954)

115. Ibid, Arkiv. Fysik, 8, 257, (1954)

116. Ibid, Arkiv. Fysik, 8, 433, (1954)

117. E. Gustafsson and E. Lindholm, Arkiv Fysik, 18, 219, (1960)

118. H. Von Kock and E. Lindholm, Arkiv Fysik, 19, 123, (1961)

119. P. Wilmenius and E. Lindholm, Arkiv Fysik, 21, 97, (1962)

120. E. Pettersson and E. Lindholm, Arkiv. Fysik, 24, 49 (1963)

121. W. B. Maier II, J. Chem. Phys. 41, 2174, (1964)

122. W. A. Chupka and E. Lindholm, Arkiv. Fysik, 25, 349, (1963)

123. W. A. Chupka, J. Chem. Phys. 30, 191, (1959)

124. B. Steiner, C. F. Giese and Mark G. Inghram, J. Chem. Phys. 34, 189, (1961)

125. R. I. Schoen, J. Chem. Phys. 37, 2032, (1962)

126. E. Murad and M. G. Inghram, J. Chem. Phys. 40, 3263, (1964)

127. H. Inghram, J. D. Morrison, Hurzeller, H. and H. E. Stanton, J. Chem. Phys. 33, 821-824, (1960)

128. J. D. Morrison, Rev.. Pure and Appl. Chem. 5, 22, (1955)

and J. Appl. Phys. 28, 1409, (1957)

129. H. E. Stanton, J. Chem. Phys. 30, 1116, (1959)

130. R. M. S. Hall, Nature, 187, 683, (1960)

131. R. M. S. Hall, Chem. and Ind. (London), p.369, (1961)

132. J. E. Monaham and H. E. Stanton, Bull. Am. Phys. Soc. II, 6, 356, (1961)

133. W. A. Chupka and M. Kaminsky, J. Chem. Phys. 35, 1991, (1961)

134. Toshikazu Tsuchiya, J. Chem. Phys. 36, 568, (1962)

135. J. Olmsted III, K. Street, Jr. and A. S. Newton, J. Chem. Phys. 40, 2114, (1964)

136. H. E. Stanton, J. Chem. Phys. 41, 3604, (1964)

137. K. R. Ryan and J. H. Futrell, J. Chem. Phys. 42, 824, (1965)

138. K. R. Ryan and J. H. Green, J. Sci. Instr. 42, 461 (1965).

139. W. E. Stephen, Bull. Am. Phys. Soc. 21, No. 2, p.22, (1946)

140. A. E. Cameron and D. F. Eggers, Jr., Rev. Sci. Instr., 19, 605, (1948)

141. R. Keller, Helv. Phys. Acta, 22, 386, (1949)

142. W. E. Glenn, UCRL-1628, 1952, Univ. of Calif. Radiation Lab. Contract No. W-7405-eng-48
See also U.S. Patent 2, 758, 214, 7 Aug. 1956

143. N. I. Ionov and B. A. Mamyrin, Zh. Tekhn. Fiz. 23, 2101, (1953) (in Russian)

144. M. M. Wolff and W. E. Stephens, Rev. Sci. Instri. 24, 616, (1953)

145. W. E. Stephens, U. S. Patent 2, 612, 607

146. E. E. Hays, TOFMS (Abstract), Phys. Rev. 96, 1454, (1954)

147. H. S. Katzenstein and S. S. Friedland, Rev. Sci. Instr. 26, 324-27, (1955)

148. W. C. Wiley and I. H. McLaren, Rev. Sci. Instr. 26 1150-1157, (1955)

149. W. C. Wiley, Science, 124, 817, (1956)

150. W. C. Wiley, (Bendix Aviation Corp)
U. S. Patent 2, 759, 105, 14 Aug. 1956
U. S. Patent 2, 762, 927, 11 Sept. 1956
U. S. Patent 2, 794, 125, 28 May, 1957
U. S. Patent 2, 797, 330, 25 June, 1957

151. H. Ezoe and T. Hayashi, Sci. Pap. Inst. Phys. Chem. Res. (Tokyo) 53, 1-8, (1958)

152, L. G. Hall and H. W. Washburn (Consolidated Electrodynamics Corp) U. S. Patent 2, 810, 075, 15.10.1957

153. A. C. Hall, T.O.F.M.S. for rocket combustion analysis, Aviation Week, 25, 47-49, (1957)

154. E. I. Agishev and N. I. Ionov, Zh. Tekhn. Fiz. 26, 203, (1956). 'Soviet Physics' Technical Physics 1, 201-5, (1956)

155. Ibid, 3, 1638, (1958)

156. D. B. Harrington, 'TOF Mass Spectrometry' in Encyclopedia of Spectroscopy ed. by C. F. Clark, pp.628-647, Reinhold Pub. Corp. N.Y., 1960

157. W. W. Hunt, Jr., R. E. Huffman, J. Saari, G. Wassel, J. F. Belts, E. H. Paufue, W. Wyess and R. A. Fluegge, Rev. Sci. Instr. 35, 88, (1964)

158. Marjorie Comstack, 'Vacuum Ultra Violet Spectroscopy', Bibliography, 1960, U.S.A.E.C. TID-3905

159. J. M. Kelble, 'Bibliography of Vacuum Ultra-Violet Spectroscopy', Feb. 1963
Technical Documentary Rep. No. ASD-TDR-62-915, Project No. 7340, Task No. 734007 No. Ad-401498

160. W. R. S. Garton, 'Spectroscopy in the Vacuum Ultra-Violet' in Advances in Atomic and Molecular Physics ed. D. R. Bates, Academic Press, N. Y. and London, 1965

161. J. H. Dowell, J. Sci. Instr. 17, 208, (1940)

162. R. A. Sawyer, 'Experimental Spectroscopy', Prentice Hall, Inc., Englwood Cliffs, N.J., 1944, 2nd Ed. pp.161-164

163. Y. Fujoka and R. Ito, Science of Light 1, 1, (1951)

164. R. Tousey, F. S. Johnson, J. Richardson and N. Toran, J. Opt. Soc. Am. 41, 696, (1951)

165. F. S. Johnson, K. Watanabe, R. Tousey, J. Opt. Soc. Am. 41, 702, (1951)

166. M. S. Robin, Rev. Opt. (theor. Instrum.), 33, 193, (1954)

167. Y. Tanaka and M. J. Zelikoff, J. Opt. Soc. Am. 44, 254, (1954)

168. P. D. Johnson, Rev. Sci. Instr. 28, 833, (1957)

169. R. Onaka, Sci. of Light, 7, 23, (1958)

170. R. Romond, B. Vodar, Rev. Sci. Instr., 29, 732, (1958)

171. Th. J. M. Sluyters and E. Hass, Rev. Sci. Instr. 29, 597, (1958)

172. F. J. P. Clarke and W. R. S. Garton, J. Sci. Instr. 36, 403, (1959)

173. L. D. Isaacs, W. C. Price and R. G. Ridley, Optica Acta, 1, 263, (1960)

174. W. M. Powell, Phys. Rev. 45, 154, (1934)

175. E. P. Little, J. Opt. Soc. Am. 36, 168, (1946)

176. W. W. Parkinson and F. E., WILLIAMS J. Opt. Soc. Am. 39, 705, (1949)

177. J. H. Bolton and S. E. Williams, Nature (London), 169, 325, (1952)

178. M. Seya, Sci. of Light (Tokyo), 2, 8, (1952)

179. T. Namioka, Sci. of Light, 3, 15, (1954)

180. T. Namioka, J. Opt. Soc. Am. 49, 951, (1959)

181. H. Greiner and S. Schaffer, Optik 14, 263, (1957)
Optik 15, 51, (1958)

182. V. J. Hammond and W. C. Price, J. Opt. Soc. Am. 43, 924 (1953)

183. W. F. Meggers and V. Westfall, J. Research Natl. Bur. Standards 44, 447 (1950)

184. D. E. Kerr and R. D. Deslattes, Tr. No. X, Contract No. 238, T.O. VIII

185. M. Zelakoff, P. H. Wyckoff, L. M. Aschenbrand and Loomis, J. Opt. Soc. Am. 39, 12 (1949)

186. E. Jacobsen, G. R. Harrison, J. Opt. Soc. Am. 39 1054 (1949)

187. M. Zelakoff, P. H. Wyckoff, L. M. Aschenbrand and Loomis, J. Opt. Soc. Am. 42, 818 (1952)

188. P. G. Wilkinson and Y. Tanaka, J. Opt. Soc. Am. 45 344 (1955)

189. F. S. Tomkins and M. Fred, J. Opt. Soc. Am. 47, 1087 (1957)

190. L. Bovey and H. Wise, AERE-R 2976 (1959)

191. F. W. Schlag and F. J. Comes, J. Opt. Soc. Am. 50, 866 (1960)

192. N. N. Axelrod, J. Opt. Soc. Am. 51, 898 (1961)
53, 297 (1963)

193. P. Warneck, Applied Optics, 1, 721 (1962)

194. E. F. Worden, R. G. Gutmacher and J. G. Conway, Applied Opt. 2, 707 (1963)

195. J. M. Vaugham, J. Opt. Soc. Am. 54, 318 (1964)

196. A. A. Vashman, L. V. Lipis and N. A. Teterina, Optics and Spectroscopy, Vol. VI, 168 (1959)

197. P. M. Murphy and H. E. Edgerton, J. Appl. Phys. 12, 848 (1941)

198. H. E. Edgerton, J. Opt. Soc. Am. 36, 390 (1946)

199. J. N. Aldington, Trans. Illum. Engineering Soc. (London), 13, 1, (1948)

200. J. N. Aldington, Ibid, 14, 19 (1949)

201. R. G. W. Norrish and G. Porter, Nature, 164, 658 (1949)

202. G. Porter, Discussion Faraday Soc. No. 9 (1950)

203. W. D. McGrath and R. G. W. Norrish, Proc. Roy. Soc. (London) A242, 265 (1957)

204. W. R. S. Garton and A. Rajaratnam, Proc. Phys. Soc. A70, 815 (1957)

205. W. R. S. Garton, J. Sci. Instr. 36, 11 (1959)

206. W. R. S. Garton et al., Proc. Fourth Int. Conf. on Ionization Phenomena in Gases, Uppsala, 1959 (North-Holland Publishing Company, Amsterdam) pp 518

207. W. R. S. Garton, Proc. Fifth Int. Conf. on Ionization Phenomena in Gases, edited by H. Maecker, Vol. 11, 1962, (North-Holland Publishing Co., Amsterdam) pp 1884

208. R. E. Huffman, Y. Tanaka and J. C. Larrabee, J. Opt. Soc. Am. 52, 857 (1962)

209. F. F. Marmo, J. Opt. Soc. Am. 43, 1186 (1953)

210. M. Seya and F. Masuda, 'Science of Light' (Tokyo), 12, 9 (1963)

211. K. Watanabe and E. C. Y. Inn, J. Opt. Soc. Am. 43

212. F. Masuda and Masao Seya, Science of Light (Tokyo) 9, 99 (1960)

213. K. Krukowski, Die Naturwissenschaften, 45, 509, (1958)

214. J. F. Hammann, Z. Angew. Phys. 10, 187 (1958)

215. Abbott M. Smith, Thesis, Institute of Optics, University of Rochester, 1961

216. N. Kristianpoller and R. A. Knapp, Applied Optics, 3, 915 (1964)

217. N. Kristianpoller, J. Opt. Soc. Am. 54, 1285 (1964)

218. R. A. Knapp and A. M. Smith, Applied Optics, 3, 637 (1964)

218a. J. A. R. Samson, J. Opt. Soc. Am, 54, 6 (1964)

219. K. J. Nygaard, Brit. J. Appl. Phys. 15, 597 (1964)

220. E. C. Bruner, Jr., The absolute quantum efficiency of sodium sodicylate excited by extreme ultra-violet. Lab. for Atmospheric and Space Physics, University of Colorado, Boulder, Colorado, NASA Sci. Rept. No. 3, April 1964, 104pp AD427 095

221. R. Allison, J. Burns and A. J. Tuzzolino 'Absolute fluorescent quantum efficiency of sodium salicylate', Labs. for Applied Sciences, University

of Chicago, NASA CR-53230 15pp 1962 N64-17573

222. R. A. Allison, J. Burns and A. J. Tuzzolino, J. Opt. Soc. Am. 54, 747 (1964)
J. Opt. Soc. Am. 54, 1381 (1964)

223. K. R. Spangenberg, 'Vacuum Tubes', McGraw-Hill Book Co. Inc., N.Y. 1943, pp.751

224. R. Tousey, Applied Optics, 1, 679-694 (1962)

225. M. Michel Clerc Rev. Sci. Instr. 36, 1160 (1965)

226. K. Watanabe, E. C. Y. Inn, and M. Zelikoff, J. Chem. Phys. 21, 1026 (1953)

227. K. Watanabe, M. Zelikoff, and E. C. Y. Inn, Geophys. Res. Pap. (Geophys. Res. Directorate), Air Force Cambridge Research Center, No. 21 (1953)

228. Y. Tanaka, E. C. Y. Inn and K. Watanabe, J. Chem. Phys. 21, 1651 (1953)

229. J. P. Curtis, Phys. Rev. 94, 908 (1954)

230. M. I. Al-Jabory, Ph.D. Thesis, Chemistry Dept. Imperial College, University of London, 1964

231. W. Bleakney and J. T. Tate, Phys. Rev. 35, 658 (1930)

232. F. H. Field and J. L. Franklin 'Electron Impact phenomena and the properties of gaseous ions' Academic Press Inc. N.Y. 1957

233. W. Bleakney, Phys. Rev. 35, 1180 (1930)

234. W. Lozier, Phys. Rev. 36, 1285 (1930)

235. H. D. Hagstrum and J. T. Tate, Phys. Rev. 59, 354 (1941)

236. C. E. Berry, Phys. Rev. 78, 597 (1950)

237. R. Taubert in 'Advances in Mass Spectrometry' edited by J. D. Waldron, Pergamon Press, London 1959, pp.489

238. R. C. Tolman, 'The principles of statistical mechanics' Oxford University Press, London 1958, Capt. IV

239. Tables of the Error Function and its Derivative, National Bureau of Standards, Circular: Applied Mathematics Series 41, Washington 1954, U.S. Superintendent of Document; Government Printing Office

240. H. E. Stanton and Mark G. Inghram (private communication)

241. D. P. Stevenson, J. Chem. Phys. 17, 101 (1949)

242. J. E. Monahan and H. E. Stanton, J. Chem. Phys. 37, 2654 (1962)

243. A. Hustrulid, P. Kusch, J. T. Tate, Phys. Rev. 54, 1037 (1938)

244. F. L. Mohler, V. H. Dibeler and R. M. Reese, J. Chem. Phys. 22, 394 (1954)

245. A. O. Hurley and V. W. Maslen, J. Chem. Phys. 34, 1919 (1961)

246. J. Franck, H. Sponer and E. Teller, Z. Physik Chem. B18, 88 (1932)